2013-09-16

Accurate and Precise Iron Isotope Amount Ratios Measured by Multi-Collector Inductively Coupled Plasma Mass Spectrometer

McKiernan, Breege

UNIVERSITY OF CALGARY

Accurate and Precise Iron Isotope Amount Ratios Measured by Multi-Collector Inductively Coupled Plasma Mass Spectrometer

by

Breege Agnus McKiernan

A THESIS

SUBMITTED TO THE FACULTY OF GRADUATE STUDIES

IN PARTIAL FULFILMENT OF THE REQUIREMENTS FOR THE

DEGREE OF MASTER OF SCIENCE

DEPARTMENT OF PHYSICS AND ASTRONOMY

CALGARY, ALBERTA

SEPTEMBER, 2013

Abstract

An analytical technique to accurately measure iron isotope amount ratios by multi collector inductively coupled plasma mass spectrometer was developed. The analytical technique consisted of sample purification using ion exchange chromatography and measurement by the mass spectrometer. Numerous factors affecting the measured data including magnet stability, and chromium interferences were encountered during development. At the completion of this projects, the precision in $\delta(^{56/54}Fe)$ is 0.09 ‰. Iron isotope measurements were completed on three data sets: a source identification study for the Cardium formation, anoxic brine samples from Lake Vida and a bioremediation study for Nova Chemicals. For the Cardium formation no definite source of iron can be identified based solely on the iron data. Similarly with the Lake Vida samples, three possible mechanisms are discussed which could produce the unique $\delta(^{56/54}Fe)$ values. For the bioremediation study, the data highlight difficulties during sample acquisition and improvements to sample acquisition are suggested.

Acknowledgments

I am grateful for my supervisor Dr. Michael Wiser and all his support and guidance throughout my maters. I would also like to thank Dr. Ronny Schoenberg for the assistance and knowledge provided while visiting his laboratory.

For the Cardium formation study, I would like to thank Dr. Bernhard Mayer and Michael Nightingale for the samples and their help in data interpretation. Thank you to Dr. Alison Murray and Dr. Bernadette Promese for the Lake Vida samples and their expertise regarding this sampling location. I would also like to acknowledge Chris Jackson, Bernhard Mayer and Nova Chemicals for the bioremediation samples.

Funding for the stable isotope laboratory from the national sciences and engineering research council (NSERC) is gratefully acknowledged. Similarly, funding from Les Stelmeier and Kathleen McCormick at Nova Chemicals, the Queen Elizabeth II Graduate Scholarship and the Alberta Graduate Student Scholarship is acknowledged. Finally, I would like to thank the Department of Physics and Astronomy, University of Calgary for their funding.

Finally I would like to acknowledge Nenita Lozano and Kerri Miller for their valuable input and moral support. Tony Cade for his technical assistance and Dr. Dieter Buhl for the knowledge gained while visiting his laboratory.

Table of Contents

Abstract ii

Acknowledgments iii

Table of Contents iv

List of Tables vii

List of Figures viii

List of Symbols and Abbreviations xi

Epigraph xii

Chapter 1: Introduction 1

1.2 Isotope Fractionation 3

1.2 Mass Dependent Isotopic Fractionation 4

1.2.1 Equilibrium Fractionation 4

1.2.2 Kinetic Fractionation 5

1.3 Mass Independent Isotope Fractionation 6

1.4 Three Isotope Plot 7

1.5 Iron Geochemistry 8

1.6 Iron Isotope Fractionation 10

1.7 Background of the Sample Obtained to Test the Iron Analytical Technique 16

1.7.1 The Pembina Oil Field, Cardium Formation 17

1.7.2 Lake Vida 19

1.7.3 Nova Chemicals Bioremediation Study 20

Chapter 2: Instrumentation 23

2.1 Mass Bias 23

2.2 Mass Bias Corrections 26

2.3 Resolving Power 29

Chapter 3: Analytical Methods 33

3.1 Mass Spectrometer 33

3.2 Sample Preparation 37

3.3 Sample Measurement on the Mass Spectrometer 42

3.4 Accurate Measurement of Iron Signal Intensities by MC-ICP-MS 49

3.5 Optimal Measurement Position on the Low Mass Shoulder 49

3.6 Intensity Matching 53

3.7 Signal Stability 56

3.8 Preparation of the IRMM-014 Standard 57

3.9 Preparation of the Iron-54 Spike 58

3.10 Clean Room Contamination 62

Chapter 4: Results and Discussion 66

4.1 Precision and Reproducibility 66

4.2 The Cardium Formation 74

4.2.1 Optimal Digestion Conditions for Siderite from the Cardium Formation 74

4.2.2 What is the Source of Increased Iron? 75

4.2.3 Future Investigations 82

4.3 Lake Vida 82

4.3.1 Dissimilatory Iron Reduction 84

4.3.2 Weathering of Existing Iron Minerals 85

4.3.3 Sorption of Iron 86

4.3.4 Future Investigations 86

4.4 Nova Chemicals Bioremediation Results 86

5. Conclusion 91

References 94

Appendix 1 103

List of Tables

Table 1: Certified Iron Isotope Amount Ratios of the IRMM-014 Standard..... 4

Table 2: The resolving power need to optically resolve all isotope of iron from their respective interferences..... 31

Table 3: The cup configuration on the MC-ICP-MS for iron isotope measurements..... 37

Table 4: Natural iron abundances compared to the iron abundances in the double spike 45

Table 5: Results from an intensity matching experiment preformed with varying concentrations of a standard. All measurements were bracketed by a 2 ppm iron standard..... 55

Table 6: Results from an intensity matching experiment preformed where varying concentrations the same ion exchanged sample were measured with respect to a 3 ppm iron standard. 56

Table 7: Natural iron abundances compared to iron abundances in the ^{54}Fe spike 59

Table 8: Comparison between data obtained in the early stages of development to the true iron delta values obtained through research in Germany and in Calgary. 67

Table 9: Comparison of iron isotope data obtained using two mass bias correction techniques, as well as two different laboratories. Samples are from the Cardium formation..... 69

Table 10: Type A uncertainty calculated using the GUM guide for the data in Table 9. Samples with (*) have replicate analyses not shown in Table 9. 71

Table 11: Comparison of nitric acid and hydrochloric acid siderite digestion 75

Table 12: Iron isotope data for Lake Vida brine 83

Table 13: Iron concentration data measured using isotope dilution for the Nova Chemicals bioremediation study. Selected data on iron delta values are also presented. Error in iron concentration is ± 2 %..... 89

List of Figures

Figure 1: A hypothetical three isotope plot for iron. The mass dependent fractionation line is shown (MFL). Red squares show samples with mass dependent fractionation and green triangles are samples where mass independent fractionation has occurred. 9

Figure 2: Iron isotope variations in terrestrial minerals, aqueous environments and the human body (BIF=Banded iron formations). 16

Figure 3: Schematic representation of the mass bias of the MC-ICP-MS which occurs at an interface consisting of two nickel cones (sample and skimmer). There is a buildup of charge at the interface resulting in a preferential transmission of heavy isotopes (Albarède & Beard, 2004). 25

Figure 4: Diagram of the resolving power for the MC-ICP-MS. Species A and B are unresolved and flat topped peaks are obtained. 32

Figure 5: Diagram of the inside components of the MC-ICP-MS. Components relevant to the discussion are labelled. 34

Figure 6: Calculation of the resolving power on March 21 2013 for high resolution on the MC-ICP-MS in Calgary, Alberta. The resolving power is sufficient to resolve all the isotopes of iron from their respective interferences 39

Figure 7: Panel A shows the ion exchange method. Panel B shows an elution curve for the ion exchange (what each mL corresponds to is give in panel A). All measured elements, except copper, elute before iron elution. 41

Figure 8: Data from a sample standard bracketing session on March 21st 2013 is shown. The overall mass bias offset and mass bias drift can be seen. A linear mass bias drift is assumed to calucate the iron delta values for a sample 44

Figure 9: Schematic representation of the algorithm used to reduce the measured double spike results for a sample and obtain the true iron isotope fractionation 47

Figure 10: A typical mass scan for iron measurements. All four isotopes of iron are viewed simultaneously in four faraday cups L2 (^{54}Fe), C (^{56}Fe), H1 (^{57}Fe) and H2 (^{58}Fe). Multiplicative factors (shown at the bottom of the diagram) are applied to signal intensities. Three regions can be defined (A, B and C) based on the ions contributing to the signal intensity..... 51

Figure 11: A mass scan of the low mass shoulder for ^{56}Fe in the standard, dark red line, and the wash, light red line. Iron delta values were calculated for each position using position 6 as the reference. A small range in mass, 0.008 u, produces delta values within expected analytical uncertainty of 0 ‰. Measurement of iron signal intensities should be performed between positions 4 to 9. 52

Figure 12: Magnet instability experience in late 2012 and early 2013. The fluctuations experienced December 2012 were detrimental to iron isotope amount ratio measurements causing significant shifts in iron peak mass position. The set measurement point deviated from optimal positioning when these fluctuations occurred..... 54

Figure 13: Iron ion exchange columns. The column on the left (A) was made from disposable pipettes notice the straight end holding the frit. Column B were manufactured by the machine shop, University of Calgary, notice the tapered end to keep the frit in the column 61

Figure 14: Three isotope plot for iron measurements May 2012. The $\delta(^{56/54}\text{Fe})$ value deviates towards negative values indicating the presence of excess 54 atoms. Error bars are shown for a reasonable value of uncertainty based on literature. Chromium contamination was the suspected source of the increased 54 atoms 64

Figure 15: Picture of the fume hood in Calgary, Alberta. Note the close proximity of the heat lamps and the hot plate. 65

Figure 16: Iron isotope data obtained on March 21st 2013. There is no excess 54 atoms measured in these samples indicating no chromium contamination occurred during sample preparation 73

Figure 17: A three isotope plot for the iron delta values obtained for the siderites, reservoir waters and pipe in the Cardium formation study. Typical error bars are shown in the lower right side of the diagram. 77

Figure 18: Plot of iron delta value verse the inverse in concentration to determine the iron isotopic composition of a potential source if BSR is occurring in the Cardium formation. 81

List of Symbols and Abbreviations

Abbreviations

BIF = Banded iron formation

BSR = Bacterial sulfate reduction

DIR = Dissimilatory iron reduction

DS = Double Spiking

IRMM-014 = Institute for reference materials and measurements: 014

M = Molar

MC-ICP-MS = Multiple collector inductively coupled plasma mass spectrometer

ORNL = Oak Ridge National Laboratory

RBS 50 = Detergent solution

RPM = Revolutions per minute

SSB = Sample standard bracketing

TI-MS = Thermal ionization mass spectrometer

Symbols

α = Equilibrium constant

β or f = Instrumental fractionation factor

δ = Delta value

s = Standard deviation

R = Resolving power

u = unified mass unit

V = Volts

Epigraph

Trust in the Lord with all your heart and lean not on your own understanding; in all your ways submit to Him and He will make your paths straight. Proverbs 3:5-6

The Bible, New International Version (NIV)

Chapter 1: Introduction

Atoms are fundamental building blocks of our universe. Atoms consist of a nucleus containing protons and neutrons which is surrounded by a cloud of electrons. Each element has a different number of protons in its nucleus and atoms with the same number of protons and different number of neutrons are called isotopes. There are four isotopes of iron with 28, 30, 31 and 32 neutrons in the nucleus. All isotopes of an element have the same electronic structure and therefore, similar chemical properties. However, isotopes of an element have different masses and thus react at different rates in chemical reactions and bacterial processes (Chang, 2007). The different reaction rates results in variation in isotope abundances where the ratio between isotopes or the isotopic composition in a system is altered commonly referred to as isotope fractionation.

Interest in stable isotope fractionation has existed since the 1930's and motivated the development of mass spectrometers to measure the isotopic composition of a sample and thus characterize the isotope fractionation. Mass spectrometry has evolved significantly since the early days including improvements to existing mass spectrometers and the development of new mass spectrometers. A large variety of mass spectrometers exist and in general a mass spectrometer consists of four components: an inlet system, an ion source, a mass analyzer and an ion detector (Hoefs, 2010). Early instrumental limitations, including low precision and reproducibility, limited measurements to light elements such as C, N, O and S (Groot, 2009)**.** The range in isotopic fractionation of these elements is large, approximately 9 % for sulfur (Hoefs, 2010), therefore fractionation in samples could still be observed even if measurement uncertainties were high. However, heavier elements such as Cu, Zn, and, Fe have a smaller range

in isotopic variation, about a tenth of a percent and thus their variability in isotopic composition would have been obscured due to instrumental uncertainty.

Interest in measuring precisely these small isotope fractionations has motivated the development of increasingly precise mass spectrometry. Recent advancements in mass spectrometry including improvements to thermal ionization mass spectrometry (TI-MS) and the development of multi-collector inductively coupled plasma mass spectrometry (MC-ICP-MS) have resulted in routine isotopic abundance analyses of heavier elements (Yang, 2009). Both TI-MS and MC-ICP-MS can offer precision as low as 0.001 % which allows small isotopic fractionations to be resolved and accurately measured.

1.1 Objective

The goal of this thesis was to develop an analytical technique to measure iron isotope amount ratios with the highest precision and accuracy possible. High accuracy enables interpretation of the data and high precision data provides confidence in the measured data. The analytical technique consisted of two components: a sample purification step using ion exchange chromatography and measurement of iron isotope amount ratios using a multi-collector inductively coupled plasma mass spectrometer. Once developed, the analytical technique was tested on a variety of samples including mineral, water and biological samples.

The analytical methods will be outlined highlighting the problems overcome during its development. A discussion on the reproducibility of the obtained data will precede the presentation of data used to test the analytical technique. From the obtained data, conclusions will be presented supported by literature.

1.2 Isotope Fractionation

Isotopic fractionation occurs when the isotopes of a given element are separated between two phases of a single system. In general, isotope fractionation is governed by the relative mass difference between the atoms (Hoefs, 2010) but can also be affected by redox state and bonding environment (Johnson et al., 2004a) This leads to large isotopic fractionation for elements such as C, N, and O where the relative mass difference between isotopes is large (i.e. $\Delta M/M \approx 1/12$ for C) and smaller isotopic fractionation for elements such as Fe, Cu, and Mo (i.e. $\Delta M/M \approx 1/56$ for Fe). Isotopic fractionation is expressed as a delta value where the measured isotope amount ratios of a sample are compared to a standard, shown in Equation I.

$$\delta^{56/54}Fe = \left(\frac{n(^{56}Fe)/n(^{54}Fe)_{Sample}}{n(^{56}Fe)/n(^{54}Fe)_{Standard}} - 1 \right) * 1000\ (‰)$$

Equation I

Due to the small extent of isotopic fractionation, a delta value is expressed in per mil (‰), or parts per thousand. Delta values, by convention, use the ratio of the number of heavy isotopes over light isotopes. Therefore, a negative delta value indicates a sample enriched in the light isotopes of a given element, "isotopically light", where as a positive delta value indicates enrichment in the heavier isotopes, "isotopically heavy". Delta values are expressed with respect to a standard which has certified isotope amount ratios and allows for inter-laboratory comparison of data. This standard is generally easily obtainable, homogeneous in composition and readily prepared for analysis (Groot, 2009). For example, iron isotope amount ratios are reported with respect to IRMM-014 and this standard was calibrated by Taylor et al., 1992. The certified isotopic abundances are given in Table 1 (Taylor et al., 1992). The numbers in

parentheses indicate the standard deviation of the measured isotope amount ratios at the two sigma level.

Table 1: Certified Iron Isotope Amount Ratios of the IRMM-014 Standard (Taylor et al., 1992)

Ratio	**Isotope Amount Ratio**
n(^{54}Fe)/n(^{56}Fe)	0.06370(27)
n(^{57}Fe)/n(^{56}Fe)	0.023096(72)
n(^{58}Fe)/n(^{56}Fe)	0.003071(29)

1.2 Mass Dependent Isotopic Fractionation

With a few exceptions, isotope fractionation in terrestrial environments can be characterized as mass dependent. Mass dependent extent of isotope fractionation is governed by the relative mass difference between the isotopes. In systems where mass dependent fractionation occurs, delta values scale proportionally to the mass difference between the isotopes. For example, $\delta(^{56/54}Fe)$ values for iron are approximately twice the measured $\delta(^{57/56}Fe)$ values due to the doubling of the mass difference between isotopes. In general, mass dependent fractionation can be described as either equilibrium or kinetic fractionation (Hoefs, 2010).

1.2.1 Equilibrium Fractionation

Equilibrium isotope fractionation involves the distribution of isotopes between two or more phases of a system which are in equilibrium. Equilibrium fractionation is driven by the difference in vibrational energies between compounds containing different isotopes and can be described by quantum mechanical processes (Johnson et al., 2004a; Urey, 1947). A closed container filled with water contains both the liquid and vapor phases of water. The isotopic fractionation, of oxygen or hydrogen isotopes, between the liquid and vapor phase would be an example of equilibrium isotopic fractionation. There is a constant exchange of both oxygen and

hydrogen isotopes between the two phases of this system and only oxygen isotopes will be discussed further. Both reservoirs possess a distinct isotopic signature; the water enriched in the heavier isotopes of oxygen whereas the vapor is enriched in the light isotopes. The exchange between the two phases is shown in Equation II for oxygen isotopes.

$$H_2{}^{16}O_l + H_2{}^{18}O_v \Leftrightarrow H_2{}^{16}O_l + H_2{}^{18}O_v$$

Equation II

For this system equilibrium, the constant α can be defined at room temperature based on the rate of the reaction of the products and reactants, Equation III. In this situation, α=1.0094 which indicates there is a 0.94 % difference in the isotopic composition between the reactants and products.

$$\alpha = \frac{[H_2{}^{16}O_l][H_2{}^{18}O_v]}{[H_2{}^{16}O_v][H_2{}^{18}O_l]} = 1.0094$$

Equation III

The extent of equilibrium isotopic fractionation between the two phases of a system is dependent on temperature of the system with smaller isotopic fractionations at higher temperatures; the decrease is generally proportional to inverse temperature (Johnson et al., 2004a). Pressure and bond strength can also affect the extent of equilibrium isotope fractionation between the two phases.

1.2.2 Kinetic Fractionation

Kinetic isotope fractionation is characterized by unidirectional or incomplete processes such as evaporation from an open system, precipitation, chemical reactions, or biological processes (Hoefs, 2010). For example, if the lid was removed from the container in the system described above the water vapor would escape into the environment. This would result in the

remaining liquid becoming enriched in the heavier isotopes heavy of oxygen compared to the initial system and the escaped vapor enriched in the lighter isotopes.

Kinetic isotopic fractionation can also be observed in bacterial processes. For example, bacteria can transform solid iron compounds to iron dissolved in water and isotopic fractionation is observed between the two iron reservoirs (Wu et al., 2011). The solid iron compounds become enriched in the heavier isotopes of iron and the aqueous iron enriched in the lighter isotopes of iron as bacterial preferentially use the lighter isotopes of an element due to the lower energy needed to break the bonds in compounds (Aelion et al., 2010).

1.3 Mass Independent Isotope Fractionation

Both the processes described above are mass dependent processes. There are systems where the difference between the delta values do not scale proportional to the mass difference between the isotopes ($2\delta(^{57/56}Fe) \neq \delta(^{56/54}Fe)$). These processes exhibit mass independent isotope fractionation which is less common than mass dependent fractionation and has been observed in meteorites, sediments deposited before the oxidation of the atmosphere and the ozone (Johnson et al., 2004a; Lyons, 2001; Pavlov & Kasting, 2002). For example, magnesium in meteoritic material can exhibit mass independent isotope fractionation. Excess magnesium-26 has been observed in meteorites and is produced by beta-plus decay or electron capture of ^{26}Al. The presence or absence of magnesium excess (isotope anomalies) in meteorites can help constrain the timing between nucleosynthesis and solar system formation because in the absence of magnesium anomalies, the lower limit between nucleosynthesis and solar system formation is approximately 3 Mya (Johnson et al., 2004a; Clayton, 1978). A lower limit is determined based on the half-life of aluminum-26 (0.7 Mya). Magnesium isotope anomalies could also provide evidence of a late injection of nucleosynthetic material into the protostellar cloud.

Another element which demonstrates mass independent fractionation in extraterrestrial materials is calcium. Calcium anomalies manifest on the neutron-rich isotope ^{48}Ca (Birck, 2004) which can only be produced in massive stars by the slow neutron capture or neutron-rich Si-burning. Calcium-48 anomalies could also result from injection of material during supernovae. The presence of calcium anomalies therefore, provides insight into the interstellar conditions prior to solar system formation. Finally, excess ^{60}Ni isotope anomalies in meteorites can arise from the beta-minus decay of ^{60}Fe. However, the presence of these anomalies is highly debated because only small increases in ^{60}Ni are expected, on the order of analytical uncertainties (Dauphas et al., 2008; Bizzaro et al., 2007). If present, these anomalies can provide insight into conditions during the early stages of solar system formation because if there are ^{60}Ni anomalies this would suggest that our solar system formed alongside a massive star which, at the time of its death, injected ^{60}Fe into the protoplanetary disk approximately one million years after solar system formation (Bizzaro et al., 2007). If there are no ^{60}Ni anomalies, this suggests that ^{60}Fe was injected into the molecular cloud that formed our solar system prior to its collapse. Type II supernovae could produce the expected conditions and could have been responsible for the initial collapse of the molecular cloud which formed our solar system (Dauphas et al., 2008).

1.4 Three Isotope Plot

A useful tool in characterizing mass dependent and mass independent isotope fractionation is a three isotope plot. In a three isotope plot, the mass dependent fractionation line (MFL) will have a slope that corresponds to the approximate mass difference between the plotted isotopes. For example, a $\delta(^{56/54}Fe)$ vs. $\delta(^{57/54}Fe)$ graph would have mass dependent fractionation slope of approximately 1.5 due to the mass difference between the isotope amount ratios (a $\delta(^{57/56}Fe)$ vs. $\delta(^{56/54}Fe)$ graph would have a slope of 2) . If mass independent processes have

occurred then, deviation from the MFL will be measured, see Figure 1. Figure 1 shows hypothetical situation with $\delta(^{56/54}Fe)$ vs. $\delta(^{57/54}Fe)$ values. In this graph both mass dependent fractionation (red squares) and mass independent fractionation (green triangles) are shown. Three isotope plots can also be useful in determining problems with the data. If mass dependent fractionation is expected and deviation from the mass dependent fractionation line has occurred, either there is contamination from an external source on one of the plotted isotopes or issues arose during sample measurement possibly due to low signal intensities or instrumental problems. Some situations that could be experience in this these are summarized (relevant discussions in Methods). If there was chromium or single spike (^{54}Fe) contamination both the $\delta(^{56/54}Fe)$ and $\delta(^{57/54}Fe)$ values would decrease. If there was a contribution from $^{40}Ar^{16}O^{+}$ tailing then the $\delta(^{56/54}Fe)$ would increase. Finally if there was contamination from the double spike (^{57}Fe and ^{58}Fe), the $\delta(^{57/54}Fe)$ value would increase.

1.5 Iron Geochemistry

Isotopic abundance analyses can provide unique insight into a variety of systems and the element of interest in this thesis is iron. Iron is the 26th element on the periodic table with four stable isotopes ^{54}Fe, ^{56}Fe, ^{57}Fe and ^{58}Fe. The abundances of these isotopes are 5.845 %, 91.754 %, 2.119 % and 0.282 % respectively (Dauphas & Rouxel, 2006). Iron was not created in the primordial big bang but through successive stellar evolution. Due to its large binding energy per nucleon (8.8 MeV for ^{56}Fe) (Chang, 2007) iron is the end point of stellar nucleosynthesis and ^{54}Fe, ^{56}Fe and ^{57}Fe can be formed through explosive silicon burning in pre-supernovae stars (Woosley & Heger, 2002). These three isotopes are also formed through rapid neutron capture in supernovae remnants. The neutron rich isotope, ^{58}Fe, is formed through slow neutron capture

during the helium burning phase of pre-supernovae red giants and in accreting white dwarf stars (Dauphas & Rouxel, 2006; Woosley & Heger, 2002).

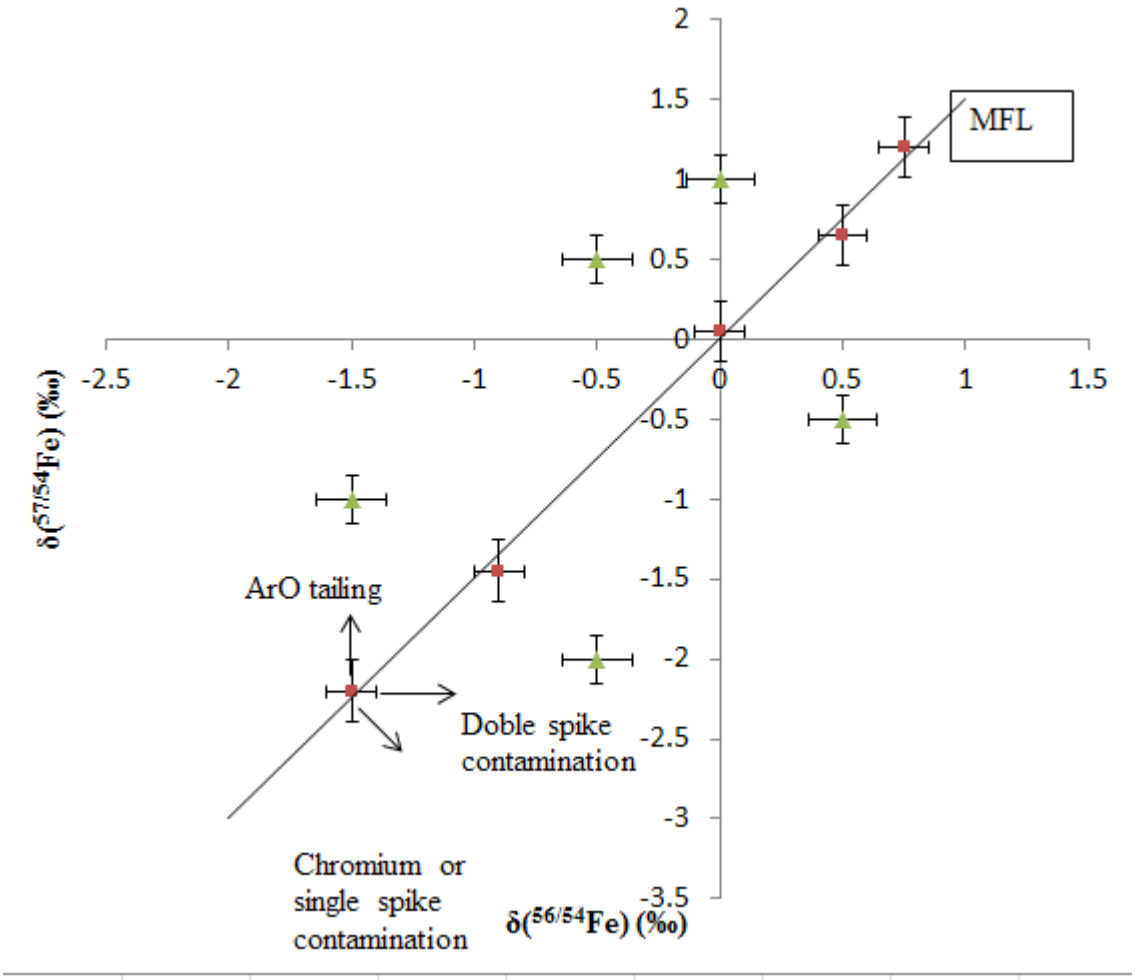

Figure 1: A hypothetical three isotope plot for iron. The mass dependent fractionation line is shown (MFL). Red squares show samples with mass dependent fractionation and green triangles are samples where mass independent fractionation has occurred.

On Earth, iron is the fourth most abundant element and makes up about 5 % (by weight) of the Earth's crust (Frey & Reed, 2012). Iron can exist in a variety of oxidation states the most common of which are Fe (II) (Fe^{2+}, ferrous) and Fe (III) (Fe^{3+}, ferric). Iron changes its oxidation state through oxidation-reduction (redox) reactions and bacterial processes (Johnson et al.,

2004b; Newman & Nealson, 2004; Johnson & Beard, 2005). The oxidation state of iron is highly dependent on the surrounding environment with ferric iron being favored in oxic environments and ferrous iron in anoxic environments. One important distinction between the two primary oxidation states of iron is their solubility in water; ferrous iron is highly soluble and ferric iron is insoluble. Ferric iron then precipitates and can from ferric iron minerals. The iron isotopic fractionation observed between the ferrous and ferric states of iron can be as high as 0.15 % per atomic mass unit with the ferric form being enriched in the heavy isotopes of iron (Johnson et al., 2008).

Early in Earth's history, anoxic conditions prevailed and ferrous iron was more abundant than ferric iron. As microorganisms evolved, they utilized the soluble ferrous iron. However, as an oxic atmosphere developed the ferric form of iron became more abundant. The ferric insoluble form of iron was harder for the microorganisms to obtain resulting in a limited amount of bioavailable iron causing microorganisms to develop specialized pathways for iron absorption. Even today, aerobic organisms existing in oxygen rich conditions, humans for example, have difficulty acquiring the iron needed to maintain necessary iron stores. This has forced humans to evolve into a closed system where little iron is lost from the body (Walczyk & von Blanckenburg, 2005).

1.6 Iron Isotope Fractionation

Recent developments in mass spectrometry have opened the door for iron isotope abundance analyses and iron fractionation has been measured in numerous systems and environments (Bizzaro et al., 2007; Hotz et al., 2011; Johnson et al., 2008). To compare results from different laboratories, a common reference material is needed. Two standards exist for iron isotope measurements, IRMM-014 and igneous rocks. Igneous rocks, or "bulk earth", was found

to have a homogeneous iron isotopic composition and has a $\delta(^{56/54}Fe) = 0.09(5)$ ‰ with respect to the IRMM-014 (Johnson et al., 2004b). The homogenous iron isotopic composition of bulk Earth was determined through measurement of igneous and sedimentary rocks in both the continental and oceanic crusts. The iron isotopic composition of bulk earth suggests that, during magma formation, any pre-existing isotopic fractionation was homogenized (Johnson & Beard, 2005). Weathering of surface rocks can remove iron from the mineral phase and place it into solution as Fe^{2+}. This process does not significantly alter the iron isotopic composition of the mineral iron as relatively low amounts of iron are removed during weathering compared to the total iron content of the minerals. Processes such as transport and deposition of iron also do no significantly affect the measured $\delta(^{56/54}Fe)$ values of surface rocks (Johnson et al., 2008).

In addition to weathering, there are three other processes in low temperature fluids that result in a distinct iron concentration/iron isotopic composition relationship (Johnson et al., 2008): bacterial sulfate reduction (BSR), dissimilatory iron reduction (DIR) and iron oxidation. Two of these pathways are mediated by bacteria: dissimilatory iron reduction (DIR) and bacterial sulfate reduction (BSR). The BSR reaction is shown in Equation IV and occurs in reducing or anoxic conditions. In marine environments BSR is the main pathway for organic matter degradation (Johnson et al., 2008).

$$SO_4^{2-} + 2CH_2O \rightarrow 2HCO_3^- + H_2S$$

Equation IV

The sulfate is used as an electron accepter during the oxidation of organic matter (CH_2O). The hydrogen sulfide (H_2S) produced dissociates and becomes HS^- which reacts with aqueous Fe^{2+} ions forming reduced iron-sulfur compounds. Bacterial sulfate reduction is therefore critical in the formation of compounds including pyrite (FeS_2), smythite (Fe_9S_{11}) and greigite (Fe_2S_4). If

the initial isotopic signature of aqueous iron ranged between $\delta(^{56/54}Fe)$ = -1 to 0 ‰, after BSR has occurred the iron isotopic signature of the aqueous iron would be $\delta(^{56/54}Fe)$ = 0 to 0.5 ‰. The isotopic composition of the remaining aqueous iron depends on both the initial isotopic composition of the water and the precipitated minerals. Typical aqueous iron concentrations in aqueous environments where BSR has occurred are around 1 ppm (Johnson & Beard, 2005; Johnson et al., 2008).

The second microbial mediated iron fractionation mechanism, DIR, is given in Equation V where ferric hydroxide is reduced in anoxic conditions and organic matter is oxidized. Dissimilatory iron reduction is thought to have developed early in the Earth's history and to be one of the oldest forms of respiration (Vargas et al., 1998). DIR contributes to the iron cycling in marine environments (Johnson et al., 2008; Percak-Dennett et al., 2011) and in environments where high rates of BSR are occurring DIR is inhibited.

$$4Fe(OH)_3 + CH_2O + 8H^+ \rightarrow 4Fe^{2+}_{aq} + CO_2 + 11H_2O$$

Equation V

Dissimilatory iron reduction is responsible for the creation of aqueous Fe^{2+} and ferrous iron minerals such as magnetite and siderite. The aqueous iron produced during DIR has low $\delta(^{56/54}Fe)$ values (-1.0 to -2.5 ‰) and high iron concentrations are observed in aquatic environments where dissimilatory iron reduction is occurring, 1-50 ppm.

Weathering of iron, as mentioned, does not significantly affect the $\delta(^{56/54}Fe)$ value of bulk Earth and during weathering the ferrous iron is typically removed from the surface environments and placed into solution. The weathered ferrous iron has $\delta(^{56/54}Fe)$ values between -1 and 0 ‰. Iron concentrations in weathered, or ravine, environments are generally low, 1 ppb to 10 ppm (Johnson et al., 2008).

Finally, iron oxidation which is given in Equation VI a significant contributor to iron fractionation observed in aqueous environments. During oxidation, a change in $\delta(^{56/54}Fe)$ between the reduced and oxidized iron of up to 3 ‰ can be observed. The oxidized iron is enriched in the heavy isotope of iron and fractionation during oxidation of iron follows the Rayleigh fractionation law an empirical law relating the isotopic composition of the product and reactant based on the amount of produced used up by a reaction (Johnson et al., 2008).

$$4Fe^{2+} + O_2 + 4H^+ \rightarrow 4Fe^{3+} + 2H_2$$

Equation VI

Since oxidized iron is insoluble, it then precipitates to form ferric compounds such as ferric hydroxide, hematite and goethite. The iron fractionation observed between the aqueous iron and the iron compound is compound specific with $\delta(^{56/54}Fe(II)_{aq})$-$\delta(^{56/54}Fe_{hematite})$ = -3.16 ‰ ($\Delta^{56/54}Fe_{Fe(II)aq\text{-}hematite}$= -3.16) and $\Delta(^{56/54}Fe(II)_{aq\text{-}goethite})$ = -1.05 ‰ (Wu et al., 2011).

The iron isotopic composition of precipitated minerals is highly dependent on the iron isotopic composition of the aqueous iron from which they formed. Using these principles, the study of banded iron formations (BIF), regions of high iron precipitation, can provide insight into early conditions on Earth. The timing of the oxidation of the atmosphere as well as the redox state of the ocean can be inferred from the iron isotopic composition of iron minerals in banded iron formations (Rouxel et al., 2005).

Iron isotopic fractionation has also been studied in hydrothermal fluids. Small, yet significant fractionation was observed in hydrothermal waters compared to bulk Earth, -0.3 to -0.77‰ (Sharma, et al., 2001). They proposed that the iron isotopic fractionation was non-biological and could have derived from leaching of deep sea basalts, during fluid transport or differences in the iron isotope composition of the rocks from which the fluid derived.

Iron fractionation has also been observed in Podzols, the typical soils of the coniferous or boreal forests. Podzols form through a process called podzolization, where there is a downward migration of organic material along with Al and Fe. This results in an increased concentration of metals in the deeper soils (Wiederhold et al., 2007). Before podzolization, the soils show a uniform depth profile of iron isotopic composition and concentration. After podzolization, a translocation of the light isotopes of iron was observed with $\Delta(^{56/54}Fe) \approx 0.6$ ‰ between two regions in a Podzol. The iron concentration was also non-uniformly distributed throughout the soil. This provides evidence of iron fractionation during soil formation (Wiederhold et al., 2007).

Our understanding of iron fractionation mechanisms in terrestrial systems has advanced significantly over the past few decades owing in part to the development of MC-ICP-MS (Walczyk & von Blanckenburg, 2005). Recently, interest in the iron isotopic signature of living organisms, such as the human body, has emerged.

Iron in blood is enriched in the light isotopes of iron compared to the bulk earth (Hotz et al., 2011; Walczyk & von Blanckenburg, 2002) in both humans and pigs. The iron isotopic composition of blood remains constant throughout a year due to the relatively low iron losses, 1 mg per day, compared to the total body iron, 3 g (Beard et al., 1996; Ohno et al., 2004). Iron is absorbed by the body in the intestinal tract and iron absorption was studied in the intestine. Significant variations in $\delta(^{56/54}Fe)$, ranging from -0.97 ‰ to -1.67 ‰, were measured in different sections of a pig intestine (Hotz et al., 2011). Hotz et al. (2011) suggested that differences in iron uptake efficiency throughout the intestine could be responsible for the observed variation; they also noted that the light isotopes of iron were preferentially absorbed by the body leading to blood enriched in the light isotopes of iron. Organ and tissue samples were also analyzed for iron isotope amount ratios. The liver and spleen were found to be enriched in the heavy isotope of

iron compared to the blood and tissues/muscles have similar isotopic composition to the blood. There is an inhomogeneity in the iron isotopic composition of the human body however; the reason behind this inhomogeneity is not yet understood.

There are two iron metalloproteins, transferrin and ferritin. Iron binds to transferrin and is transported throughout the body. Ferritin binds iron and stores it in a non-toxic form for storage and future use by the body (Beard et al., 1996). Previous studies have found an isotopic enrichment in the heavy isotopes of iron in the liver compared to blood. Ferritin is the primary iron species in the liver (Hotz et al., 2011). Iron bound to ferritin is oxidized before storage therefore the ferritin may be enriched in the heavy isotopes of iron compared to the blood (Walczyk & von Blanckenburg, 2005). The isotopic composition of the two metalloproteins, transferrin and ferritin, has yet to be studied. However, previous studies suggest that the isotopic composition of these proteins could provide insight into iron cycling in the body.

Figure 2 shows the variation in iron isotopic composition for terrestrial systems including aqueous environments, minerals and in the human body (Dauphas & Rouxel, 2006; Dideriksen et al., 2006; Johnson et al., 2004b; Walczyk & von Blanckenburg, 2002; Rouxel & Auro, 2010).

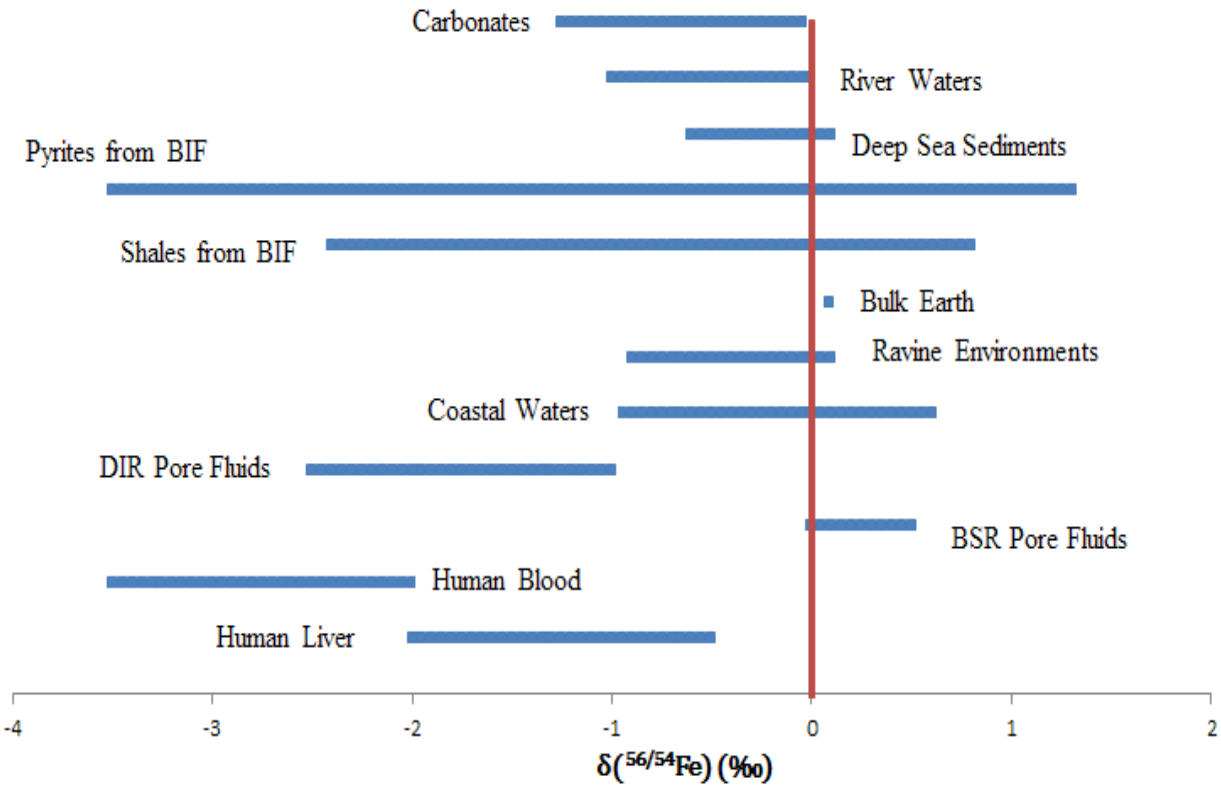

Figure 2: Iron isotope variations in terrestrial minerals, aqueous environments and the human body (BIF=Banded iron formations).

1.7 Background of the Sample Obtained to Test the Iron Analytical Technique

In order to develop a reliable analytical technique, samples from a variety of environments were gathered: the Cardium Formation, Lake Vida and Nova Chemicals. The Cardium Formation samples represent a source identification study where iron minerals, waters and production piping were analyzed. High salinity brine samples were obtained from Lake Vida. From Nova Chemicals, biological growth medium were obtained. These samples can be used to demonstrate the robust nature of the iron analytical technique and under which circumstances careful preparation of the samples is required.

1.7.1 The Pembina Oil Field, Cardium Formation

The Pembina Oil Field is situated in Northern Alberta near the town of Drayton Valley. The Pembina Oil field is approximately 4000 square kilometers, one of Canada's largest oil fields (King, 1997). Oil extraction from this site started in 1953 and this oil field has historically been one of Canada's largest producers with peak oil production of 25,000 m^3 of oil produced per day in the 1970's. Today production has decreased as the oil reserves are being depleted, 10,000 m^3 of oil in recent years (Dashtgard et al., 2008). Oil is extracted from the Cardium formation with is a three tiered sandstone formation that dates back to the Cretaceous period.

All three layers of the formation consist of fine grained sandstone. The upper sandstone layer is 0 to 4 m thick and is separated from the middle sandstone (0.3 to 6.5 m thick) layer by shale and interbedded sandstone (0.1 to 4 m thick). The middle sandstone layer is again separated from the lower sandstone layer (0.5 to 3.5 m thick) by shale (3.5 to 8 m thick) (Dashtgard et al., 2008). The formation contains unusually large siderite ($FeCO_3$) nodules (personal communication M. Nightingale). Oil production occurs primarily in the upper and middle sandstone layers.

Elemental analysis was completed on the sandstone layers, shale and siderite nodules present in the formation (Nightingale, 2010). The sandstone is primarily silicon (~92 %) with small amounts of other elements. The shale is primarily silicon (~65 %), aluminum (~13 %) and iron (~5 %). Siderite nodules are primarily iron (~46 %) and carbonate carbon (~32 %).

Oil is initially extracted from the formation using a production well which relies on the pressure difference between the oil and the base of the well to extract the oil. This pressure difference drives the oil up a production well, this is primary oil extraction. Once the pressure difference decreases, secondary production methods are needed. Secondary production methods

use injection wells and inject water into the formation forcing the oil from an injection well towards the production well. Secondary oil production at the Cardium formation started in 1960 and recently tertiary techniques including CO_2 injection have been employed in this formation. The water injected into the formation was sourced from the Paskapoo aquifer and the North Saskatchewan River (Nightingale, 2010).

As mentioned, CO_2 injection has also recently used to extract oil from the Cardium formation. For tertiary oil recovery, a variety of gasses can be used however; carbon dioxide gas was chosen to test the feasibility of carbon capture (Johnson et al., 2009). When the injected CO_2 contacts water it can form hydrogen carbonate, Equation VII.

$$CO_2 + H_2O \leftrightarrow H_2CO_3$$

Equation VII

The hydrogen carbonate then interacts with the minerals present in the formation, specifically calcium carbonate and siderite, Equation VIII and Equation IX.

$$CaCO_3 + H_2CO_3 \leftrightarrow Ca^{2+} + 2HCO_3^-$$

Equation VIII

$$FeCO_3 + H_2CO_3 \leftrightarrow Fe^{2+} + 2HCO_3^-$$

Equation IX

CO_2 injection can also cause acidification of the reservoir water enabling acid leaching of the iron pipes used in the production and injection wells, Equation X.

$$Fe_{Metal} + H_2CO_3 \leftrightarrow {Fe^{2+}}_{aq} + 2HCO_3^- + H_2O$$

Equation X

After CO_2 injection commenced, increased iron concentrations were measured in the reservoir waters sourced from injection wells used during secondary oil extraction (Nightingale, 2010). Reservoir water sampled after CO_2 injection, ground siderite nodules and a piece of

production pipe were obtained. Iron isotopic analyses on these samples will be used to aid in the determination of the source of increased iron in the reservoir water.

1.7.2 Lake Vida

Lake Vida is located in an Eastern Antarctic dessert in the Victoria Valley (77°23'S 161°56'E). Lake Vida is one of the largest lakes in the area encompassing 6.8 km^2 (Doran et al., 2003). Lake Vida has the thickest ice layer of a sub-aerial lake with approximately 19 m of ice cover. Under the ice is a pocket of slightly acidic (pH=6.2) liquid water or brine at -13.4°C (Murray et al., 2012). This brine remains liquid because of its high salinity, approximately 7 times the salinity of sea water (Doran et al., 2003).

Currently, Lake Vida is an ice sealed lake which implies the lake is covered by a layer of ice year-round so that the brine does not interact with the surrounding environment. There is also no outflow of water from the lake. Carbon-14 isotope analyses of organic matter in the ice cover suggest that the lake has been isolated for approximately 2800 years (Doran et al., 2003). Elemental and isotopic analyses of Lake Vida ice and brine have been completed in recent years to help probe and understand the conditions of the lake and any processes that may be occurring in the brine, for example bacterial activity. The presence of microbes in both the ice and brine has been well documented despite the extreme conditions present (Mondino et al., 2009; Murray et al., 2012).

Brine samples, ice cores and mineral samples were collected from the lake in 2010 (Murray et al., 2012). Extensive elemental analyses as well as selected isotopic analyses have been completed on the brine. Isotopic analyses of dissolved inorganic carbon, sulfate, and nitrogen compounds (NO_3^-, NH_4^+ and N_2) all suggest inorganic origins of these compounds implying no microbial activity is occurring in the brine. Lake Vida brine is supersaturated in

nitrous oxide and has high dissolved iron content. These conditions have been suggested to result from abiotic brine-rock interactions (Murray et al., 2012).

All evidence currently suggests that no active microbial processes are occurring in the brine. However, studies looking at possible activity and DNA of the microbes found at the site have been completed (Mondino et al., 2009; Murray et al., 2012). Mondino et al. (2009) melted the ice from Lake Vida and studied the conditions when the microbes became active. They found that at -8 °C one strain of bacteria grew suggesting than conditions at Lake Vida may be too cold for microbes present in the brine to be active. However, conditions in the brine do not exclude the possibility of microbial growth (Doran et al., 2003).

Because of the unique environment Lake Vida processes, it has been suggested as an analog for Jupiter's moon Europa. Understanding the conditions in Lake Vida and the potential for microbial growth, can provide insight into the cold, dark conditions expected in extraterrestrial environments. To further investigate the conditions of the Lake, six brine samples were received, three filtered (0.2 μm) and three unfiltered, from the 2010 sampling session. The high iron concentration of the brine (13 ppm) is unique and iron isotopic analyses may provide insight into processes that may be occurring in the brine.

1.7.3 Nova Chemicals Bioremediation Study

Hydrocarbons, such as gasoline, are used frequently by consumers and require transport from their production source to the consumer. Occasionally, spills occur and large amounts of hydrocarbons enter the surrounding environment. These hydrocarbons can negatively impact both human and environmental health. Therefore, the quick and complete removal of these compounds from the environment is of vital importance (Beckett & Huntley, 1998). This has led to the development of numerous bioremediation techniques.

One type of bacteria, dissimilatory iron-reducing bacteria, can provide a unique method of hydrocarbon bioremediation. These bacteria simultaneously oxidize organic material and reduce iron in low oxygen environments such as soils, via Equation V above. The oxidized hydrocarbons are converted into carbon dioxide which can then escape from the soils. For this process to occur, reducing conditions are needed as well as a supply of mineral iron, any ferric iron compound would suffice. Successful bioremediation of a site is highly dependent on the environmental conditions such as the availability of iron, the metabolic activity of the bacteria, and the type dissimilatory iron-reducing bacteria used (Boopathy, 2000).

Large iron isotope fractionations are expected between the mineral form of iron and the aqueous ferrous iron, upwards of 2 ‰ with the aqueous iron depleted in the heavier isotopes of iron compared to the mineral form (Crosby et al., 2007). Therefore, Nova Chemicals would like to use iron isotope analyses to determine how effectively a cultured bacteria can oxidize organic matter and if complete removal of organic matter can be accomplished. Initially, a laboratory experiment was performed at Nova Chemicals with the goal of performing a similar field experiment in the future.

The experiment was performed in an anoxic chamber and ferric oxyhydroxide was used as the iron source. Bacteria were cultured from a site in Alberta where Nova Chemicals hopes to apply this technique in the future. Bacteria, in a growth medium, were added to the chamber and the experiment was allowed to progress. Samples were collected from the growth chamber and collection occurred every three days for 24 days and three replicates were obtained each collection session. Samples were kept under anoxic conditions before sub sampling occurred at the University of Calgary to prevent the oxidation of iron. A small aliquot, approximately 5 mL,

of the growth medium containing the aqueous iron was removed from each sample for iron concentration and isotopic analyses.

As the experiment progressed, the measured isotopic composition of the aqueous iron should trend towards the isotopic composition of the ferric oxyhydroxide based on mass balance considerations. Since the experiment is performed in a closed system a relationship between the $\delta(^{56/54}Fe)$ and iron concentration initial solution (i), reacted aqueous (a) and reacted ferric oxyhydroxide (f) can be obtained and is shown in Equation XI. When c_f approaches zero, $\delta(^{56/54}Fe)_a$ trends towards the initial isotopic composition of the ferric oxyhydroxide.

$$c_i\delta(^{56/54}Fe)_i = c_a\delta(^{56/54}Fe)_a + c_f\delta(^{56/54}Fe)_f$$

Equation XI

There are two scenarios where the $\delta(^{56/54}Fe)_a$ value would stop changing in time. First, if the reacted ferric oxyhydroxide is depleted. This would cause the aqueous iron to possess the isotopic composition of the initial ferric oxyhydroxide due to mass balance considerations. Secondly, the hydrocarbons could be depleted indicating successful bioremediation. In this case the isotopic composition of the aqueous iron remains constant over time but is not necessarily identical to the initial ferric oxyhydroxide value. Iron isotopic analyses of the growth medium can then provide insight into the bioremediation conditions.

Chapter 2: Instrumentation

This chapter will discuss relevant analytical considerations for iron isotope amount ratio measurements. Two mass spectrometers methodologies will be discussed briefly including the mass spectrometer of interest to this thesis, the MC-ICP-MS. Sample measurements on the MC-ICP-MS suffer from a mass bias where the measured isotope amount ratios of a sample differ from their true values. The mass bias of the MC-ICP-MS will be presented and various correction techniques will be discussed. Finally, conventional definitions of resolution cannot be applied to medium and high resolution measurements on the MC-ICP-MS as interferences are not optically resolved completely from iron. A new definition, the resolving power will be discussed.

2.1 Mass Bias

Iron isotopic fractionation can provide insight into the oxidation of the atmosphere, the source of iron in a system or the transport mechanisms for iron in the human body. The measured range of iron isotope fractionation $\delta(^{56/54}Fe) \approx -2.5$ ‰ to 1.5 ‰ represents approximately a 4 ‰ difference (Johnson et al., 2008). Therefore, precise measurement techniques are required to resolve the small extent of iron fractionation and accuracy is required to infer sources of iron fractionation. Two types of mass spectrometers are generally used to measure iron isotope amount ratios in a sample: thermal ionization mass spectrometry (TI-MS) and multi-collector inductively coupled mass spectrometry (MC-ICP-MS). TI-MS was the primary measurement technique for iron isotope amount ratios until the development of MC-ICP-MS in the early 2000's (Yang, 2009). The TI-MS ionizes a prepared sample, which has been deposited on a rhenium filament. Deposition of the sample onto a filament and heating of the filament are time consuming processes. Also, achieving optimal ionization of iron is difficult due to the high first

ionization potential of iron leading to poor ionization efficiency. Therefore, careful optimization of analytical parameters such as filament heating time and sample deposition on the filament is required (Johnson & Beard, 1999). In comparison, samples can be introduced into the MC-ICP-MS in aqueous form simplifying sample preparation. Samples are ionized by a high temperature inductively-coupled plasma that efficiently ionizes iron (Yang, 2009). Shorter analysis times are also achieved due to the elimination of filament heating and shorter sample measurement times allowing for higher sample throughput.

Isotopic composition measurements on both the TI-MS and MC-ICP-MS are affected by a mass bias where the measured isotope amount ratios differ from the true isotope amount ratios (Yang, 2009). The mass bias on TI-MS arises during filament heating where the lighter isotopes are preferentially evaporated and ionized (Albarède & Beard, 2004). Therefore, the mass bias on the TI-MS is time dependent and either internal normalization or double spiking is used to correct the isotope amount ratios (double spike discussed below and in the Methods section).

The mass bias of the TI-MS may be time dependent but it is relatively small compared to the mass bias of the MC-ICP-MS by about a factor of 10. The mass bias on the MC-ICP-MS is approximately 3 %/u, compared to approximately 0.2 %/u for TI-MS. For example, a $^{56}Fe/^{54}Fe$ isotope amount ratio for IRMM-014 of approximately 16.8 would be measured by the MC-ICP-MS when the true ratio is 15.698. The source of the mass bias on the MC-ICP-MS is thought to result from the so called space charge effect, which occurs at a sample interface (Albarède & Beard, 2004) (see Methods section for a description of the mass spectrometer). The sample interface consists of two nickel cones, the sample and skimmer cone, (Figure 3) positioned after the inductively coupled plasma. As positive ions are transferred through the cones, there is a buildup of positive charge

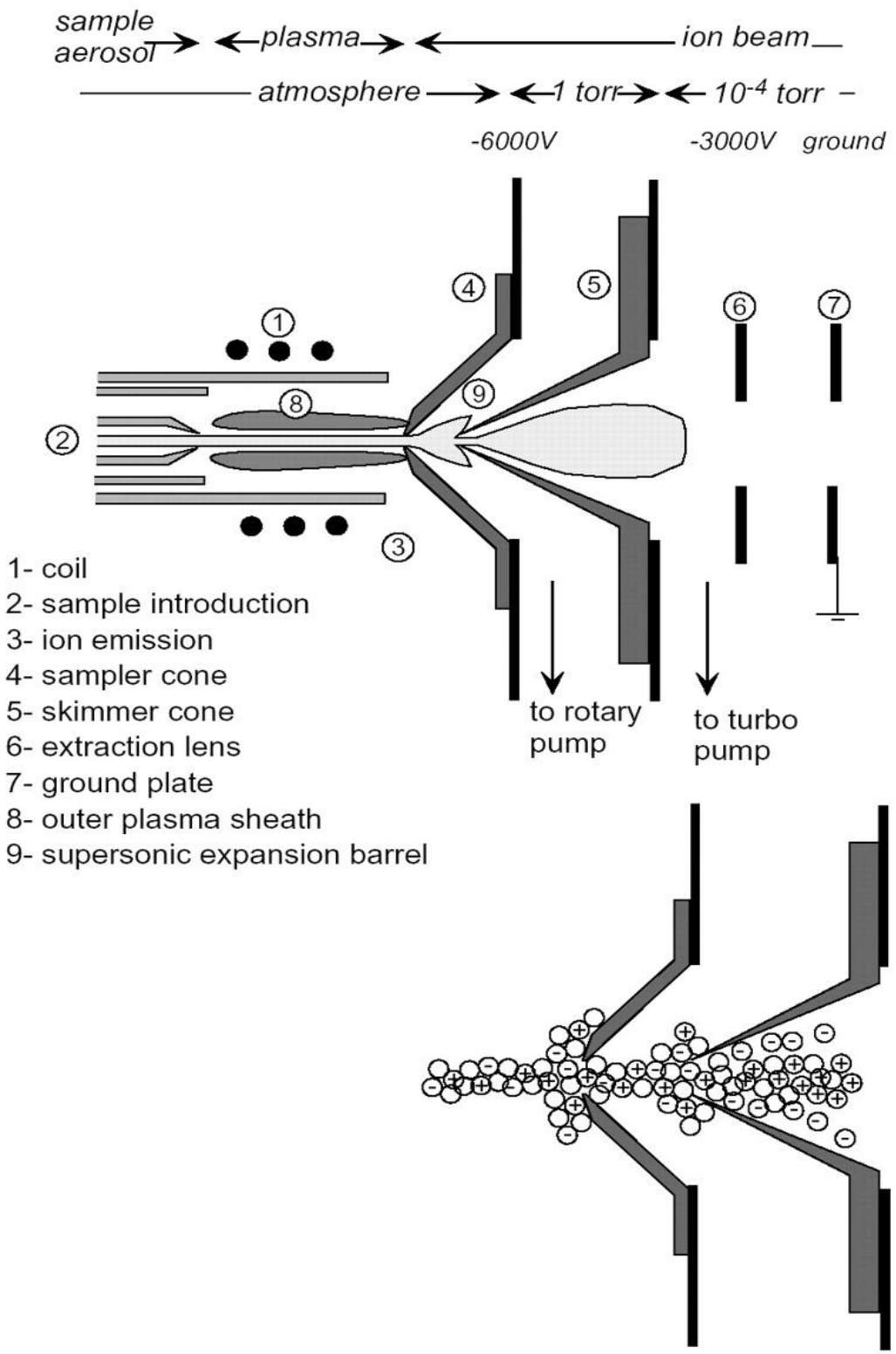

Figure 3: Schematic representation of the mass bias of the MC-ICP-MS which occurs at an interface consisting of two nickel cones (sample and skimmer). There is a buildup of charge at the interface resulting in a preferential transmission of heavy isotopes (Albarède & Beard, 2004).

in the space between the cones. The accumulated charge then affects the ion beam causing ions to be scattered away from the central beam. The scattered ions do not enter the orifice of the skimmer cone and thus are not transmitted to the inside components of the mass spectrometer. Lighter ions, due to their lower mass and momentum, are preferentially scattered (Heumann et al., 1998).

Therefore, the ion beam exiting the skimmer cone is relatively enriched in the heavier isotopes than the initial ion beam. The space charge effect makes the largest contribution to the mass bias however; there are other factors such argon gas flows in the torch and the potential differences in the lens system that can also affect the mass bias (Heumann et al., 1998).

2.2 Mass Bias Corrections

The mass bias of the MC-ICP-MS is large, approximately 3 %/u. However, it is relatively time independent with variations as small as <1 ‰/u per day and <0.01 ‰/u in 30 minutes (Weyer & Schwieters, 2003). In order to obtain accurate and precise iron isotope amount ratios the mass bias of the mass spectrometer needs to be corrected for. Three techniques have been developed to correct for the mass bias on both TI-MS and MC-ICP-MS: internal normalization, double spike (DS) and sample standard bracketing (SSB). All three techniques will be discussed briefly as they apply to mass bias corrections on the MC-ICP-MS. The double spike and sample standard bracketing were used in this thesis to correct for the mass bias on the MC-ICP-MS.

All three mass bias correction techniques require the correct characterization of the mass bias. The mass bias of the MC-ICP-MS has been modeled successfully using the exponential fractionation law given in Equation XII (Maréchal et al., 1999).

$$R_M = R_T \left(\frac{m_1}{m_2}\right)^f$$

Equation XII

Where R_M is a measured isotope amount ratio, for example $n(^{56}Fe)/n(^{54}Fe)$, R_T is the true isotope amount ratio, f is a fractionation factor and m_1 and m_2 are the masses of the measured isotopes, ^{56}Fe and ^{54}Fe. To quantify the mass bias, f needs to be determined.

When using sample standard bracketing to correct for the mass bias of the mass spectrometer the measurement of a sample is bracketed by measurements of a standard of known isotopic composition immediately before and after the sample. An average fractionation factor, f, can be determined for the standards and then used to find the R_T of the sample. Alternatively, an average of the measured isotope amount ratios for the standard can be used to calculate a delta value for the sample based on Equation I. Bracketing must occur immediately before and after the sample to reduce error in the data caused by any drift in mass bias. The SSB mass bias correction assumes a linear mass bias drift as well as identical sample and standard matrixes, or the elements in a sample. Matrix effects arise from the presence of elements other than the element of interest in the sample, for example Cu in a Fe measurement. These elements affect the mass bias of the MC-ICP-MS altering the transmission of sample ions into the mass spectrometer (Yang, 2009). Therefore, concentrations of matrix elements need to be minimized to obtain an identical mass bias between samples and standards ensuring precise isotope ratios. Matrix effects can significantly alter the measured isotope amount ratios especially when the concentration of matrix components increases (Dauphas et al., 2009). Dauphas et al. (2009) looked at the effect varying concentrations of numerous elements in a sample, including Ni, on the measured $\delta(^{56/54}Fe)$ value. They found that, for matrix concentrations below approximately 10 ppm, there was no significant change in the measured $\delta(^{56/54}Fe)$ value. However, as the concentration of matrix elements increased there was a noticeable effect on the $\delta(^{56/54}Fe)$ value. Therefore, chemical purification of samples is necessary to obtain precise and accurate isotope amount

ratios when applying the standard sample bracketing technique. The importance of chemical purification can also be seen when considering the nature of the space charge effect. An increase in matrix elements in a sample will affect the transmission of the sample ions into the mass spectrometer changing the mass bias of a sample. The assumption of identical mass bias between bracketing standards and the sample is then invalid and error is introduced into the delta value. When all these factors are considered, the reproducibility of the $\delta(^{56/54}Fe)$ value can be as low as 0.049 ‰ for SSB (2s) (Schoenberg & von Blanckenburg, 2005).

To apply double spiking, a solution artificially-enriched in two isotopes of the desired element (a double spike) is needed. The concentration and isotopic composition of the spike are known and a small aliquot is added to the sample prior to sample preparation and analysis. Adding the double spike prior to sample preparation allows one to correct for any isotopic fractionation encountered during sample preparation as well as to correct for the mass bias of the mass spectrometer (Dideriksen et al., 2006). Numerous data reduction techniques have been developed to obtain the true isotopic ratios of a sample from double spike data (Siebert et al., 2001; Yang et al., 2009; Krabbenhoft et al., 2009). The data reduction technique of Krabbenhoft et al. 2009 was used in this thesis (see Methods for a detailed description). To successfully apply double spiking, careful and time consuming calibration of the spike is required and only mass dependent fractionation can be resolved by a single double spike run due to assumptions made during data reduction (Yang, 2009). When mass independent effects are expected, a spiked and unspiked run are required. The advantage of double spiking is that the mass bias correction is applied directly to the sample eliminating the need for careful matching of sample and standard matrix. The precision reported for iron double spike data is $\delta(^{56/54}Fe)$ value can be as low as 0.04 ‰ (2s) (Millet et al., 2012).

Finally, elemental doping can be used to correct for the mass bias of the mass spectrometer. For elemental doping, an elemental spike is added to the sample after chemical purification and prior to analysis. This elemental spike is of similar mass to the measured element and the isotopic composition of the elemental spike is known. For example, Cu and Ni spikes can be used for Fe measurements. However, it has been well documented that the mass bias produced by the MC-ICP-MS is element dependant (Meija et al.,2009) therefore sample measurements must be bracketed by standard measurements spiked with the same element similar to sample standard bracketing (Yang, 2009). Copper-doping has been applied to iron isotope amount ratio measurements. However, Dauphas et al. (2009) showed that increased matrix components can affect the measured isotope amount ratios. Precision for the copper-doping has been quoted as $\delta(^{56/54}Fe)$ =0.11‰ (2s) (Arnold et al., 2004).

All the mass bias correction techniques, discussed above, produce isotope amount ratios which are then compared to a standard to obtain a delta value for a sample and the delta value is dependent on the standard. Therefore, certified reference materials are needed to compare isotope amount ratios between laboratories. The isotope amount ratios of these certified standards are very well characterized and the reference material used for iron isotope amount ratio measurement in this thesis is IRMM -014 (Table 1).

2.3 Resolving Power

MC-ICP-MS was the preferred method for the measurement of iron isotope amount ratios for this thesis. A detailed description of the mass spectrometer as used for iron isotope amount ratio measurements is provided in the Analytical Methods section. The mass bias of the MC-ICP-MS can be corrected for using either mass bias correction technique discussed in Section 2.2. On top of the mass bias, iron measurements on the MC-ICP-MS are affected by polyatomic

interferences specifically argon oxides and argon nitrides. To ionize the sample, a high temperature inductively coupled plasma is used. The plasma is formed using an argon gas flow and the argon atoms then form ionized compounds such as argon oxides and argon nitrides with the oxygen and nitrogen atoms in the sample. These compounds can be detrimental to iron isotope amount ratios as $^{40}Ar^{14}N^{+}$, $^{40}Ar^{16}O^{+}$, $^{40}Ar^{16}O^{1}H^{+}$ and $^{40}Ar^{18}O^{+}$ have similar masses to $^{54}Fe^{+}$, $^{56}Fe^{+}$, $^{57}Fe^{+}$, and $^{58}Fe^{+}$, respectively. Therefore, high resolution is essential for iron measurement on the MC-ICP-MS (Weyer & Schwieters, 2003). Conventional definitions of resolution, 10 % valley definition, cannot be applied to the MC-ICP-MS as unresolved flat topped iron-interference peaks are obtained (see Figure 4) Flat topped peaks are created using an entrance slit that is narrower than the exit slit. The entrance slit is positioned after the cones and the width of the entrance slit is adjustable to low (250 μm), medium (30 μm) and high (16 μm) settings (ThermoFinnigan, 2003). Therefore, as the ion beam sweeps across the exit slit, the entire ion beam would be incident on the detectors resulting in a flat topped peak. Instead of resolution a new definition, resolving power, was defined (Weyer & Schwieters, 2003). Resolving power is given by Equation XIII and shown schematically in Figure 4.

$$R = \frac{m}{\Delta m^{*}} = \frac{m}{m(95\%) - m(5\%)}$$

Equation XIII

In this equation, m(95%) and m(5%) denote the mass at 95 % and 5 % of peak height respectively and m is the mass at peak height. Using this definition, a resolving power of 2500 is sufficient to resolve all the isotopes of iron from their argon interferences, Table 2. The MC-ICP-MS has three resolution settings with low resolution (resolution 400), medium resolution (resolving power 8,000-9,000) and high resolution (resolving power 10,000-12,000) (Weyer & Schwieters, 2003). Therefore, medium resolution is sufficient to resolve all iron isotopes from

their relevant interferences. The presence of interferences results in low mass and high mass shoulders shown in Figure 4 and discussed in detail in the Methods section.

Table 2: The resolving power need to optically resolve all isotope of iron from their respective interferences

Isotope of Iron	Interference	Resolving Power (Approx.)
$^{54}Fe^{+}$	$^{40}Ar^{14}N^{+}$	2100
$^{56}Fe^{+}$	$^{40}Ar^{16}O^{+}$	2500
$^{57}Fe^{+}$	$^{40}Ar^{16}O^{1}H^{+}$	1900
$^{58}Fe^{+}$	$^{40}Ar^{18}O^{+}$	2000

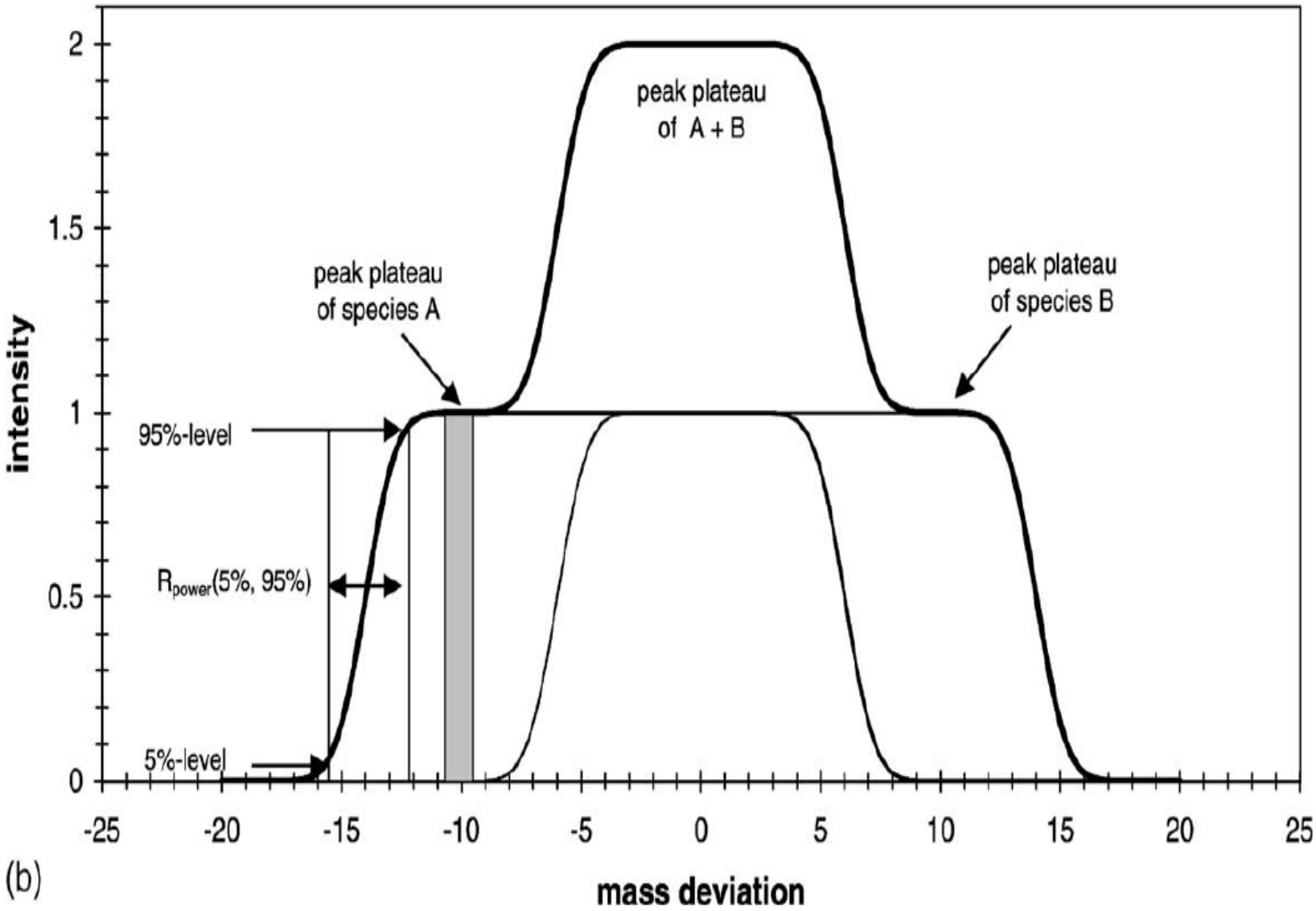

Figure 4: Diagram of the resolving power for the MC-ICP-MS. Species A and B are unresolved and flat topped peaks are obtained.

Chapter 3: Analytical Methods

This section will discuss the analytical technique for the measurement of iron isotope amount ratios. A general overview of the MC-ICP-MS will be presented focusing on the relevant aspects for iron measurements. Sample preparation techniques will be discussed including sample digestion where the iron is removed from mineral form and placed into solution, and ion exchange chromatography where the sample is chemically purified for analysis. The measurement method for analysis of samples using the MC-ICP-MS will be outlined focusing on the mass bias correction techniques used, and optimal measurement conditions. Experiments performed to ensure high quality data are highlighted including optimal magnet position and intensity matching. Finally, factors that affected the measured delta values including magnet instability and chromium interference will be discussed.

3.1 Mass Spectrometer

Iron isotope amount ratios were measured using a Thermo Fisher Neptune multiple collector inductively coupled plasma mass spectrometer (MC-ICP-MS). The MC-ICP-MS is a double focusing mass spectrometer with a Nier-Johnson geometry consisting of three components: plasma ion source (A), mass analyzer section (B), and ion collectors (C) (Figure 5) (ThermoFinnigan, 2003).

A prepared sample in 3% nitric acid is introduced into the mass spectrometer through an inlet system consisting of tubing, nebulizer, and spray chamber. An argon gas flow, “the sample gas”, is used to create a low pressure region at the base of the nebulizer and draw in the sample using the Venturi principle (Dean, 2005). The nebulizer produces an aerosol which is aspirated into a spray chamber where sample droplets are sorted by size. Larger droplets exit the spray chamber into a waste container while smaller droplets are drawn into the mass spectrometer

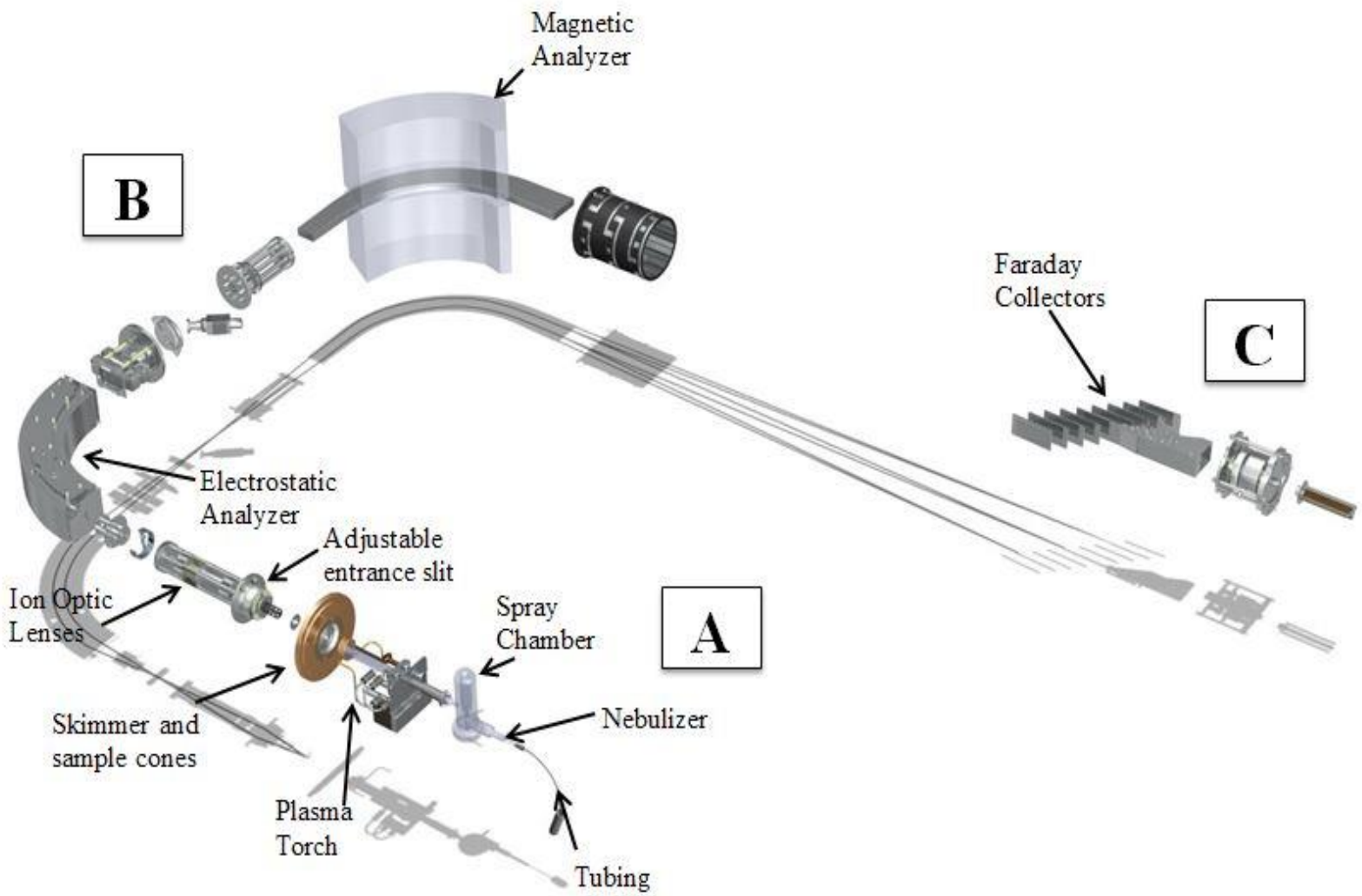

Figure 5: Diagram of the inside components of the MC-ICP-MS. Components relevant to the discussion are labelled. Permission obtained from ThermoFinnigan for reproduction in the thesis (Appendix)

by a pressure differential between the inside components (ESA module/ICP Module) of the mass spectrometer and inlet system. Large droplets should not be injected into the mass spectrometer as they could cause a cooling of the plasma enhancing matrix effects or extinguishing the plasma completely (Dean, 2005).

High temperature inductively coupled plasma is used to ionize the sample. The inductively coupled plasma is generated by coupling a strong oscillating electromagnetic field (27.12 MHz) to the argon gas flow using a load coil. The plasma was created in a plasma torch which consisted of two concentric quartz glass tubes. Auxiliary argon gas was introduced tangentially into the inner tube and a cooling argon gas flow in the outer tube which prevents the torch from melting as the plasma can reach 10,000 K. The aspirated sample was then introduced into the center of the plasma torch (ThermoFinnigan, 2003; Thomas, 2008).

The sample exits the spray chamber and enters the plasma where it is dried, vaporized, atomized, and ionized as it travels through the plasma. The positive sample ions exit the plasma at a temperature of 6000-7000 K. An interface, consisting of two nickel cones (sample and skimmer cones) and a skimmer valve make up the interface where a pressure differential transports the sample from atmospheric pressure to the high vacuum inside the mass spectrometer (10^{-7} Torr) (Figure 3) (ThermoFinnigan, 2003). The sample and skimmer cones are made of nickel due to its hardness, high thermal conductivity, high melting point, and ability to dissipate heat quickly (Hacettepe University, 2013). This interface is the primary source of the mass bias discussed in the Chapter 2.1. The ion beam then enters the transfer lens or ion optics which consists of a system of lenses that focus and accelerate the ion beam towards the entrance slit of the electrostatic analyzer. The width of the entrance slit can be adjusted to either low (250 μm), medium (30 μm) or high resolution (16 μm). Increasing the resolution results in decreased

signal intensity but the increased resolution allows iron to be resolved from interferences, for example $^{40}Ar^{16}O^{+}$ (55.95729 u) from $^{56}Fe^{+}$ (55.93494 u) and $^{40}Ar^{14}N^{+}$ (53.96545 u) from $^{54}Fe^{+}$ (53.93961 u). As mentioned, the MC-ICP-MS is a double focusing mass spectrometer with Nier Johnson geometry, in which an electrostatic analyzer precedes the magnetic analyzer to allow simultaneous high resolution measurements of multiple isotopes. The electrostatic analyzer consists of two cylindrical plates; there is a potential difference between the plates, with the outer plate held at a positive potential and the inner plate at a negative potential. The electrostatic analyzer focuses ions of different energies to its exit slit (de Hoffmann & Stroobant, 2002).

After exiting the electrostatic analyzer, the ions enter the magnetic analyzer where they are focused based on their mass to charge ratio. The ions of a desired mass are then directed into graphite cups, Faraday detectors fitted with graphite liners, connected to amplifiers. The amplifiers convert the incoming ion current into a voltage reading, which is measured by the mass spectrometer; the amplifiers used for iron measurements employ $10^{11}\ \Omega$ resistors ($1*10^{-11}$A = 1 V). There are nine graphite Faraday cups, labelled H4, H3, H2, H1, C, L1, L2, L3 and L4. The Faraday cups are all positioned along the focal plane and the position of the high (H) and low (L) cups are adjustable these cups can be arranged to simultaneously detect all isotopes of iron as well as ^{53}Cr and ^{60}Ni. Table 3 shows the cup configuration for iron isotope amount ratio measurements.

Table 3: The cup configuration on the MC-ICP-MS for iron isotope measurements

Cup	Measured ion
L4	$^{53}Cr^{+}$
L2	$^{54}Fe^{+}$
C	$^{56}Fe^{+}$
H1	$^{57}Fe^{+}$
H2	$^{58}Fe^{+}$
H3	$^{60}Ni^{+}$

3.2 Sample Preparation

Sample purification prior to analysis by MC-ICP-MS was achieved using anion exchange chromatography, discussed below, which is of vital importance since changes in the sample matrix can significantly affect the mass bias of the mass spectrometer (Dauphas et al., 2009). Of particular importance is the separation of nickel and chromium from iron since the resolving power needed to distinguish between ^{58}Fe and ^{58}Ni is R= 28,000 and then for ^{54}Cr and ^{54}Fe R= 78,000 which is greater than the available high resolution, R ≈ 12,000. The resolving power of the MC-ICP-MS in Calgary was been determined periodically and ranged from 11,500 - 13,000 in high resolution. Changes in argon gas flows, the voltages applied to ion optic lenses and the integrity of the entrance slit can affect the resolving power. The sharp edges on the entrance slit degrade with use causing the resolving power to decrease over time. Calculations are shown in Figure 6 for a measurement of the resolving power (March 21st 2013).

Some samples required digestion prior to ion exchange including mineral samples, such as siderite ($FeCO_3$), and the iron production pipe to remove the iron from its mineral form and

release it into solution. Siderite samples were weighed into 1.5 mL polypropylene centrifuge tubes to which 0.5 mL of concentrated HNO_3 (≈ 15.4 M) was added. The siderite digested for 3-5 days then, 1 mL of polished water was added. A small aliquot containing the desired amount of iron for chemical purification was transferred to a Teflon beaker and dried under a heat lamp or on a hot plate. For the production pipe, small cubes (d < 1cm) were cut. A cube was then placed in 6 M HCl on the hot plate for an hour in a closed Teflon beaker to remove any surface contamination. The cube was then weighed and placed in 6 M HCl in a clean Teflon beaker for one hour. The pipe was removed from the acid and weighed to determine how much of the pipe dissolved into solution. A small aliquot of the 6M HCl-pipe solution was then transferred to a Teflon beaker and dried under a heat lamp in preparation for ion exchange. Samples requiring no digestion, such as water samples, were weighed into Teflon beakers and dried under a heat lamp or on a hot plate.

All dried samples were dissolved in 1 mL 6M HCl in preparation for ion exchange. Iron forms $FeCl_3^-$ ions in high molarity HCl which then adhere to the resin during ion exchange chromatography. As mentioned, separation of iron from the sample matrix was achieved using ion exchange chromatography and is shown schematically in Figure 7-A. The procedure was adapted from Schoenberg & von Blanckenburg (2005). Glass columns were filled with 1 mL of EiChrom AG 1-X 100-200 mesh resin. The resin was cleaned with 5 mL 5 M HNO_3 and 2 mL of MQ water to remove any trace surface iron from the resin before sample loading. The resin was preconditioned with 4 mL 6M HCl. Preconditioning the resin with the exact molarity of acid used in sample loading to ensure all the iron is retained by the resin. The sample is then passed through the ion exchange column. In high molarity HCl, iron has a high distribution coefficient (Saito, 1984) thus ensuring all the iron is retained by the resin bed (greater than 99 %).

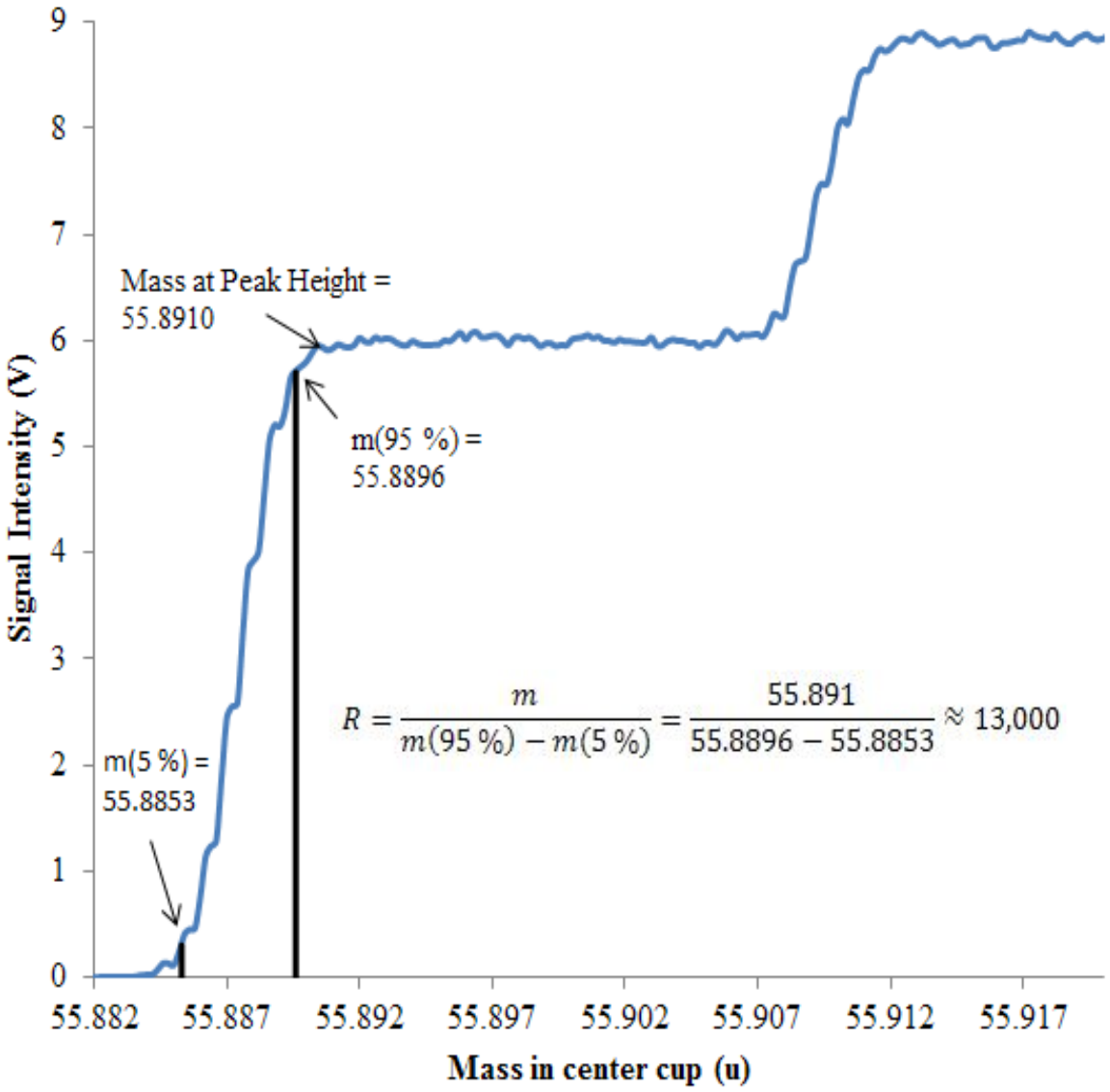

Figure 6: Calculation of the resolving power on March 21 2013 for high resolution on the MC-ICP-MS in Calgary, Alberta. The resolving power is sufficient to resolve all the isotopes of iron from their respective interferences

After sample loading, matrix elements such as nickel and chromium are removed by passing 6 mL of 6 M HCl through the column. These elements have low distribution coefficients in 6M HCl and are thus eluted from the column. Other elements such as copper, manganese and cobalt have slightly larger distribution coefficients and are only partially eluted from the resin during this matrix elution step. However, these elements do not interfere isobarically with iron and in low concentrations do not significantly affect the mass bias during a measurement session (Dauphas et al., 2009). Once the matrix elements are eluted from the resin, the iron is removed using 2 mL MQ water followed by 5 mL 5 M HNO_3. High molarity nitric acid is used to remove the iron from the resin because high molarity nitric efficiently breaks $FeCl_3^-$ complexes better than either water or low molarity HCl. Therefore, volumetrically less 5 M nitric is needed to remove all of the iron from the resin in comparison to water or low molarity HCl.

An elution curve is shown in Figure 7-B. The eluent is collected in Teflon beakers and dried under a heat lamp or on a hot plate and once the sample is dry, it is dissolved in 100 μL concentrated nitric acid and heated on a hot plate at 100°C. The addition of nitric acid to the sample breaks any remaining iron chloride complexes or residual organic complexes. Iron in its chloride form and organic complexes, can affect the reproducibility of the measured delta values thus increasing analytical uncertainty (Schoenberg et al., 2005). The iron in concentrated nitric acid was dried down and samples were dissolved in 3 % nitric acid for analysis by the mass spectrometer.

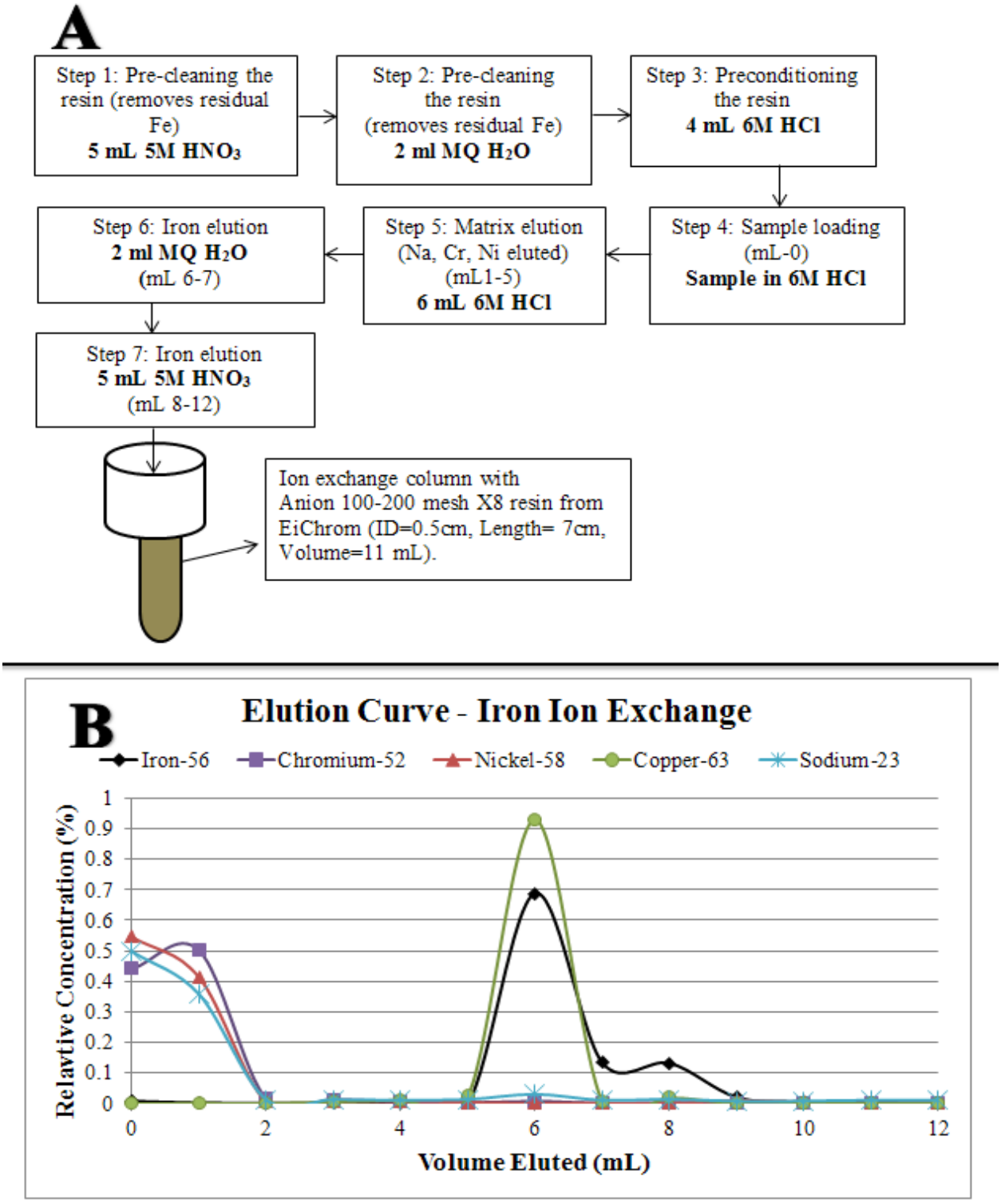

Figure 7: Panel A shows the ion exchange method. Panel B shows an elution curve for the ion exchange (what each mL corresponds to is give in panel A). All measured elements, except copper, elute before iron elution.

3.3 Sample Measurement on the Mass Spectrometer

Correction techniques are needed to correct for both the overall mass bias and the time dependent mass bias drift to obtain the true iron isotopic ratios of a sample. Correction techniques are needed because; the mass bias of the MC-ICP-MS can be as high as 3 % per mass unit and the range of iron fractionation is at most 0.4 %. On top of the overall offset, small time dependent variations also occur, approximately 0.1 ‰ during a day. Two techniques were used to correct for the mass bias of the mass spectrometer: sample standard bracketing (SSB) and double spike (DS). Both these techniques have been shown to accurately correct for instrumental mass bias and obtain the true isotopic ratios of a sample. Using these techniques, precision (2s) in $\delta(^{56/54}Fe)$ values has been reported as 0.04 ‰ and 0.05 ‰ for DS and SSB respectively (Schoenberg et al., 2005; Millet et al., 2012).

SSB is shown schematically in Figure 8 where measurement of a sample is bracketed by measurements of a standard. Measured data points are given by the triangles and the solid red and black lines represent the average measured $n(^{56}Fe)/n(^{54}Fe)$ ratio for the sample or standard. From Figure 8, we can see the mass bias offset between the measured $n(^{56}Fe)/n(^{54}Fe)$ isotope amount ratio and the true $^{56}Fe/^{54}Fe$ isotope amount ratio (15.698) of the standard. A linear drift in mass bias towards decreasing $^{56}Fe/^{54}Fe$ isotope amount ratio can also been seen as time progressed. For this measurement session, approximately 0.5 ‰ variation in the $^{56}Fe/^{54}Fe$ isotope amount ratio was observed in an hour. When measuring samples and applying SSB, the mass bias drift must be considered. First measurement time between samples and standards should be reduced to ensure the drift in mass bias is small between the bracketing standards. Also due to the linear drift in mass bias the wash out time between samples and standards should be identical. This ensures the fractionation factor of the averaged standards represents the actual

fractionation factor of the sample. For this thesis, the bracketing standard used for iron measurements was the Iron ICP/DCP standard from Sigma-Aldrich with a measured isotopic composition of $\delta(^{56/54}Fe) = 0.2(1)$ ‰ with respect to IRMM-014. This correction was applied to all measured data such that all delta values reported in this thesis are with respect to the certified iron standard IRMM-014 used in literature. This enables the comparison of the data to published values ensuring accurate conclusions are made. For sample standard bracketing (SSB), 25 iterations of 8 seconds of sample signal intensities were collected (1 block of 25). Internal precision during a SSB measurement was typically 0.03 ‰ (1s).

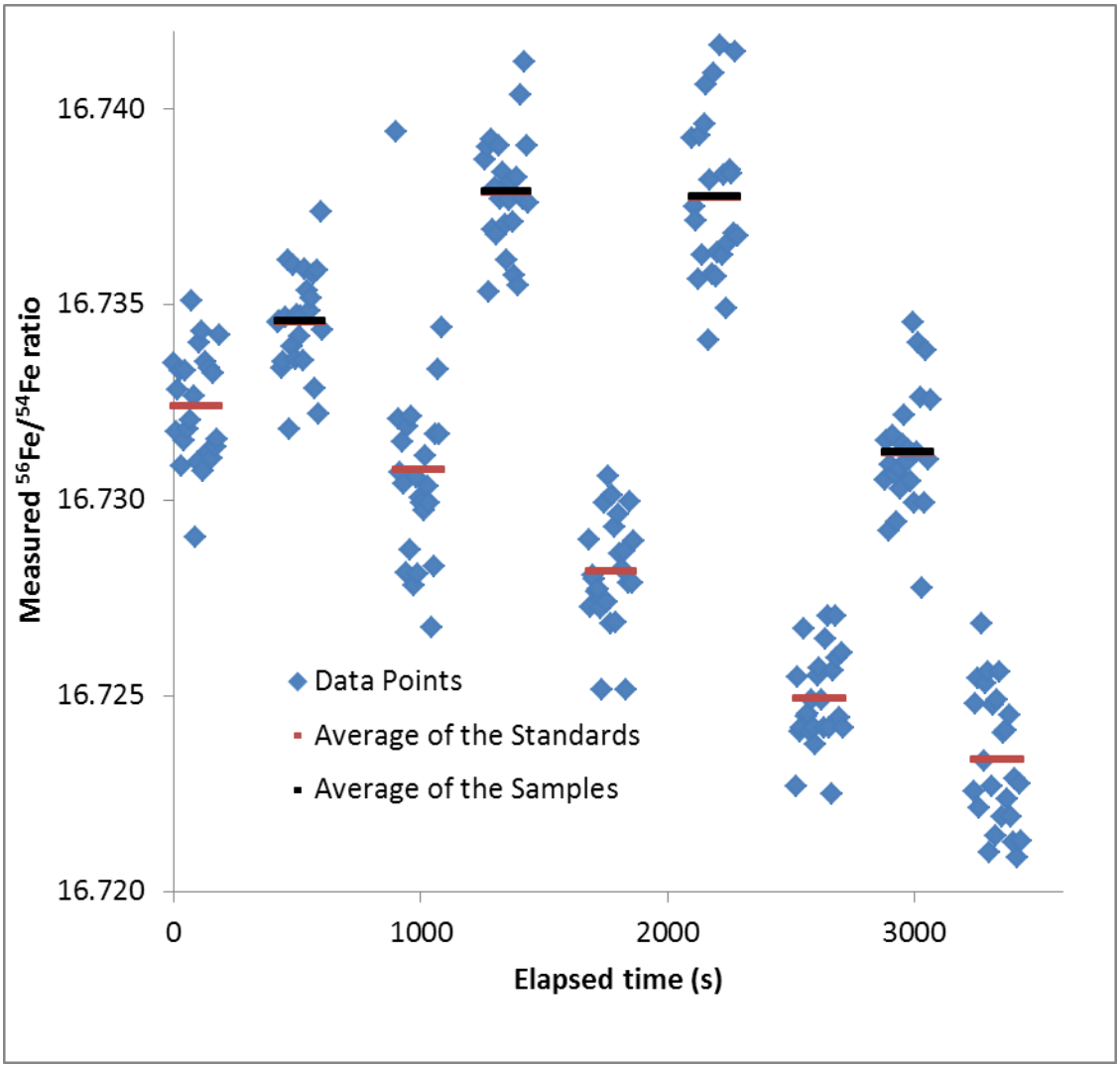

Figure 8: Data from a sample standard bracketing session on March 21st 2013 is shown. The overall mass bias offset and mass bias drift can be seen. A linear mass bias drift is assumed to calucate the iron delta values for a sample

The second method, double spike, uses a solution enriched in ^{57}Fe and ^{58}Fe which is added to the sample prior to ion exchange chromatography. Adding the double spike prior to ion exchange chromatography eliminates any fractionation introduced during sample preparation because preparation will affect all the isotopes, including those added from the double spike (Dideriksen et al., 2006). The double spike used in this thesis was prepared and calibrated by Ronny Schoenberg, University of Tübingen. The double spike contains 186 ppm of iron and a $n(^{57}Fe)/n(^{58}Fe)$ ratio of approximately 0.979 which is normally 7.514 in unspiked materials. Iron isotope abundances in double spike are given in Table 4.

Table 4: Natural iron abundances compared to the iron abundances in the double spike

Isotope	Natural (%)	Double Spike (%)
^{54}Fe	5.85	0.002
^{56}Fe	91.75	1.37
^{57}Fe	2.12	48.79
^{58}Fe	0.28	49.84

To reduce uncertainty in double spike measurements, a 1:1 ratio between amount of iron in the double spike and in the sample is required (Rudge et al., 2009). Measurement of double spiked samples consisted of two measurements by the mass spectrometer: measurement of the sample intensities and measurement of the relevant background intensities. Background intensities were measured during aspiration of a clean 3 % nitric acid solution; these background intensities were subtracted from the measured sample double spike intensities prior to data reduction to eliminate their contribution to the signal intensity. Sample measurement on the mass spectrometer consisted of 80 iterations of 8 seconds each (4 blocks of 20).

After sample measurement, the measured signal intensities were used to obtain a delta value for the sample using a double spike algorithm obtained from Ronny Schoenberg (University of Tübingen), shown in Figure 9. The algorithm used an iterative method to determine the true isotopic ratios of a sample (Krabbenhoft et al., 2009) this involved using the measured intensities of $^{54}Fe^{+}$, $^{56}Fe^{+}$, $^{57}Fe^{+}$, $^{58}Fe^{+}$, $^{53}Cr^{+}$, and $^{60}Ni^{+}$. With the chromium and nickel intensities, interference corrections were applied to the measured ^{58}Fe and ^{54}Fe intensities.

The iron isotope amount ratios measured on the MC-ICP-MS for double spiked samples can be broken down into the contribution from the sample and from the spike, Equation XIV.

$$\left(\frac{^{56}Fe}{^{58}Fe}\right)_{measured} = \frac{\#^{56}Fe_{Spike}atoms + \#^{56}Fe_{Sample}\ atoms}{\#^{58}Fe_{Spike}atoms + \#^{58}Fe_{Sample}atoms}$$

Equation XIV

To account for the contribution of the double spike in an iron isotope amount ratio and obtain the true iron isotope amount ratios for the sample an algorithm is used. The algorithm starts with assumed (but reasonable) values for an instrumental fractionation ($\beta_{Instrumental}$) and natural fractionation factor ($\beta_{natural}$). $\beta_{Instrumental}$ is approximately 2 and $\beta_{natural}$ is generally between -1 and 1 (Siebert et al., 2001) (Figure 9-1). Using these fractionation factors and the exponential mass fractionation equation, the mass bias corrected iron isotope amount ratios (calculated mix - CM) and "true" iron isotope amount ratios (sample new - SN) can be obtained (Figure 9-2). Using the calculated mix and sample new ratios Q58(54) and Q58(56) values can be obtained, Equation XV and Equation XVI. These Q values relate the amount of ^{58}Fe in the sample to that in the spike and can be derived from Equation XIV (Figure 9-3).

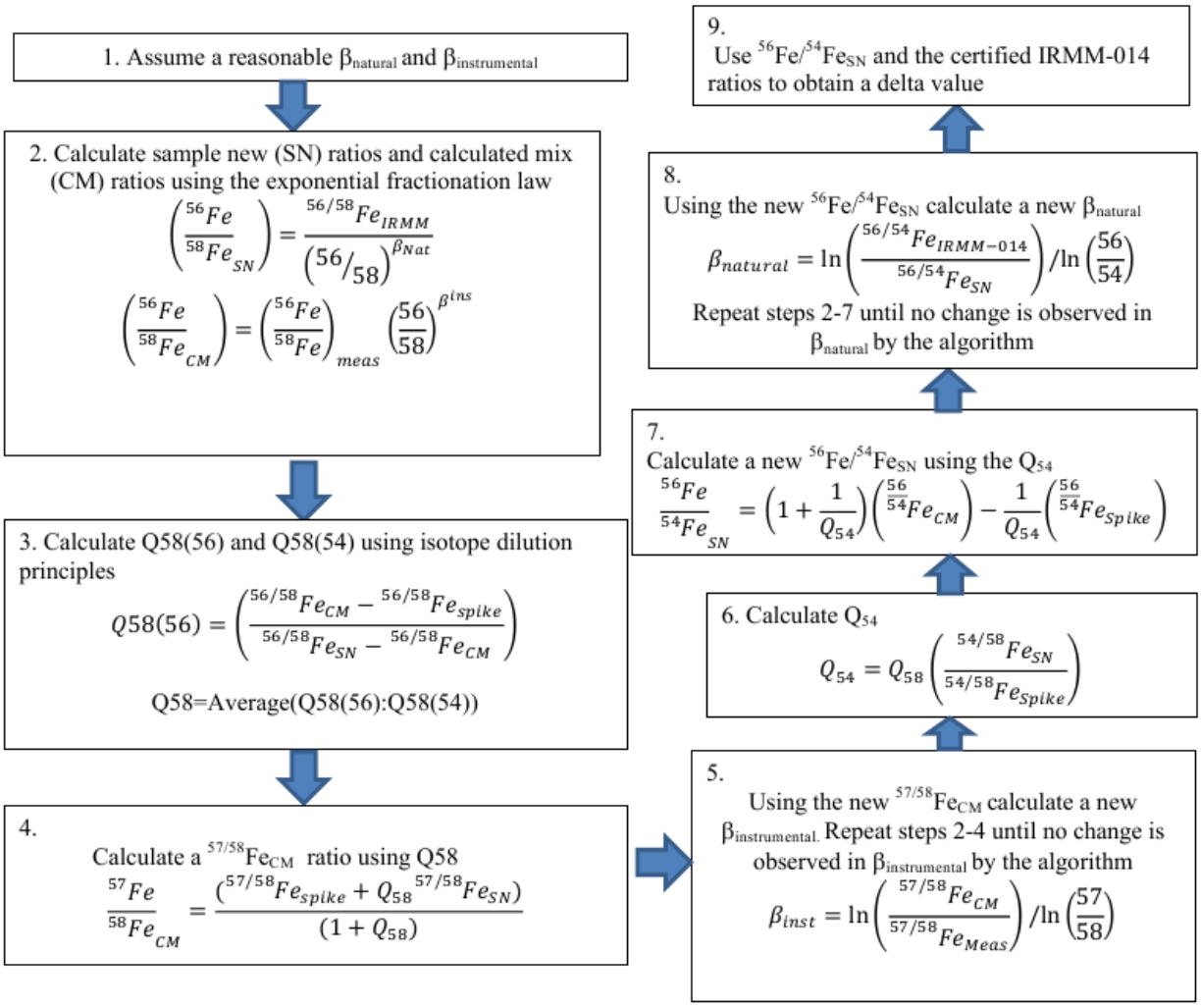

Figure 9: Schematic representation of the algorithm used to reduce the measured double spike results for a sample and obtain the true iron isotope fractionation

$$Q58(56) = \left(\frac{^{58}Fe_{sample}}{^{58}Fe_{Spike}}\right) = \frac{^{56/58}Fe_{CM} - ^{56/58}Fe_{Spike}}{^{56/58}Fe_{SN} - ^{56/58}Fe_{CM}}$$

Equation XV

$$Q58(54) = \left(\frac{^{58}Fe_{sample}}{^{58}Fe_{Spike}}\right) = \frac{^{54/58}Fe_{CM} - ^{54/58}Fe_{Spike}}{^{54/58}Fe_{SN} - ^{54/58}Fe_{CM}}$$

Equation XVI

Both Q values should be equal, since the amount of ^{58}Fe is constant, irrespective of the isotope amount ratio measured.

Using the averaged Q value, the mass bias corrected measured ^{57}Fe/^{58}Fe (calculated mix) isotope amount ratio can be obtained (Figure 9-4). Using the ^{57}Fe/^{58}Fe (calculated mix) ratio and the exponential fractionation law, a first iteration instrumental fractionation factor was determined. The algorithm repeated until the change in the instrumental fractionation factor between successive iterations was less than a defined value (Figure 9-5). Once the true instrumental fractionation factor was determined, the contribution from the mass bias on the measured iron isotope amount ratios was eliminated. With the mass bias corrected iron isotope amount ratios and a Q_{54} value (Q_{54}=n($^{54}Fe_{sample}$)/n($^{54}Fe_{spike}$)) (Figure 9-6), a sample new n(^{56}Fe)/n(^{54}Fe) iron isotope amount ratio was obtained (Figure 9-7). From this ratio and using the exponential fractionation law, a new natural fractionation factor was calculated ($\beta_{natural}$). The algorithm repeats until the change in this fractionation factor between successive iterations was less than a defined value (Figure 9-8). Once the true $\beta_{natural}$ was determined, a final n(^{56}Fe)/n($^{54}Fe_{SN}$) ratio is calculated using the empirical exponential fractionation law. The n(^{56}Fe)/n($^{54}Fe_{SN}$) ratio was then used to calculate a delta value with respect to the certified IRMM-014 standard, Equation I (Figure 9-9).

3.4 Accurate Measurement of Iron Signal Intensities by MC-ICP-MS

To apply either mass bias correction technique (DS and SSB) successfully, iron signal intensities need to be accurately measured by the MC-ICP-MS. A typical mass scan obtained using high resolution MC-ICP-MS is shown in Figure 10. As mentioned, the MC-ICP-MS can simultaneously detect all four isotopes of iron in four different collectors (L2 (green), C (red), H1 (light blue), H2 (dark blue)). In Figure 10, there are three distinct regions: the low mass shoulder (A), the middle plateau (B), and the high mass shoulder (C). The ions contributing to the measured signal intensity are shown for the center cup, ^{56}Fe. As mentioned, iron is subject to polyatomic interferences such as argon oxides. Fortunately, all atoms with mass lighter than 90 u are lighter than their respective polyatomic interferences (Nelms, 2005). This allows high resolution mass spectrometry to resolve the three distinct regions, A, B and, C. In region A, only the desired isotope of iron contributes to the signal intensity, in region B iron as well as the interference contribute to the signal intensity, and in region C, only the interference contributes to the signal intensity. Therefore, all iron isotopic measurements are made on the low mass shoulder.

3.5 Optimal Measurement Position on the Low Mass Shoulder

The magnet position, or measurement position, on the low mass shoulder can affect the measured iron isotope amount ratios, see Figure 11. Figure 11 shows a mass scan of the low mass shoulder for ^{56}Fe in a standard (dark red line) and a wash solution (clean 3 % nitric acid aspirated into the mass spectrometer, signal intensity $\times$ 4000) (light red line). The resolving power needed to optically resolve $^{56}Fe^{+}$ from its interference is larger than any other iron isotope/interference resolving power. Therefore, only the position on the $^{56}Fe^{+}$ peak will be considered. Ideally all measurements should be obtained with the set mass position in the axial

cup at the center of the low mass shoulder (LMS) (Weyer & Schwieters, 2003). As is shown in Figure 11, the LMS spans a smaller mass range during measurement of clean nitric solution, wash solution, compared to the standard. In the wash, the contribution of the interference can be easily seen due to the low iron signal intensities. Due to this effect, a scan of the wash and standard should be made before the optimal magnet position is determined. To determine optimal magnet position on the LMS, an experiment was performed where the iron isotope amount ratios were measured at various points along the low mass shoulder. The measurements along the LMS were bracketed by iron isotope amount ratios measured at the center, 55.900, and delta values were calculated. Results are summarized in Figure 11. Between points 4 and 9, covering a 0.008 u range, delta values are within expected uncertainty of 0 ‰ (Chapter 4.1). Figure 11 clearly demonstrates that careful positioning of the magnet is needed to obtain accurate iron isotope amount ratios. Because of the small mass range in which accurate delta values can be obtained, the peak position should not shift during measurement. Fluctuations in magnetic field strength can cause measurable shifts in peak position which are detrimental to iron isotope amount ratio measurements. Therefore, magnet stability is of vital importance in high or medium resolution iron measurements. Shifts in the magnetic field were encountered frequently until January 2013. This instability was a significant contributor to analytical uncertainty in the early stages of method development. The problem was identified and was fixed in January 2013.

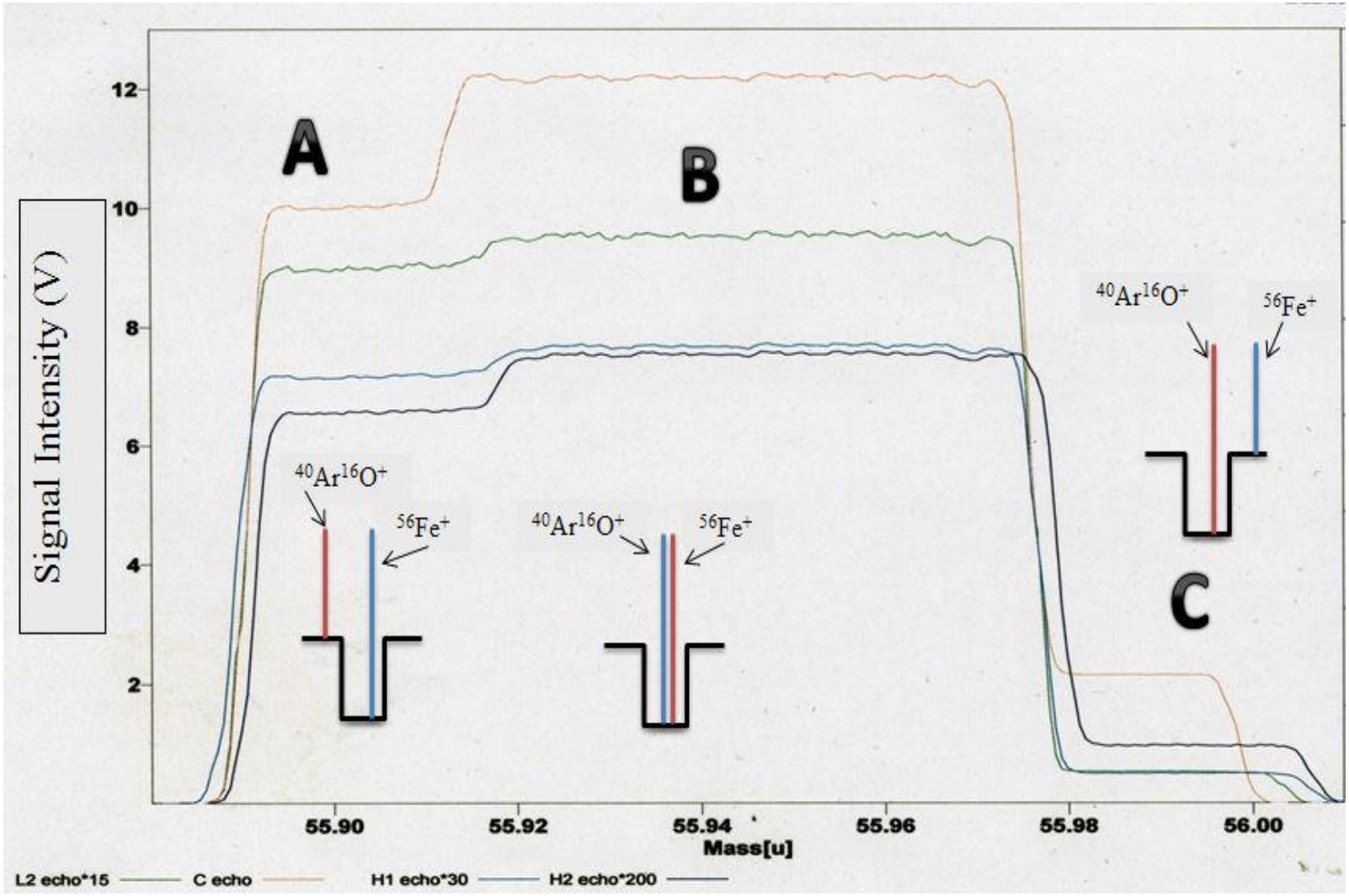

Figure 10: A typical mass scan for iron measurements. All four isotopes of iron are viewed simultaneously in four faraday cups L2 (^{54}Fe), C (^{56}Fe), H1 (^{57}Fe) and H2 (^{58}Fe). Multiplicative factors (shown at the bottom of the diagram) are applied to signal intensities. Three regions can be defined (A, B and C) based on the ions contributing to the signal intensity

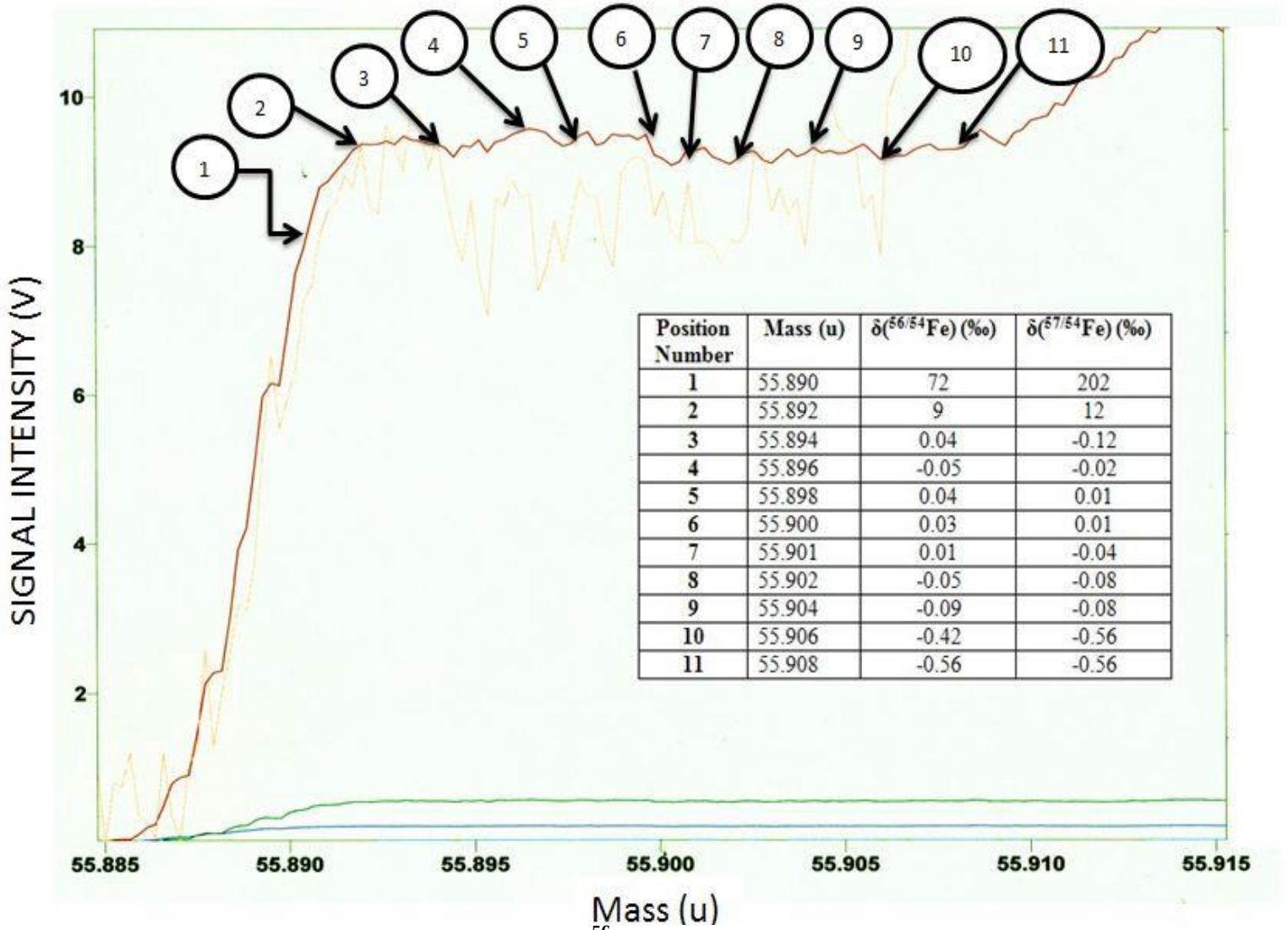

Position Number	Mass (u)	$\delta(^{56/54}Fe)$ (‰)	$\delta(^{57/54}Fe)$ (‰)
1	55.890	72	202
2	55.892	9	12
3	55.894	0.04	-0.12
4	55.896	-0.05	-0.02
5	55.898	0.04	0.01
6	55.900	0.03	0.01
7	55.901	0.01	-0.04
8	55.902	-0.05	-0.08
9	55.904	-0.09	-0.08
10	55.906	-0.42	-0.56
11	55.908	-0.56	-0.56

Figure 11: A mass scan of the low mass shoulder for ^{56}Fe in the standard, dark red line, and the wash, light red line. Iron delta values were calculated for each position using position 6 as the reference. A small range in mass, 0.008 u, produces delta values within expected analytical uncertainty of 0 ‰. Measurement of iron signal intensities should be performed between positions 4 to 9.

The magnetic field of the MC-ICP-MS is measured by a field probe which outputs to the mass spectrometer software. The fluctuations in magnetic field strength, as displayed by the software, were recorded. Figure 12 shows magnetic field strength fluctuations during periods of significant instability (blue) and after stability had been restored (red). The instability in magnetic field strength was caused by magnet power supply board was providing an unstable voltage to the magnet. To fix this problem a 1 nF capacitor was soldered across a specific resistor to smooth the voltage. This resulted in tolerable fluctuations in magnetic field strength.

3.6 Intensity Matching

Intensity matching, where the iron concentrations of samples and standards are within 10 % of each other, is essential to the accuracy and reproducibility of iron isotope amount ratios according to literature (Weyer & Schwieters, 2003). Of particular interest is the contribution from the $^{40}Ar^{16}O^{+}$ peak at the optimal set mass position in the axial cup for measuring $^{56}Fe^{+}$. The tailing of the interference peak can be as high as 10 ppm of the $^{56}Fe^{+}$ signal. If SSB is used to correct for the mass bias of the mass spectrometer, and intensities of samples and standards are not matched, the tailing would contribute a different portion of the measured signal intensity in samples and standards. The contribution of the tailing to the sample signal intensity would then be either under or over corrected during SSB, affecting the measured sample delta values.

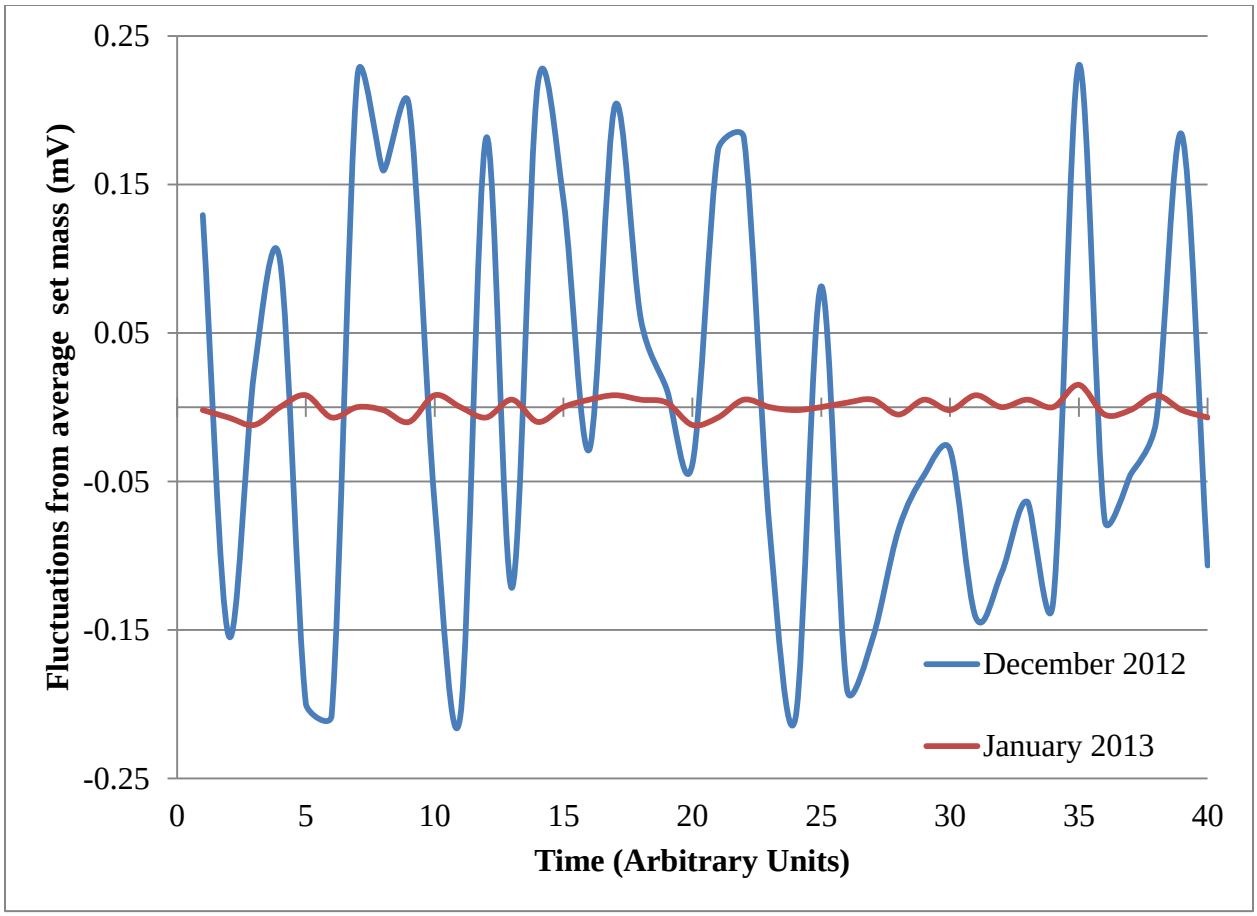

Figure 12: Magnet instability experience in late 2012 and early 2013. The fluctuations experienced December 2012 were detrimental to iron isotope amount ratio measurements causing significant shifts in iron peak mass position. The set measurement point deviated from optimal positioning when these fluctuations occurred.

However, if iron concentrations are matched between samples and standards, the contribution of the interference tail to the measured intensity would be eliminated by using SSB (Schoenberg & von Blanckenburg, 2005). It is also possible that the tailing from the $^{40}Ar^{16}O^{+}$ peak is negligible, in which case the measured delta values would not be affected by mismatched sample/standard intensities. To test the importance of intensity matching for high resolution iron measurements on the MC-ICP-MS varying concentrations of a standard and ion exchanged sample were prepared. First, iron isotope amount ratios were obtained for varying concentrations of the

standard. Delta values were calculated by bracketing each measurement with the same standard with an iron concentration of 2 ppm. Results are shown in Table 5. For concentrations greater than 0.5 ppm (1.4 V ^{56}Fe, 0.028 V ^{57}Fe), mismatched intensities did not significantly affect the measured delta values, compared to analytical uncertainty (see Discussion).

Table 5: Results from an intensity matching experiment preformed with varying concentrations of a standard. All measurements were bracketed by a 2 ppm iron standard.

Iron Concentration (ppm)	Intensity ($^{56}Fe^{+}$) (V)	$\delta(^{56/54}Fe)$ (‰)	$\delta(^{57/54}Fe)$ (‰)
0.25	0.7	-0.60	0.07
0.5	1.4	0.12	-0.45
1.5	3.9	-0.03	-0.08
1.9	4.8	-0.001	0.1
2	5.2	0.03	0.05
2.1	5.4	0.04	0.03
2.5	6.3	0.03	0.09
3	7.7	0.07	0.03

Changes in the sample matrix can affect the measured delta values so the same experiment was performed using an ion exchanged sample bracketed by a standard. Results are summarized in Table 6. In this intensity matching experiment, little variability is observed in the delta values, all are within expected analytical uncertainty.

Table 6: Results from an intensity matching experiment preformed where varying concentrations of the same ion exchanged sample were measured with respect to a 3 ppm iron standard.

Iron Concentration (ppm)	Intensity ($^{56}Fe^{+}$) (V)	$\delta(^{56/54}Fe)$ (‰)	$\delta(^{57/54}Fe)$ (‰)
1.2	3.5	0.14	0.33
2.0	5.8	0.13	0.26
2.3	7.3	0.13	0.23
2.4	7.3	0.10	0.16
2.7	8	0.15	0.27
3.2	9.1	0.11	0.18
Standard Deviation (2σ)	--	0.04	0.10

From both experiments, statistically significant deviations from the expected delta values are only observed when measuring low concentration samples. This is due to low signal intensities, (< 50 mV) measured for the minor isotopes of iron. At these intensities, electronic noise form the detectors is > 50 ppm and can affect the measured delta values (Weyer & Schwieters, 2003). Therefore, from both experiments it can be concluded that so long as the intensity of all desired isotopes are large enough (approximately 100 mV) (Weyer & Schwieters, 2003) matching concentrations of samples and standards is unnecessary. Despite these results, sample/standard concentrations were matched to the best of our ability. This was done to reduce any possible effect from mismatched samples and standards based on literature.

3.7 Signal Stability

Stability of the ion signal can affect the measured iron isotope amount ratios (Yang, 2009). Two factors were found to influence the stability of the ion beam: mass spectrometer source settings and the cleanliness of the inlet system. Source settings on the mass spectrometer include argon gas flows (auxiliary and sample gas), torch position and the voltages applied to the

ion optic lenses. Generally, torch position and ion optic voltages only required adjustments after maintenance to the mass spectrometer. In contrast, the optimal argon gas flows varied especially, when adjustments were made to the inlet system or the argon tank was changed. The gas flows were always optimized prior to a measurement session.

The cleanliness of the inlet system proved to be a significant problem causing unstable ion beams, varying mass bias, low signal intensities, high backgrounds and clogging of the nebulizer where no sample was aspirated into the mass spectrometer. Cleanliness of the inlet system was found to degrade when a large number of samples had been measured or when an element incompatible with iron was measured. Sulfur was found to be significantly incompatible with iron isotope amount ratios causing large changes in mass bias during a measurement session. Elements such as Cu, U and Mo did not affect iron isotope amount ratios to the same extent. Therefore, two separate inlet systems were used for iron and sulfur. The inlet system was also periodically removed from the mass spectrometer and cleaned. The spray chamber was immersed in RBS 50 solvent and placed in an ultrasonic bath. The nebulizer was placed in 3 M HNO_3 and heated on a hot plate. Both cleaning of the spray chamber and nebulizer was found to have a favorable effect on the signal stability, signal intensity and background intensities.

3.8 Preparation of the IRMM-014 Standard

Initially, difficulties were encountered in obtaining the certified iron standard IRMM-014 as production was discontinued. A small piece (15 mg) of unsealed IRMM-014 wire was obtained from Michael Berglund (IRMM-Geel, Belgium), and prepared on July 30th 2012. The wire was carefully broken into to two approximately equal pieces in a clean room using acid cleaned plastic tweezers. Half of the wire was kept in the original packaging and half was digested.

To digest the IRMM-014 wire, 7.44 mg piece was placed in a clean Teflon beaker and 2 mL 6 M HCl was added. The beaker was left for 12 days until no visible wire remained. The acid was then transferred to a clean 15 mL centrifuge tube and centrifuged at 2500 rpm for 45 minutes. A small amount (1.040 mL) of the prepared IRMM-014 was then pipetted and weighed into at 1 L Teflon bottle. The IRMM-014 was diluted with 3 % nitric acid to yield a solution with an iron concentration of 1.56(3) μg/g. The certified isotope ratios for the IRMM-014 are given in Table 1.

3.9 Preparation of the Iron-54 Spike

Using isotope dilution accurate iron concentration measurements can be obtained using an iron single spike. An iron-54 metal spike (20 mg) was obtained from Oak Ridge National Laboratory (ORNL). The quoted abundances are shown in Table 7 and from these abundances the spike has an atomic weight of 53.979. The metal spike was placed in a clean Teflon beaker and 2 mL concentrated HCl was added. After approximately 24 hours, no metal remained and the spike solution was diluted to yield a stock solution concentration of approximately (948 $\pm$ 5) ppm. From the stock iron spike solution, two more dilutions were made one to approximately (90.2 $\pm$ 0.5) ppm iron and a working solution at approximately (5.33 $\pm$ 0.03) ppm iron. Two tests were performed on the working spike solution, one to investigate the quoted abundances and another to determine the exact concentration of the iron spike.

To verify the quoted iron isotopic composition of the 54-spike solution, 0.5 mL of the working solution was dried down and once dry dissolved in 2 mL 3 % HNO_3 for analysis by the mass spectrometer. The iron spike was measured using SSB and the bracketing standard was the IRMM-014. Since the isotopic composition of the IRMM-014 is known, a fractionation factor, f, was calculated and applied to the measured iron isotope amount ratios of the spike using the

Table 7: Natural iron abundances compared to iron abundances in the ^{54}Fe spike

Isotope	Natural Abundance (%)	^{54}Fe Spike Abundance (%)
^{54}Fe	5.85	97.26
^{56}Fe	91.75	2.60
^{57}Fe	2.12	0.07
^{58}Fe	0.28	0.04

exponential fractionation law. Using the true ratios of the spike and Equation XVII below, the measured abundances of all four isotopes of iron were obtained

$$^{54}Fe(\%) + {}^{56}Fe(\%) + {}^{57}Fe(\%) + {}^{58}Fe(\%) = 100$$

Equation XVII

For example, when finding the percent abundance of ^{54}Fe, the other three isotopes of iron are expressed as ^{54}Fe(^{5x}Fe/^{54}Fe) where x=6, 7 or 8 in Equation XVII. This leaves one variable, ^{54}Fe, which can be solved for to yield the percent abundance of that isotope in the spike solution. The abundances in the iron spike were determined to be ^{54}Fe (97.31%), ^{56}Fe (2.22%), ^{57}Fe (0.22%) and ^{58}Fe (0.17%). The discrepancy observed between the ORNL quoted and measured values is a result of instrumental measurement uncertainty, particularly on the isotopes with low abundances, ^{57}Fe and ^{58}Fe. Therefore, the ORNL quoted abundances are used for all future calculations.

To determine the exact iron concentration of the working spike solution, IRMM-014 and the working spike solution were weighed using a high accuracy scale into a test tube and dried under a heat lamp. Once dry, the samples were dissolved in 2 mL of 3 % HNO_3 for analysis by the mass spectrometer. For this experiment, samples were measured using SSB. The bracketing

standard was IRMM-014. The fractionation factor determined for the bracketing standards was used to obtain the true $^{56}Fe/^{54}Fe$ isotope amount ratio in the spiked IRMM-014. Using the true isotope amount ratio and the isotope dilution equation, Equation XVIII, the ratio between the number of 54 atoms in the spike and standard was determined.

$$\left(\frac{^{54}Fe_{sample}}{^{54}Fe_{spike}}\right) = \frac{^{56/54}Fe_{measured} - {}^{56/54}Fe_{spike}}{^{56/54}Fe_{sample} - {}^{56/54}Fe_{measured}}$$

Equation XVIII

Since the atomic weight of the standard, percent abundance of ^{54}Fe in the standard and the amount of standard added are known, the number of ^{54}Fe atoms in the analyzed solution belonging to the added standard can be determined. Then, using the $^{54}Fe_{spike}/^{54}Fe_{standard}$ isotope amount ratio from the isotope dilution equation the number of ^{54}Fe atoms in the added spike can be calculated. Then, using the atomic weight of the spike and the percent abundance of ^{54}Fe in the spike, the iron concentration of the spike can be determined. Three measurements were made and concentrations of 5.93 μg/g, 6.02 μg/g and 5.93 μg/g were determined averaging to 6.0 ± 0.1 μg/g. Both of these calibrations were completed on August 26 2012. On January 23 2013 a new working solution was made and its concentration calibrated following the above procedure. The new iron-54 spike working solution has an iron concentration 5.2 ± 0.1 μg/g.

With the calibrated single spike, recovery experiments were performed for the ion exchange procedure. In a recovery experiment, a known amount of IRMM-014 passed through the ion exchange column. After ion exchange, a known amount of ^{54}Fe spike was added to the eluent. By comparing the measured concentration to the expected concentration a percent recovery for the ion exchange method can be determined. Initially, recoveries varied from 40 - 100 % when using in house made iron ion exchange columns from disposable pipettes (Figure 13-A). The low recoveries were likely due to a loose fit between the column and frit allowing

resin and thus iron to elute from the column during matrix elution. Glass columns were made and percent recovery for these columns was greater than 99 % which is sufficient to ensure no significant isotope fractionation occurred during ion exchange (Stenberg et al., 2003).

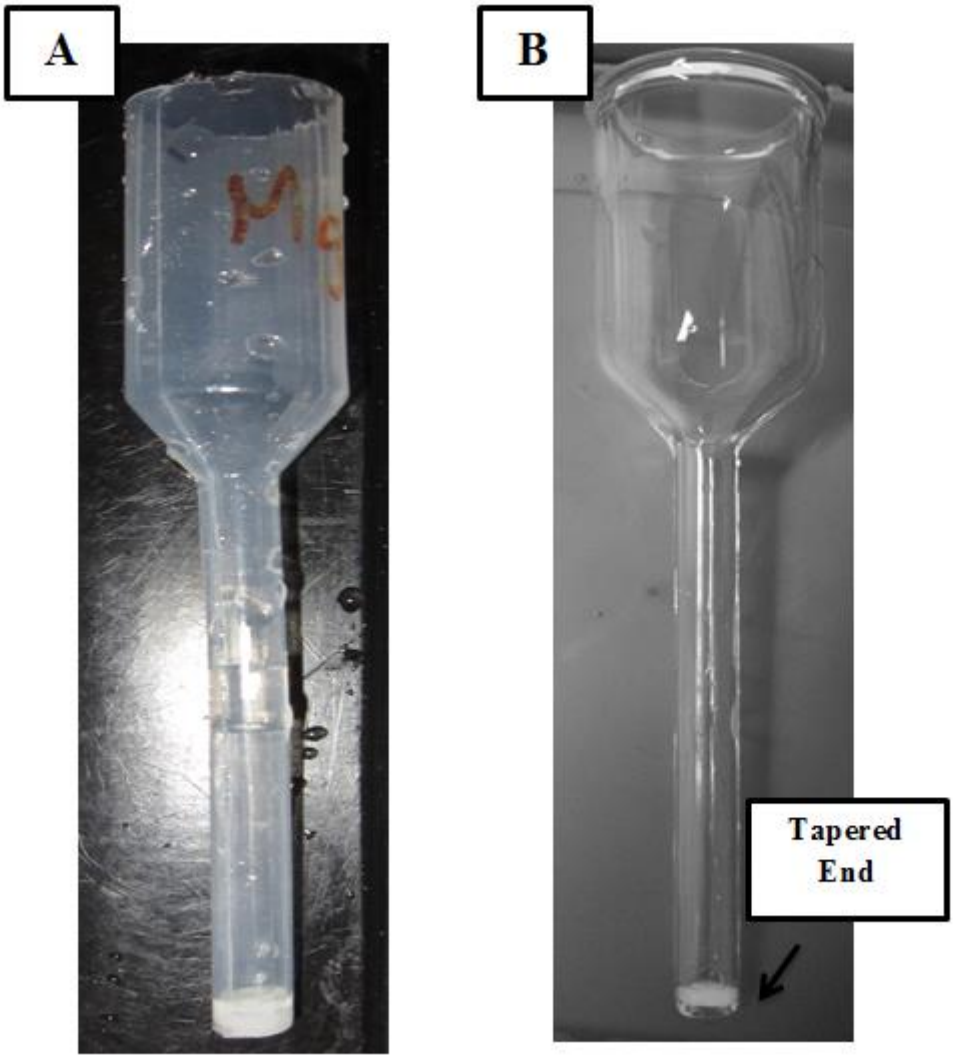

Figure 13: Iron ion exchange columns. The column on the left (A) was made from disposable pipettes notice the straight end holding the frit. Column B were manufactured by the machine shop, University of Calgary, notice the tapered end to keep the frit in the column

The glass columns were designed with a tapered end (Figure 13-B) to keep the frit in place and ensure no resin escaped the column during ion exchange.

Along with recovery experiments, blank measurements were made using the iron-54 spike. Analytical blanks can affect the measured delta values for a sample if they represent a significant contribution to the amount of iron in a sample. To measure the ion exchange blank either no sample was loaded onto the column or clean 6M HCl was added as the sample onto the column. As with the recovery experiment, after ion exchange the iron-54 single spike was added to the sample. The isotope dilution equation can be used to determine the amount of iron that was introduced during sample preparation, ion exchange, and evaporation under a heat lamp. Typical ion exchange blanks were between 15-20 ng of iron which represents a 0.7% contribution to 3 μg of iron. This contribution is insignificant introducing less than a 0.02 ‰ uncertainty in the $\delta(^{56/54}Fe)$ and ion exchange iron blanks are in agreement with similar laboratories (Personal communication Dr. Ronny Schoenberg).

3.10 Clean Room Contamination

Chromium blanks were a major concern throughout the development of the iron analytical technique. As mentioned, ^{54}Cr and ^{54}Fe cannot be resolved by the MC-ICP-MS and complete chemical separation of these elements is needed. Ion exchange had been shown to effectively remove chromium from the sample matrix (Figure 7-B) however, high chromium blanks were still observed during measurement on the mass spectrometer. The exact source of the chromium contamination was difficult to isolate. Precautions were taken including switching to glass columns, as plastics could leach chromium and acquiring a pipette specifically for iron measurements. Chromium can be introduced into a sample using a pipette if acid had come into contact with the internal components of the pipette. These precautions helped reduce the chromium contamination however; the chromium blanks were not eliminated and still significantly affected the measured delta values. The effect of high chromium blanks on the

measured delta values can be seen in Figure 14. Samples unexpectedly deviate from the mass dependent fractionation line. The deviation towards negative $\delta^{56/54}$Fe values was observed however there was no systematic offset. Throughout this thesis the goal was to obtain the highest precision data possible. The precision needed make meaningful interpretations of iron isotope amount data is less than 0.1 ‰ in the $\delta(^{56/54}$Fe) ratio. This uncertainty is shown in Figure 14 for data obtained early on in the project. From Figure 14, it can be noted that the chromium contamination significantly affects the measured iron delta values. Delta values do not lie within our desired uncertainty of the mass dependent fractionation line. This deviation was traced back to chromium contamination based on measurements ^{53}Cr by the mass spectrometer. Therefore, chromium contamination must be addressed in order to obtain high precision data. All samples at some point during their preparation were dried either on a hot plate or under a heat lamp. It was noted that metal on the heat lamps in the clean room was oxidizing due to high levels of acid fumes present. A test was performed to determine the effect the rusting heat lamps were having on the iron and chromium blanks. Numerous pipettes were also tested to determine their contribution to the iron and chromium blanks. All test solutions were compared to an acid solution which had not been pipetted or left open in the fume hood. All pipettes showed negligible blanks compared to the reference solution. However, samples dried in the fume hood, both on the hot plate and under the heat lamp, showed an increase in iron and chromium contamination, the hot plate is adjacent to the heat lamps (Figure 15). So even samples dried on the hot plate can be affected by the leaching of iron or chromium from the heat lamps. The sample dried on the hot plate showed a 10-fold increase in chromium but a negligible increase in iron. In comparison, the sample dried under the heat lamp shows a 100-fold increase in chromium and a 10-fold increase in iron.

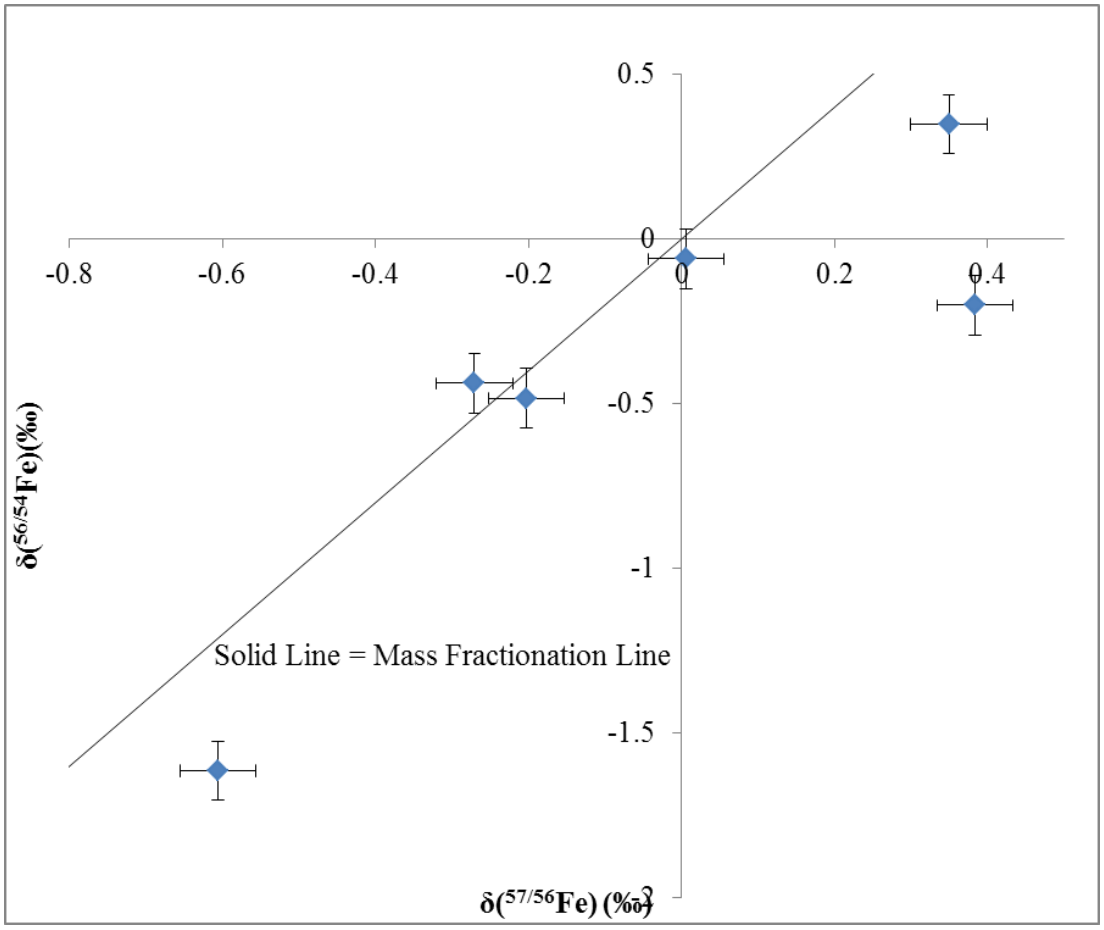

Figure 14: Three isotope plot for iron measurements May 2012. The δ($^{56/54}$Fe) value deviates towards negative values indicating the presence of excess 54 atoms. Chromium contamination was the suspected source of the increased 54 atoms

To counteract the increase in iron and chromium blanks until the heat lamp problem can be resolved, two procedures were employed. First, if possible, the amount of iron passed through the ion exchange column was increased. Therefore, the percent contribution of the blank to the total iron decreased and the effect to the measured delta values decreases as well. Secondly, all samples were dried on the hot plate rather than under the heat lamp. Additionally, while drying, a glass beaker was placed on two supports over the samples. This prevents iron falling from the heat lamps from entering the sample. Along with this, care was taken to ensure samples were open in the fume hood for the shortest possible time. Lastly, if possible while drying samples for iron isotope measurements, the heat lamps were removed from the fume hood completely and

samples dried on the hot plate. When precautions were applied to prevent heat lamp contamination, no significant chromium contamination was measured in samples evaporated on the hot plate.

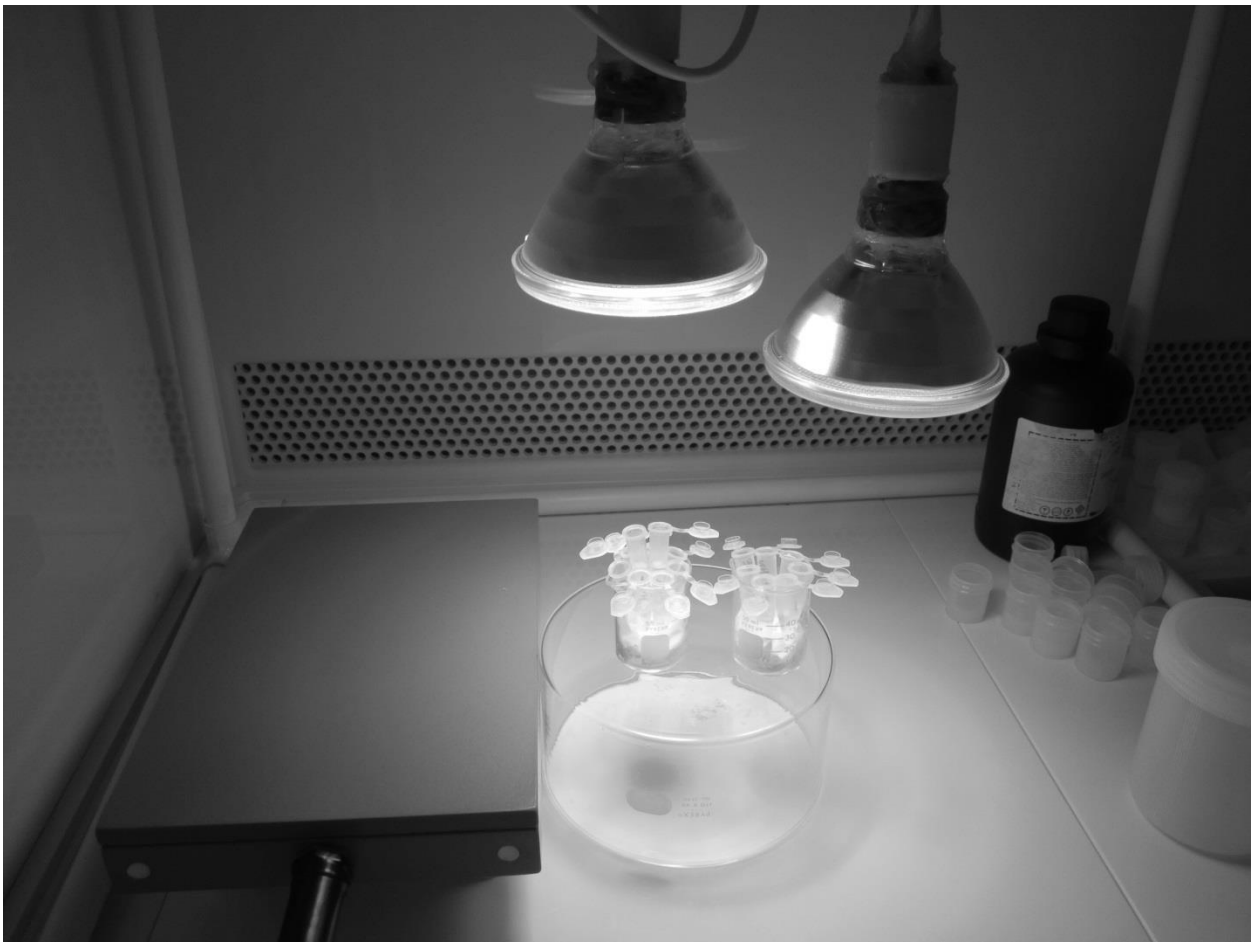

Figure 15: Picture of the fume hood in Calgary, Alberta. Note the close proximity of the heat lamps and the hot plate.

Chapter 4: Results and Discussion

Using the analytical technique, samples were measured for iron isotope amount ratios by the MC-ICP-MS. This section discusses the precision and accuracy of the measured data focusing on one data set measured multiple times in two different laboratories. Calculations are presented to determine the uncertainty in the $\delta(^{56/54}Fe)$ value. This section discusses and interprets the data for the three study sites: the Cardium formation, Lake Vida and Nova Chemicals.

4.1 Precision and Reproducibility

Accurate delta values are essential in the interpretation of data. Precise delta values provide confidence in and confirm the interpretation of the measured data. Throughout the development of the analytical technique, the goal was to obtain the highest precision and accuracy for the measured data. Early measurements of iron isotope amount ratios were met with varying degrees of success. As discussed in the methods section, problems with magnet stability, chromium contamination as well as residual chlorine complexes or organic material affected both the precision and accuracy of the measured delta values. Some early results for iron delta values are shown in Table 8. The $\delta(^{57/56}Fe)$ values are reported to highlight the negative impact in the precision and accuracy that factors such as magnet stability and chlorine complexes had on the data (BF=before problems were addressed, V= verified delta value for the sample).

Table 8: Comparison between data obtained in the early stages of development to the true iron delta values obtained through research in Germany and in Calgary.

Sample Name	$\delta(^{57/56}Fe)_{BF}$ (‰)	$\delta(^{57/56}Fe)_{V}$ (‰)
S10	-0.17	-0.01
	-0.18	
	0.19	
S27	0.13	0.03
	0.29	
	0.10	
S33	0.07	-0.03
	0.02	
	-0.12	

The $\delta(^{57/56}Fe)_{V}$ values are the delta values that have been verified for a sample based on results obtained from experience gained in an isotope laboratory in Germany. The measured $\delta(^{57/56}Fe)_{BF}$ have a poor level of precision (2 standard deviation = 0.2 - 0.4 ‰). As well as low precision, a low level of accuracy was obtained; the measured delta values differed by up to 0.3 ‰ from their true values. If the $\delta^{56/54}Fe$ values were considered in Table 8, on top of the difficulties mentioned, chromium contamination could result in up to a 1 ‰ shift from true values. All these factors resulted in the inability to quantify mass dependent fractionation and provided little confidence in the measured data resulting in difficulty interpreting the data.

Once analytical issues had been addressed samples were reanalyzed for iron isotope amount ratios. At that time, delta values for one of the analyzed data sets had been obtained using both sample standard bracketing and double spike techniques from work at the University of Tübingen, Germany with Dr. Ronny Schoenberg. The analytical technique for iron isotope measurements was well established at this laboratory (Schoenberg & von Blanckenburg, 2005) which allowed delta values measured in Calgary to be compared to the verified delta values for the samples.

Table 9 shows the $\delta(^{56/54}Fe)$ values for a set of samples measured both at the University of Calgary and the University of Tübingen. The ion exchange method used in both laboratories is comparable. The data set also demonstrates two mass bias correction techniques, double spike and sample standard bracketing (Chapter 3.3). The two sample standard bracketing-Germany columns represent the same ion exchanged sample measured twice by the mass spectrometer during a single analytical measurement session. Of all the mass bias correction techniques, the double spike technique is generally thought to provide more robust data. Double spike mass bias correction technique can provide reproducible and accurate delta values even when concentrations of matrix components are high and delta values are generally not affected by incomplete recovery during ion exchange (Dideriksen et al., 2006).

The data demonstrate that the sample standard bracketing and double spike technique can provide results identical within analytical uncertainty, 0.05 ‰ – 0.15 ‰ (Johnson et al., 2008). For example, the M 11 3-11 sample has an average $\delta(^{56/54}Fe)$ of 0.514 ‰ for double spike and 0.529 ‰ for sample standard bracketing, a 0.014 ‰ difference. Even the largest difference in delta values between SSB and DS, observed in M11 4-14 (0.087 ‰), is within expected uncertainties, 0.05 to 0.15‰, based on values reported in literature. The agreement between the data obtained using sample standard bracketing and double spike suggests than both mass bias correction techniques provide accurate and reproducible data and can be used interchangeably when required.

Table 9: Comparison of iron isotope data obtained using two mass bias correction techniques, as well as two different laboratories. Samples are from the Cardium formation.

Sample Name	DS – Germany $\delta(^{56/54}Fe)$ (‰)	DS - Calgary $\delta(^{56/54}Fe)$ (‰)	SSB-Germany $\delta(^{56/54}Fe)$ (‰)	SSB-Germany $\delta(^{56/54}Fe)$ (‰)	SSB-Calgary $\delta(^{56/54}Fe)$ (‰)
M11 3-11	0.50	0.52	0.55	0.51	0.53
M11 4-12	0.38	0.30	0.34	0.34	0.41
M9 02 12-11	0.36		0.33	0.32	0.42
M10 7-11	0.25		0.23	0.24	0.23
M9 10-11	0.36		0.26	0.32	0.30
M11 1-11	-0.32		-0.34	-0.42	-0.36
M11 9-10	0.47		0.48	0.41	0.42
M8 1-13	0.67		0.53	0.54	
M11 4-14		-0.85	-0.78	-0.75	-0.77
M8 8-11			0.37	0.38	0.38
M10 9-11			0.22	0.23	0.26
Pipe	0.14				0.13
S10	0.00		-0.02	-0.06	-0.02
S15	0.08		0.02	0.06	
S20	0.18		0.10	0.10	0.09
S24	0.09		0.09	0.07	0.04
S25	0.12		0.07	0.13	0.08
S27	0.10		0.02	0.06	0.07
S33	-0.17		-0.20	-0.16	-0.08
S39	-0.03		-0.07	-0.02	
S45	0.03				0.08
S51	-0.06				0.06

As mentioned, this data set enables the comparison of the analytical technique developed in Calgary to an established analytical technique. Comparing the sample standard bracketing data, good agreement is observed between the data obtained in Calgary and in Germany. In general, the difference between the measured delta value from Germany and Calgary is less than 0.08 ‰. One notable exception is the M9 02 12-11 sample where there is approximately a 0.107 ‰ difference.

However, the difference between the delta values is not a good estimate for the precision in the delta values. To determine the uncertainty in the measured iron delta values the Guide to the Expression of Uncertainty in Measurement (GUM) was used (JCGM, 2008) was used. In this guide, two methods for uncertainty analysis are given, Type A and B. For this thesis, Type A uncertainty, obtained from a series of observations, will be considered. Using the procedures outlined in GUM, the variability in observed values or expected experimental standard deviation (s) can be determined, Equation XIX.

$$s = \sqrt{\frac{1}{n-1}\sum_{j=1}^{n}(q_j - \bar{q})^2}$$

Equation XIX

Where n is the number of data points, q_j is a specific data point and $\bar{q}$ is the average value of all data points. The expected experimental standard deviation is then quoted as the measurement uncertainty, 1 s at the 68.2 % confidence level and 2 s at the 95.4 % confidence level. The calculated s values for all samples above are shown in Table 10, uncertainty is in the measured $\delta(^{56/54}Fe)$. Uncertainty in Table 10 is reported at the 2s level based on convention in literature.

Table 10: Type A uncertainty calculated using the GUM guide for the data in Table 9. Samples with (*) have replicate analyses not shown in Table 9.

Sample Name	Uncertainty (‰)		Sample Name	Uncertainty (‰)
M11 3-11	0.039		**S10**	0.054
M11 4-12 (*)	0.072		**S15**	0.068
M9 02 12-11 (*)	0.124		**S20**	0.083
M10 7-11	0.018		**S24**	0.046
M9 10-11	0.082		**S25**	0.056
M11 1-11	0.087		**S27**	0.062
M11 9-10	0.072		**S33**	0.106
M8 1-13	0.164		**S39**	0.062
M11 4-14	0.092		**S45**	0.072
M8 8-11 (*)	0.016		**S51**	0.170
M10 9-11 (*)	0.038		**Pipe (*)**	0.080

The largest uncertainty is observed in samples S51, M902 12-11, M8 1-13, M11 4-14 and S33. A few factors could have contributed to the increased uncertainty including low statistics (S51 and M8 1-13) or delta values obtained prior to all problems were addressed (S33, S51). The type A uncertainty gives a better representation of the uncertainty in samples when there are a high number of replicates. If we consider samples with a high number of replicate analyses (5, 6 or 7) for example M11 3-11, M11 4-12, M8 8-11 and M10 9-11 the maximum determined uncertainty is 0.072 ‰. Taking into account known factors that likely affected the measured delta values, all relevant samples except M9 02 12-11 show uncertainty (2s) less than 0.092 ‰ (95 % of considered samples). Therefore, our reported uncertainty in the $\delta(^{56/54}Fe)$ is 0.09 ‰ under ideal operating conditions. This is comparable to uncertainties reported in literature by other laboratories (Johnson et al., 2008). A similar calculation for the $\delta(^{57/54}Fe)$ value provides an uncertainty of 0.19 ‰ (2s). The uncertainty in the $\delta(^{57/54}Fe)$ value is approximately $1.5*\delta(^{56/54}Fe)$

as expected with the slight increase likely due to the lower abundance of ^{57}Fe. The $\delta(^{56/54}Fe)$ and $\delta(^{57/54}Fe)$ are the values generally reported in literature.

The agreement between the data, obtained in Calgary and Germany, suggests that procedures implemented to improve precision and accuracy were successful. The expected abundance of 54 atoms in the sample suggest than the heat lamps were indeed the primary source of chromium contamination. Therefore, in all successive iron measurements drying samples under or near heat lamps should be avoided unless heat lamps can be acquired that do not leach chromium. Figure 16 shows selected data obtained in March 2013 after all problems had been addressed. The measured delta values are within expected uncertainty of the mass dependent fractionation line demonstrating that there is no significant chromium in these samples.

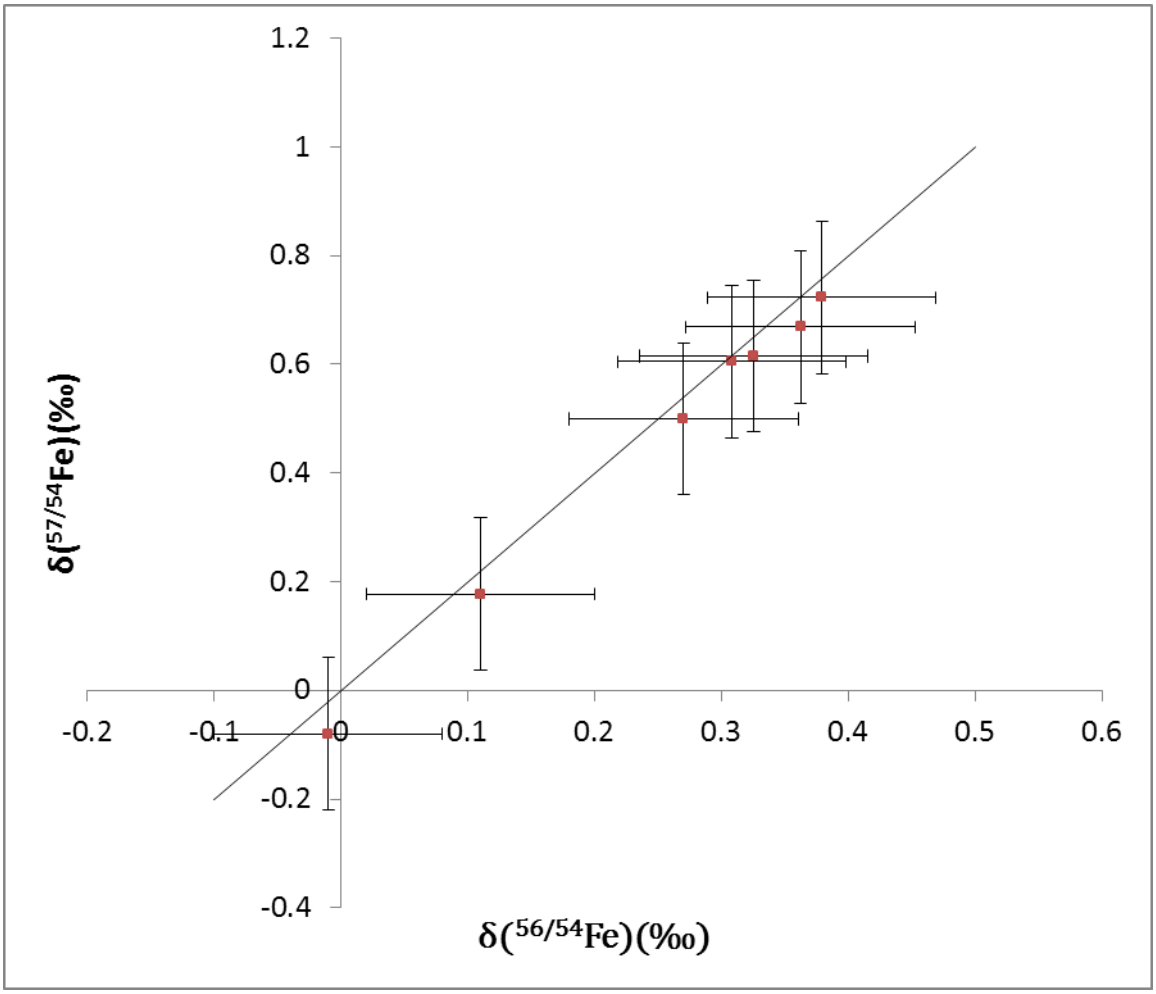

Figure 16: Iron isotope data obtained on March 21st 2013. There is no excess 54 atoms measured in these samples indicating no chromium contamination occurred during sample preparation

4.2 The Cardium Formation

The Cardium Formation is located in the Pembina oil field near Dayton Valley, Alberta, Canada. Oil extraction started in 1953 and primary, secondary and tertiary oil recovery techniques have been used to extract oil. An extensive study into the geochemistry of the site was complete by Nightingale, 2010, before and after tertiary oil recovery or CO_2 injection commenced. Increased iron concentrations were measured after CO_2 injection in reservoir waters. An extensive discussion of this site can be found in Chapter 1.5.1.

4.2.1 Optimal Digestion Conditions for Siderite from the Cardium Formation

The goal of this analysis was to determine the source of the increasing iron content in reservoir water sourced from injection wells; siderite dissolution or acid leaching of the iron production pipe were considered. Water samples were collected from numerous injection wells (samples starting with M), siderites (samples starting with S) were collected from drill cores and a piece of production pipe used in an injection well was obtained (digestion procedures are discussed in the Methods section). One of the first considerations was the type of acid used to digest the siderite samples. Previous attempts at a pyrite (FeS) digestion (not reported) suggested than nitric acid was the most effective at removing the iron from its mineral form and placing it into solution. However, previous molybdenum analyses on shale samples completed by colleagues in the laboratory suggest hydrochloric acid is more effective dissolving Mo from a mineral matrix. Therefore, two siderite samples were chosen and an HCl and HNO_3 digestion was performed on each sample using the procedure described in the methods section and iron isotope data are summarized in Table 11.

Table 11: Comparison of nitric acid and hydrochloric acid siderite digestion

Sample	Acid Used for Digestion	$\delta(^{56/54}Fe)$ (‰)
S24	HNO_3	0.10
S24	HCl	0.08
S27	HNO_3	0.08
S27	HCl	0.09

The measured $\delta(^{56/54}Fe)$ values for each digestion were within expected analytical uncertainty therefore, both digestion methods provided comparable delta values. For all reported siderite samples, a HNO_3 digestion was performed. The obtained $\delta(^{56/54}Fe)$ values for the siderites, waters and pipe are summarized in Table 9 above and shown graphically in Figure 17 below. Replicate analyses are shown in Figure 17. Error bars are not shown, the uncertainty in the $\delta(^{56/54}Fe)$ is 0.09 ‰ (2s) and the $\delta(^{57/54}Fe)$ is 0.19 ‰ (2s), based on calculations done in the Chapter 4.1. The siderite samples have approximately a 0.3 ‰ variation in the $\delta(^{56/54}Fe)$ value. The $\delta(^{56/54}Fe)$ value of the pipe is similar to the upper range in siderite values. The water samples show two distinct populations: nine samples have positive $\delta(^{56/54}Fe)$ value between 0.25 to 0.67 ‰ and two water samples have negative $\delta(^{56/54}Fe)$ between -0.36 and -0.77 ‰.

4.2.2 What is the Source of Increased Iron?

Two possible sources were suggested for the increased iron concentrations measured in the reservoir fluids: siderite dissolution and leaching of production piping. The possibility that either of these sources is the source of the increased iron will be discussed.

First, the iron isotopic composition for the two sources was determined. The iron isotopic composition of the pipe is $\delta(^{56/54}Fe)$ = 0.14(9) ‰. The $\delta(^{56/54}Fe)$ values of the siderite ranges from -0.17(9) ‰ to 0.12(9) ‰. The range of $\delta(^{56/54}Fe)$ values for the siderite in this formation is in the upper range of delta values measured for siderite (Johnson et al., 2003; Markl et al., 2006).

The delta values of the siderite could provide insight into the formation pathways for the siderite in the formation. Siderite precipitation is expected to result in a difference in $\delta^{56/54}Fe$ between the aqueous iron and siderite of +0.5 ‰ ($\Delta^{56/54}Fe_{aq\text{-}siderite} \approx +0.5‰$) (abiotic) and siderite production during DIR (biotic) results in $\Delta^{56/54}Fe_{aq\text{-}siderite} \approx +0$ ‰ (Johnson et al., 2004b). Based on these fractionations, we can then start to constrain the mechanisms involved in formation for siderite.

The iron concentration of the reservoir waters spiked after CO_2 injection commenced (Nightingale, 2010). All measured water samples were collected after CO_2 injection and only one sample from each well was obtained. After iron isotopic analyses were completed on the water samples, two distinct populations could be identified. Both waters enriched and depleted in the heavier isotopes of iron were identified suggesting different conditions in both populations. However, we cannot access how conditions in the wells changed after CO_2 injection due to sample limitations.

First, the waters depleted in the heavy isotopes have isotopic signatures similar to typical ravine environments, -1 to 0 ‰ (Johnson et al., 2008). However, the iron concentration measured in the reservoir water of these wells is higher than the source of water, the North Saskatchewan River (Nightingale, 2010) and on the upper end of iron concentrations typically observed in ravine environments (Johnson et al., 2008). Iron concentrations of 4.0 μg/g and 17.6 μg/g were previously measured in reservoir water from wells M11 1-11 and M11 4-14 respectively (Nightingale, 2010). The primary source of iron in ravine environments is weathering of iron bearing minerals. In this formation, there is likely extensive weathering of formation minerals caused by water flood. Of note, CO_2 injection in these wells started later than

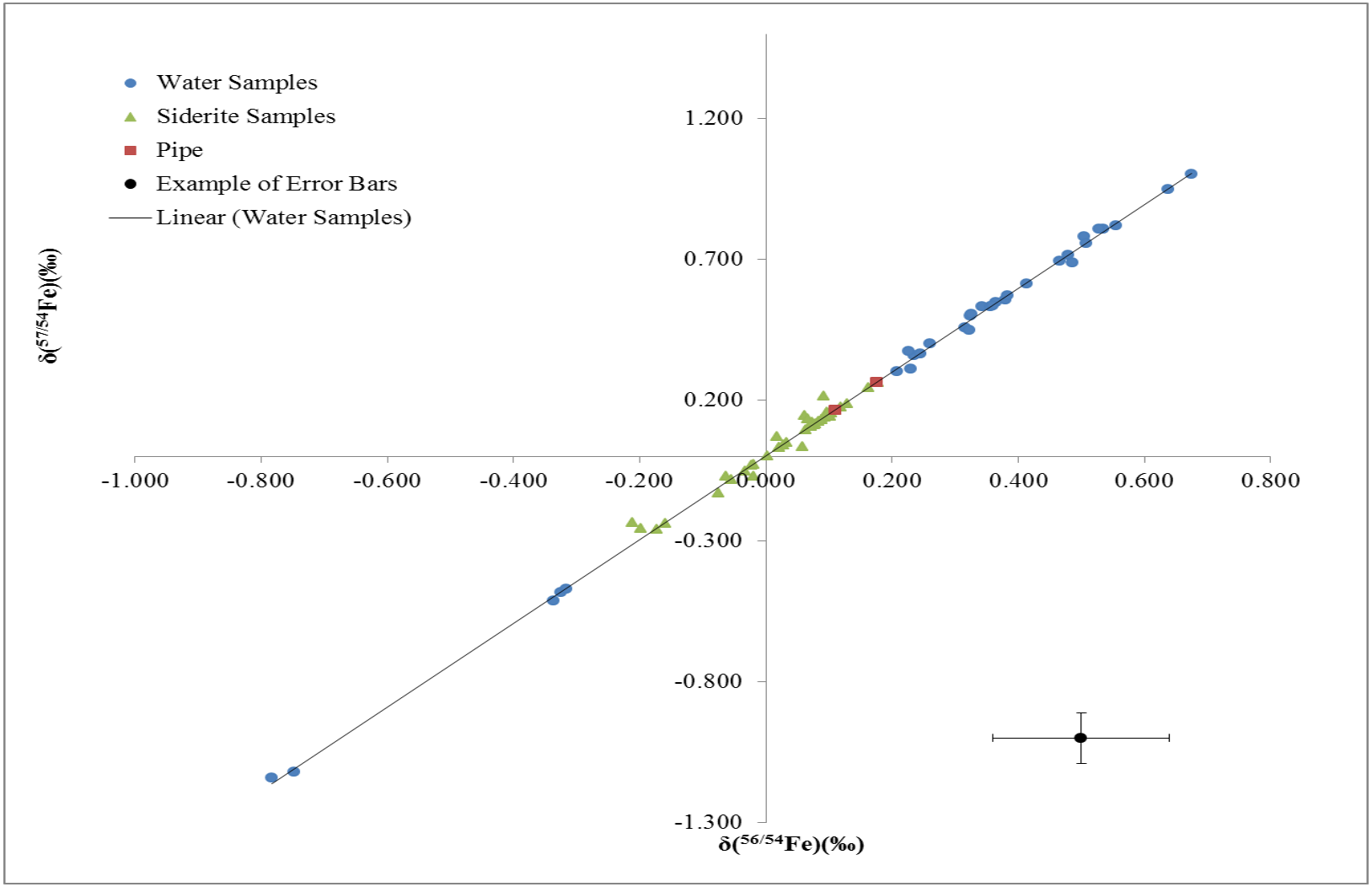

Figure 17: A three isotope plot for the iron delta values obtained for the siderites, reservoir waters and pipe in the Cardium formation study. Typical error bars are shown in the lower right side of the diagram.

the other measured wells therefore, the reservoir water from these wells has had less time to interact with the increased CO_2 environment. Therefore, the negative $\delta(^{56/54}Fe)$ values in these wells could be indicative of conditions before CO_2 injection however, more data would be needed to confirm this hypothesis.

The iron isotopic composition of the remaining nine wells is unique as aqueous iron is generally depleted in the heavier isotopes of iron (Johnson, Beard, & Roden, 2008). From the measured $\delta(^{56/54}Fe)$ values we can say that neither leaching of iron pipe or siderite dissolution is the only process occurring in the formation. If acid leaching of the production pipe was solely responsible for the increased iron in reservoir waters, the $\delta(^{56/54}Fe)_{water}$ would be less than or equal to the $\delta(^{56/54}Fe)_{pipe}$ based on the fractionation typically observed between ferric oxides and aqueous iron (Johnson et al., 2004b). Similarly, if siderite dissolution was solely responsible for the increased iron concentrations $\delta(^{56/54}Fe)_{water}$ would be isotopically lighter than the siderite based on typical mineral weathering processes (Dauphas & Rouxel, 2006). Elemental analyses also seem to suggest that siderite dissolution is not occurring in the formation. Nightingale (2010) did not see a positive correlation between magnesium and iron concentrations in the reservoir fluids as would be expected during siderite dissolution since the siderites contain significant amounts of magnesium. Therefore, either a different source is contributing to the increased iron concentrations in these reservoir fluids or the isotopic composition of the iron is being altered after leaching. Three possible explanations for the positive $\delta^{56/54}Fe$ values will be discussed: sorption, bacterial sulfate reduction and an unknown source of iron.

At some point in the formation history, aqueous iron could have been adsorbed onto the minerals in the formation. Adsorbed iron is isotopically heavier than the aqueous iron, the extent of fractionation depending on whether biotic or abiotic processes were responsible (Icopini et al.,

2004). Adsorbed iron is also in the ferrous state. In experiments studying adsorbed iron, a weak acid solution was used to remove the adsorbed iron (Crosby et al., 2007). After CO_2 injection, the pH of the reservoir waters decreased (Nightingale, 2010). The acidification of the reservoir water could have caused any adsorbed iron to be released from the minerals into solution thus increasing the iron concentrations and resulting in positive $\delta(^{56/54}Fe)$ values. To test this hypothesis, minerals could be analyzed for adsorbed iron following established procedures (Crosby et al., 2007; Johnson & Beard, 2007; Icopini et al., 2004). Also samples in new injection wells should be collected before and after CO_2 injection to measure any shift in the $\delta(^{56/54}Fe)$ values which would provide insight into how the $\delta(^{56/54}Fe)$ changed after CO_2 injection.

Siderite dissolution and acid leaching of the iron pipe were the two possible sources of iron investigated in this thesis. However, other studies propose a possible third source of iron in the formation (Zymela, 1996). Based on previous analyses by Zymela (1996), Nightingale (2010) suggested that iron oxide coatings (ferric iron) on the clays could be released during acidification of the formation. Dissolution of other iron bearing minerals, pyrite, could also increase iron concentrations in the reservoir waters. Therefore, iron isotopic analyses of the clays and pyrite in the formation could test whether iron oxide coatings or pyrite dissolution were responsible for the $\delta(^{56/54}Fe)$ values measured in the reservoir waters based on reported fractionations between these solid iron sources and aqueous iron (Dauphas & Rouxel, 2006).

Finally, positive $\delta(^{56/54}Fe)$ values in aqueous environments could be a result of bacteria sulfate reduction (BSR). If BSR were occurring, iron concentrations would be expected to decrease due to precipitation of iron bearing minerals (Johnson et al., 2008). Therefore, some other source, the acid leaching of the pipe, siderite dissolution or dissolution of other iron bearing minerals, must have been the source of increased iron concentrations. The isotopic

composition of the aqueous iron was then altered through BSR and resulted in decreased iron concentrations. Nightingale, 2010 did measure a decrease in iron concentrations of the reservoir waters after the initial spike caused by CO_2 injection. In BSR, sulfates are reduced to sulfides (Equation IV) which then precipitate with aqueous iron to form reduced iron/sulfur compounds such as pyrite ($\Delta^{56/54}Fe_{water\text{-}minerals} \approx +0.5$ ‰). As mentioned, the injected CO_2 reacts with the water in the formation to form H_2CO_3 (Equation VII) however, CH_2O can also be formed through oxygenic photosynthesis (Equation XX) (Johnson et al., 2008). The CH_2O produced then provides the necessary organic matter for BSR to occur.

$$H_2O + CO_2 \rightarrow CH_2O + O_2$$

Equation XX

If BSR were occurring in the formation we would expect to observe a decrease in sulfate concentration in the reservoir waters and a distinct isotopic sulfur composition of the sulfates. Approximately a 2.5 fold decrease in sulfate concentrations was observed however, sulfur isotopic data for the sulfates were not measured (Nightingale, 2010). We could also argue that the iron isotopic composition of reservoir waters with lower iron concentrations would be more affected by BSR than high iron concentration wells. Assuming identical conditions in all the wells and that BSR is the only mechanism affecting the iron isotopic composition of the waters, a plot of delta values verses inverse concentration could then provide the iron isotopic composition of the iron source (Figure 18).

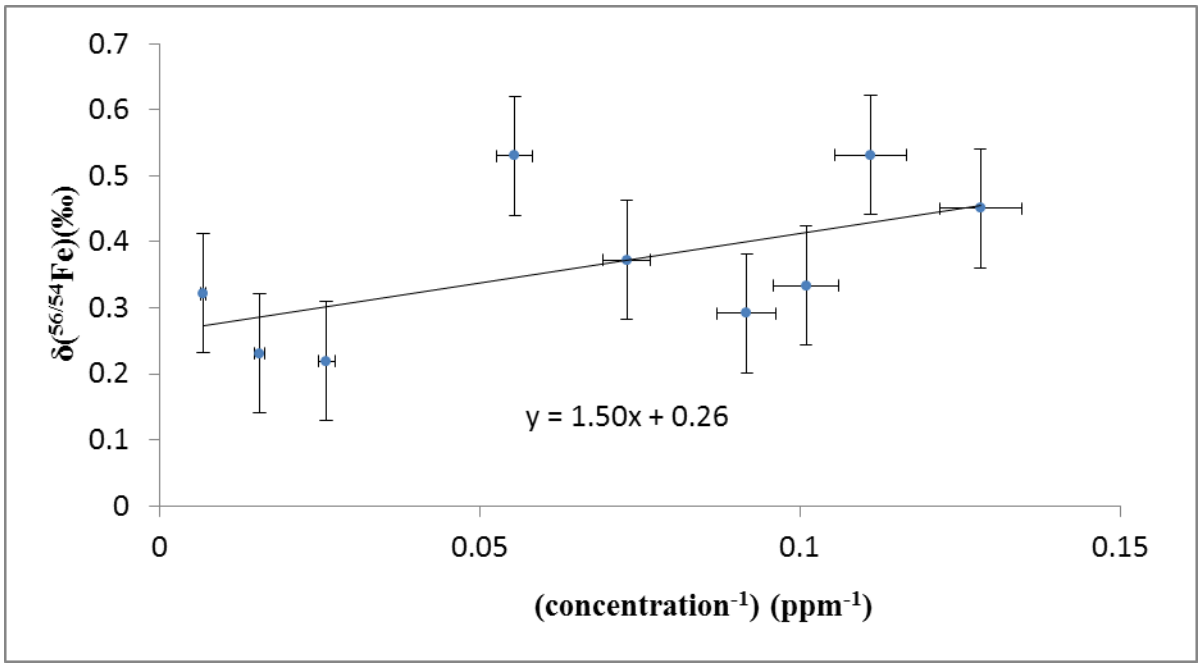

Figure 18: Plot of iron delta value verse the inverse in concentration to determine the iron isotopic composition of a potential source if BSR is occurring in the Cardium formation.

From the y intercept of the graph a source isotopic composition $\delta(^{56/54}Fe) = 0.26 \pm 0.05$ ‰ was determined which is similar to siderite and pipe values. However, due to the large uncertainty it is not possible to conclusively determine the source of iron. Uncertainty for the intercept was determined using linear regression techniques. As can be seen from the graph, a linear fit does not characterize the data possibly indicating conditions in each well may not be identical. However, this graph does point to the possibility that BSR is responsible for the measured $\delta(^{56/54}Fe)$ values.

To determine conclusively if BSR is occurring in these wells, the sulfur isotopic composition of the sulfates should be measured, the concentration of iron/sulfide minerals in the formation should be tracked or the iron isotopic composition of the reservoir waters could be measured over time to observe changes that are occurring.

4.2.3 Future Investigations

From the data, three distinct populations can be identified and informed conclusions can be made regarding the source of increased iron concentrations in reservoir waters. Possible mechanisms can be suggested and studies proposed to test the hypotheses. Specifically, in future investigations well water samples should be collected before, during and after CO_2 injection in order to quantify the changes in the iron isotopic composition of the waters. Isotopic analyses of other elements such as sulfur could be used to determine if BSR is occurring. Magnesium isotopic compositions of the siderites and waters could also suggest if siderite dissolution is occurring whereas isotopic analyses of other heavy metals (Ni, Cr, and Zn) could support acid leaching of the pipe.

4.3 Lake Vida

Lake Vida is an anoxic lake in Antarctica and conditions in Lake Vida have been suggested as an analog for Jupiter's moon Europa. Six brine samples were obtained from a 2010 expedition described in Murray et al. (2012) to study the physical and chemical conditions in the lake. Three samples of the brine were collected from a borehole in the ice of Lake Vida. During the initial sampling the goal was to collect samples at different depths. Samples at different depths could show variations in iron isotopic signatures based on the conditions in the brine. However, during sampling mixing of samples at different depths likely occurred which would result in homogeneity of all the samples. Whole brine samples and filtered brine samples were received in Calgary. The samples were filtered by the collaborators using a 0.2 μm filter to remove any precipitates. Based on the sampling methods, all samples are expected to be isotopically similar. Iron delta values are summarized in Table 12. Six un-numbered samples

were received. Once received, samples were labeled 1, 2, or 3 to allow replicate analyses of samples. Therefore, whole brine 1 is not necessarily the same as filtered brine 1.

Table 12: Iron isotope data for Lake Vida brine

Sample	$\delta(^{56/54}Fe)$ (‰)	$\delta(^{57/54}Fe)$ (‰)
Whole Brine 1	-2.79	-4.06
Whole Brine 2	-2.77	-4.12
Whole Brine 3	-2.46	-3.67
Filtered Brine 1	-2.64	-3.92
Filtered Brine 2	-2.49	-3.62
Filtered Brine 3	-2.81	-4.00

The $\delta(^{56/54}Fe)$ values measured for the Lake Vida brine are unique in terrestrial environments. The measured $\delta(^{56/54}Fe)$ values lie at the lower range of iron variation measured to date and thus constrain possible mechanisms which could have produced these unique iron delta values. At first glance, the variability in the $\delta(^{56/54}Fe)$ values, 0.16 ‰ (2s) is larger than the expected uncertainty, 0.09 ‰ (2s). Two factors could have contributed to the decrease in precision: inhomogeneity of the samples and incomplete separation of iron from the sample matrix.

Three different sets of samples were received and based on the sampling methods were expected to have similar iron isotopic compositions and iron concentrations. Small variability in iron concentration was observed between the samples suggesting not all samples were identical. Therefore, it is possible that different iron isotopic signatures exist for the samples. Secondly, the

concentration of matrix elements in the sample prior to ion exchange is high and incomplete separation could have occurred. For example sodium concentrations were approximately 25,000 ppm and sodium partially co-elutes with iron during ion exchange chromatography (Figure 7-B). Increased sodium concentrations have been found to affect signal stability and nebulizer aspiration rate thus affecting the mass bias. This would result in the observed decrease in precision and passing the samples through the ion exchange columns twice would likely reduce this effect, but this was not done. The decrease in precision was not deemed significant specifically for these samples as accurate interpretation of the data could still be achieved due to the unique isotopic signatures measured. These delta values are only observed in a small number of systems and scenarios which could produce these low delta values will be discussed.

4.3.1 Dissimilatory Iron Reduction

Dissimilatory iron reduction (DIR) is thought to be one of the oldest forms of respiration (Vargas et al., 1998) and is given by Equation V above. The early signature of DIR is preserved in banded iron formations and provides insight into DIR under anoxic atmospheric conditions (Johnson et al., 2003). For DIR to occur, anoxic conditions, organic matter and ferric iron minerals are required. The organic matter is oxidized and the iron minerals are reduced. Therefore, dissimilatory iron reduction can produce high quantities of $Fe(II)_{aq}$ and $\delta(^{56/54}Fe)$ for the aqueous iron are typically 1 ‰ to 3 ‰ lower than the mineral form of iron (Crosby et al., 2007; Johnson et al., 2008).

The measured $\delta(^{56/54}Fe)$ values for the Lake Vida samples lie in the lower range of iron fractionation measured on Earth to date. Lake Vida brine does contain organic matter and microbes were found in the lake. However, all evidence to date suggests that they are not actively processing elements. This was determined using the $\delta^{13}C$ of the dissolved inorganic

carbon, the $\delta^{34}S$ of sulfate and the $\delta^{15}N$ of NO_2 (Murray et al., 2012). Iron bearing minerals were also present around the lake which could have provided the needed iron minerals for DIR to occur. The iron isotope data cannot, on its own, confirm DIR is responsible for the measured $\delta(^{56/54}Fe)$ values as there are other mechanisms, discussed below, which could account for the measured $\delta(^{56/54}Fe)$ values. Two analyses could be performed to investigate whether DIR is occurring in the brine, $\delta^{13}C$ analyses on the CO_2 head space of the brine compared to the $\delta^{13}C$ of the dissolved organic carbon (Romanek et al., 2003) and iron isotopic analyses on the iron bearing minerals surrounding the lake. If bacteria are active in the harsh conditions of the brine, studies considering the possibility of extra-terrestrial life are provided with a unique terrestrial analog to possible extra-terrestrial conditions.

4.3.2 Weathering of Existing Iron Minerals

As mentioned, Lake Vida brine comes into contact with iron bearing minerals which could be a possible source of the iron in the lake (Murray et al., 2012). Weathering under anoxic conditions removes the soluble ferrous iron from surface minerals (Johnson & Beard, 2005). Under anoxic conditions, no fractionation would be encountered between the $\delta(^{56/54}Fe)$ of the iron mineral and aqueous weathered iron as no changes in oxidation state would occur during weathering. They also suggest that large aqueous iron contents would be observed similar to the conditions at Lake Vida. The data cannot conclusively determine if weathering has occurred, however, if weathering is the source of iron in the brine, the iron bearing minerals surrounding the lake that experience weathering would have to be significantly depleted in the heavier isotopes of iron (around the measured brine values). These $\delta(^{56/54}Fe)$ values for minerals are not typical (Johnson et al., 2003) except in iron bearing minerals in banded iron formations which were deposited before the oxidation of the atmosphere (Johnson et al., 2008). If weathering is the

source of the iron in the brine, Lake Vida could provide insight into conditions on Earth prior to the oxidation of the atmosphere.

4.3.3 Sorption of Iron

A third possible mechanism which would produce the measured $\delta^{56/54}Fe$ values is sorption. Sorption of iron occurs when aqueous iron, adsorbs onto the surface of existing minerals. This results in iron fractionation, as the heavy isotopes preferentially adsorb onto the minerals. Adsorption can be produced by both abiotic and biotic processes with $\Delta^{56/54}Fe_{aq\text{-}Fe(III)source}$ larger for biotic processes than abiotic processes (Icopini et al., 2004). In abiotic processes, the adsorbed iron is 2 ‰ heavier than the aqueous iron and in biotic experiments the adsorbed iron is up to 4 ‰ heavier than the aqueous iron (Icopini et al., 2004). Again, the data set above cannot confirm or deny the presence of adsorption, iron isotope analyses of the minerals would be required. Analyses of both isotopic analyses of total mineral and adsorbed iron could provide insight into this process.

4.3.4 Future Investigations

The iron isotope analyses of the brine samples revealed a distinct an isotopic signature which is typically not observed in current aqueous environments. Multiple processes could have resulted in the observed $\delta(^{56/54}Fe)$ values and iron isotopic analyses of iron bearing minerals surrounding the lake could provide insight into the source of iron or processes occurring in the lake. Other isotopic analyses, for example the $\delta^{13}C$ of CO_2 from the brine, could also provide insight into the unique conditions present at Lake Vida.

4.4 Nova Chemicals Bioremediation Results

A bioremediation experiment was performed by Nova Chemicals in an anaerobic environment using bacteria cultured from a future study site in Alberta, Canada. Solid ferric

oxyhydroxide was used as the iron source and bacteria were present in an aqueous growth medium. From the growth chamber, samples were removed on eight different occasions separated by three days. Three replicates were taken each time resulting in 24 samples. These samples were analyzed for iron concentrations by isotope dilution using a single ^{54}Fe spike and iron isotope amount ratios using a double spike. Results are summarized in Table 13.

The concentrations of the replicate samples from the same day varied significantly. Since all three replicates were collected at approximately the same time from the anaerobic chamber at Nova Chemicals, they should be identical in both iron concentration and isotopic composition. However, the iron concentrations measured using isotope dilution, were different. The variable iron concentrations were thought to result from ineffective sub-sampling at the University of Calgary. Iron isotope data could test this hypothesis and will be discussed below. At the Nova Chemicals laboratory, the samples were collected from the anaerobic chamber into 150 ml glass containers. The samples were sealed in an anaerobic atmosphere to prevent the oxidation of iron. Each sample contained the growth medium possessing aqueous (reduced) iron and solid ferric iron. The iron isotopic composition of the aqueous iron can provide insight into whether DIR is occurring. To isolate the aqueous iron for analyses, the bottles were placed on their sides and left over night. The ferric oxyhydroxide should settle near the bottom. A syringe was used to pierce the re-sealable opening and approximately 5 mL of solution removed and weighed. This method of sampling assumed that no ferric oxyhydroxide was in solution nor was sampled inadvertently. However, the ferric oxyhydroxide tended to settle near the opening and any small movement of the bottle disturbed the settled iron. Therefore, it is likely that despite the precautions taken to avoid sampling the ferric oxyhydroxide, it was sampled in varying amounts for each sample. The

ferric oxyhydroxide would then obscure the aqueous iron signature and iron isotopic analyses of the sub-sampled growth medium could test this hypothesis.

Iron isotope amount ratios were obtained for a sub set of data to determine if the ferric oxyhydroxide was sampled along with the aqueous iron. The analyzed sub set of samples were chosen based on the measured iron concentrations. Days where low and high iron concentrations were measured were analyzed for iron isotope amount ratios to determine if the isotopic signature of high iron concentration samples trended towards the initial isotopic composition of the ferric oxyhydroxide. The results are summarized in Table 13. All $\delta(^{56/54}Fe)$ values were determined using double spike to achieve the highest precision possible. For comparison, the ferric oxyhydroxide used in the experiment has a $\delta(^{56/54}Fe)$ of +0.33(9) ‰. The error in the measured $\delta^{56/54}Fe$ values for all samples is 0.09 ‰, discussed above. One sample, November 6th (1), has a larger error due to difficulties encountered during measurement such as large changes in the mass bias, and low statistics. The error for this measurement was assessed using the DS algorithm and the internal precision of the measured ratios. The error associated with the concentration measurements is ± 2 % based on the variability measured during calibration of the spike.

Not all samples were analyzed for iron isotope amount ratios as the proposed hypothesis for the mismatched intensities was verified with the measured data. The samples with higher iron concentrations tend towards the isotopic composition of the ferric oxyhydroxide and samples with lower iron concentrations are enriched in the light isotopes of iron compared to the ferric oxyhydroxide. The $\delta(^{56/54}Fe)$ values support the assertion that ferric oxyhydroxide was sampled with the aqueous iron. Therefore, in successive experiments modifications should be made to the sampling procedure including filtering of the sample to remove particulates. Also, if a syringe

Table 13: Iron concentration data measured using isotope dilution for the Nova Chemicals bioremediation study. Selected data on iron delta values are also presented. Error in iron concentration is ± 2 %

Sampling Date	Sample Number	Fe (ppm)	$\delta(^{56/54}Fe)$ (‰)
10/28/12	1	4.15	
10/28/12	2	1.47	
10/28/12	3	0.95	
10/31/12	1	1.21	
10/31/12	2	2.49	
10/31/12	3	1.11	
11/03/12	1	0.32	0.22(9)
11/03/12	2	0.20	0.27(9)
11/03/12	3	0.17	0.30(9)
11/06/12	1	0.11	-2.1(5)
11/06/12	2	0.62	0.33(9)
11/06/12	3	0.28	-1.11(9)
11/09/12	1	0.33	
11/09/12	2	0.62	
11/09/12	3	0.28	
11/12/12	1	0.56	
11/12/12	2	0.84	
11/12/12	3	0.26	
11/15/12	1	0.08	-1.40(9)
11/15/12	2	0.10	-1.39(9)
11/15/12	3	0.26	-0.05(9)
11/18/12	1	0.05	-0.33(9)
11/18/12	2	0.33	0.27(9)
11/18/12	3	0.28	0.32(9)

with a longer needle were used the bottles could be allowed to settle upright. No ferric oxyhydroxide would be present at the opening and fewer disturbances of the samples would occur during sampling.

From the measured delta values, the experiment can be assessed. First, some extent of dissimilatory iron reduction is occurring. In the samples with low iron concentrations, negative $\delta(^{56/54}Fe)$ values are measured, which is typical of DIR. However, due to the mixing with the ferric oxyhydroxide no trend in $\delta(^{56/54}Fe)$ values can be observed as the experiment progressed. Secondly, the conditions of the experiment were likely not ideal to facilitate DIR. For example, the type of bacteria used in this study may not efficiently reduce organic matter by DIR and the duration of the experiment was likely too short. A similar study looking at different types of DIR bacteria, shewanella putrefaciens and Geobacter sulfurreducens, was completed over 280 days and observed significantly larger aqueous iron concentrations (Crosby et al., 2007). The bacteria used in our experiment (species unknown) were cultivated from the potential bioremediation site in Northern Alberta and may not participate as effectively in DIR.

If the experiment were repeated, careful consideration should go into the type of bacteria, length of experiment and sampling methods used to obtain optimal results and accurate $\delta(^{56/54}Fe)$ values for the reduced aqueous iron.

5. Conclusion

This thesis outlines the development of an analytical technique to measured iron isotope amount ratios in samples. The analytical technique developed consisted of two components: sample purification using ion exchange chromatography and sample measurement using MC-ICP-MS. The analytical technique was tested on a variety of samples including water, mineral and a biological growth medium. Numerous difficulties were encountered throughout the development including magnet stability, blank contributions and reproducibility. As techniques were developed to address these difficulties, the precision and accuracy of the measured iron isotope amount ratios improved. As the technique stands today, analytical precision is ± 0.09 ‰ (2s) in the $\delta(^{56/54}Fe)$ values. This precision is comparable to other laboratories preforming iron isotopic analyses. This thesis can serve as a guideline for conditions and tests that should be considered or performed prior to measurement of isotope amount ratios on the MC-ICP-MS in order to obtain precise and accurate data.

During sample purification, precautions should be taken to avoid chromium contamination possibly introduced from contaminated pipettes or from external sources such as heat lamps. After, ion exchange samples should be dissolved in concentrated nitric acid to remove any residual organic material or chlorine complexes. During sample measurement, careful consideration of operating conditions, including argon gas flow, torch position and the voltages applied to the ion optic lenses, is required to obtain accurate results. Position of the magnet on the low mass shoulder, intensity matching between samples and standards, and signal stability can all affect the measured $\delta(^{56/54}Fe)$ values. The tests completed in this thesis, including intensity matching and optimal measurement position, should be performed periodically during iron isotope measurements to ensure precise and accurate data are being

obtained. Also, when relevant, these tests should be performed with every element measured on the MC-ICP-MS to ensure the highest precision data. This thesis can also serve as a guideline for the analytical precision possible under ideal operating conditions.

Using the analytical technique developed, three sample sets were analyzed and some conclusions were drawn from the data. First, a source identification experiment was performed using samples from the Cardium formation. The iron source could not be positively identified. However, future analyses were suggested to help determine the source of increased iron. For example, magnesium and sulfur isotopic analyses of the water and minerals could provide the necessary data to positively identify the source of increased iron concentrations. Second, brine samples from an anoxic lake were analyzed. These samples highlighted the importance of complete separation of iron from the sample matrix, in this case sodium, as the precision in the $\delta(^{56/54}Fe)$ values was affected by high sodium concentrations. This lake has been suggested as an analog for Jupiter's moon Europa and iron data can provide insights into the conditions in the brine. Three scenarios were proposed including sorption, mineral dissolution and DIR however, no firm conclusions can be made solely on the iron data of the brine. Future analyses were proposed including obtaining iron isotope amount ratios for the iron bearing minerals in the Lake and carbon isotopic analyses to determine the exact processes involved in placing the iron into the brine. Finally, a bioremediation study was completed and the iron isotope data obtained from this experiment provided insights into sampling limitations. The iron data will enable the success of future experiments.

These three studies highlighted the importance of iron isotope data in determining conditions present in a system. The data obtained from the measured samples provided unique insights into systems which would have been unavailable before. Using the iron isotope data,

future investigations into these systems or bioremediation experiments can be structured to obtain the desired knowledge. Also, the iron analytical technique can now be applied to biological samples such as human or animal blood proteins, hair or nails to investigate iron fractionation mechanisms in the body.

References

Hacettepe Univserity . (2013). Retrieved April 8, 2013, from http://www.icp.hacettepe.edu.tr/LAICPMS_day1b.pdf

Aelion, C. M., Höhener, P., Hunkeler, D., & Aravena, R. (2010). *Environmental isotopes in biodegradation and bioremediation.* Boca Raton, FL: Taylor & Francis Group.

Albarède, F., & Beard, B. (2004). Analytical Methods for Non-Traditional Isotopes. *Reviews in Mineralogy & Geochemistry, 55*, 113-152.

Arnold, G. L., Weyer, S., & Anbar, A. D. (2004). Fe Isotopes Variations in Natural Materials Measured Using High Mass Resolution Multi Collector ICPMS. *Analytical Chemistry, 76*, 322-327.

Beard, J. L., Dawson, H., & Pinera, D. J. (1996). Iron Metabolism: A Comprehensive Review. *Nutrition Reviews, 54*(10), 195-317.

Beard, J. L., Dawson, H., & Pinero, D. J. (1996). Iron Metabolism: A Comprehensive Review. *Nutrition Reviews, 54*, 295-317.

Beckett, G. D., & Huntley, D. (1998). Soil Properties and Design Factors Influencing Free-Phase Hydrocarbon Cleanup. *Environmental Science and Technology, 32*, 287-293.

Birck, J. L. (2004). An Overview of Isotopic Anomalies in Extraterrestrial Materials and their Nucleosyntetic Heritage. *Reviews in Mineralogy & Geochemistry, 55*, 25-63.

Bizzarro, M., Ulfbeck, D., Trinquier, A., Thrane, K., Connelly, J. N., & Meyer, B. S. (2007). Evidence for a Late Supernova Injection of 60Fe into the Protoplanetary Disk. *Science, 316*, 1178-1181.

Boopathy, R. (2000). Factors limiting bioremediation technologies. *Bioresource Technology, 74*, 63-67.

Chang, R. (2007). *Chemistry* . New York, NY: McGraw Hill.

Clayton, R. N. (1978). Isotopic Anomolies in the Early Solar System. *Annual Reviews in Nuclear Particle Science, 28*, 501-522.

Crosby, H. A., Roden, E. R., Johnson, C. M., & Beard, B. L. (2007). The mechanisms of iron isotope fractionation produced during dissimilatory Fe(III) reduction by Shewanella putrefaciens and Geobacter sulfurreducens. *Geobiology, 5*, 169-189.

Dashtgard, S. E., Buschkuehle, M. B., Fairgrieve, B., & Berhane, H. (2008). Geological characterization and potential for carbon dioxide (CO2) enhanced oil recovery in the Cardium Formation, central Pembina Field, Alberta. *Bulletin of Canadian Petroleum Geology, 56*, 147-164.

Dauphas, N., & Rouxel, O. (2006). Mass Spectrometry and Natural Variations of Iron Isotopes. *Mass Spectrometry Reviews, 25*, 515-550.

Dauphas, N., Cook, D. L., Sacarabany, A., Fröhlich, C., Davis, A. M., Wadhwa, M., . . . Gallino, R. (2008). Iron 60 Evidence for Early Injection and Efficient Mixing of Stellar Debris in the Protosolar Nebula. *The Astrophysical Journal, 686*, 560-569.

Dauphas, N., Pourmand, A., & Teng, F. Z. (2009). Routine isotopic analysis of iron by HR-MC-ICPMS: How precise and how accurate? *Chemical Geology, 267*, 175-184.

de Hoffmann, E., & Stroobant, V. (2002). *Mass Spectrometry.* West Sussex, England: John Wiley & Sons Ltd.

Dean, J. R. (2005). *Practical Inductively Coupled Plasma Spectroscopy.* West Sussex, England: John Wiley & Sons Ltd.

Dideriksen, K., Baker, J. A., & Stipp, S. L. (2006). Iron isotopes in natural carbonate minerals determined by MC-ICP-MS with a 58Fe-54Fe double spike. *Geochimica et Cosmochimica Acta, 70,* 118-132.

Doran, P. T., Fritsen, C. H., McKay, C. P., Priscu, J. C., & Adams, E. E. (2003). Formation and character of an ancient 19-m ice cover and underlying trapped brine in an "ice-sealed" east Antarctic lake. *Proceedings of the National Academy of Sciences of the United States of America, 100,* 26-31.

Frey, P. A., & Reed, G. H. (2012). The Ubiquity of Iron. *ACS Chemical Biology, 7,* 1477-1481.

Groot, P. A. (2009). *Handbook of Stable Isotope Analytical Techniques: Volume 2.* Oxford: Elsevier.

Heumann, K. G., Gallus, S. M., Rädlinger, G., & Vogl, J. (1998). Precision and accuracy in isotope ratio measurement by plasma source mass spectrometry. *Journal of Analytical Atomic Spectrometry, 13,* 1001-1008.

Hoefs, J. (2010). *Stable Isotope Geochemistry - 6th Edition.* Berlin: Springer.

Hotz, K., Augsburger, H., & Walczyk, T. (2011). Isotopic signature of iron in body tissues as a potential biomarker for iron metabolism. *Journal of Analytical and Atomic Spectrometry, 26,* 1347-1353.

Icopini, G. A., Anbar, A. D., Ruebush, S. S., Tien, M., & Brantley, S. L. (2004). Iron isotope fractionation during microbial reduction of iron: The importance of adsorption. *Geology, 32*, 205-208.

JCGM. (2008). *Evaluation of measurement data - Guide to the expression of uncertainty in measurement (GUM).* Working Group 1 of the Joing Committee Guides in Metrology .

Johnson, C. M., & Beard, B. L. (1999). Correction of instrumentally produced mass fractionation during isotopic analysis of Fe by thermal ionization mass spectrometry. *International Journal of Mass Spectrometry, 193*, 87-99.

Johnson, C. M., & Beard, B. L. (2005). Biogeochemical Cycling of Iron Isotopes. *Science, 309*, 1025-1027.

Johnson, C. M., Beard, B. L., & Albarede, F. (2004a). *Geochemistry of Non-Traditional Stable Isotopes.* Washington: Mineralogical Society of America.

Johnson, C. M., Beard, B. L., & Roden, E. E. (2008). The Iron Isotope Fingerprints of Redox and Biogeochemical Cycling in Modern and Ancient Earth. *Annual Reviews in Earth and Planetary Sciences, 36*, 457-493.

Johnson, C. M., Beard, B. L., Beukes, N. J., Klein, C., & O'Leary, J. M. (2003). Ancient geochemical cycling in the Earth as inferred from Fe isotope studies of bannded iron formations from the Transvaal Craton. *Contributions to Mineral Petrology, 144*, 523-547.

Johnson, C. M., Beard, B., Roden, E. E., Newman, D. K., & Nealson, K. H. (2004b). Isotopic Constraints on Biogeochemical Cycling of Fe. *Reviews in Mineralogy & Geochemistry, 55*(2004), 359-408.

Johnson, G., Raistrick, M., Mayer, B., Shevalier, M., Taylor, S., Nightingale, M., & Hutcheon, I. (2009). The use of stable isotope measurements for monitoring and verification of CO2 storage. *Energy Proccedia, 1*, 2315-2322.

King, R. (1997). Resolution of the Principal Formation Damage Mechanisms Causing Injectivity and Productivity Impairment in the Pembina Cardium Reservoir. *SPE Annual Technical Conference and Exhibition*, (pp. 5-8 October). San Antonio, Texas.

Krabbenhoft, A., Fietzke, J., Eisenhauer, A., Liebetrau, V., Bohm, F., & Voltstaedt, H. (2009). Determination of radiogenic and stable strontium isotope ratios (87Sr/86Sr;d88/86Sr) by thermal ionization mass spectrometry applying an 87Sr/84Sr double spike. *Journal of Analytical Atomic Spectrometry, 24*, 1267-1271.

Lyons, J. R. (2001). Transfer of Mass-Independent Fractionation in Ozone to Other Oxygen-containing Radicals in the Atmosphere. *Geophysical Research Letters, 28*, 3231-3234.

Maréchal, C. N., Télouk, P., & Albarède, F. (1999). Precise analysis of copper and zinc isotopic compositions by plasma-source mass spectrometry. *Chemical Geology, 156*, 251-273.

Markl, G., von Blackenburg, F., & Wagner, T. (2006). Iron isotope fractionation during hydrothermal ore deposition and alteration. *Geochimica et Cosmochimica Acta, 70*, 3011-3030.

Meija, J., Yang, L., Sturgeon, R., & Mester, Z. (2009). Mass Bias Fractionation Laws for Multi-Collector ICPMS: Assumptions and Their Experimental Verification. *Analytical Chemistry, 81*, 6774-6778.

Millet, M.-A., Baker, J. A., & Payne, C. E. (2012). Ultra-precise stable Fe isotope measurements by high resolution multiple-collector inductively coupled plasma mass spectrometry with a 57Fe-58Fe double spike. *Chemical Geology, 304-305*, 18-25.

Mondino, L. J., Asao, M., & Madigan, M. T. (2009). Cold-active halophilic bacteria from the ice-sealed Lake Vida, Antarctica. *Archives of Microbiology, 191*, 785-790.

Murray, A. E., Kenig, F., Fritsen, C. H., McKay, C. P., Cawley, K. M., Edwards, E., . . . Doran, P. T. (2012). Microbial life at -13 C in the brine of an ice-sealed Antarctic lake. *Proceedings of the National Academy of Sciences of the United States of America, 109*, 20626-20631.

Nelms, S. M. (2005). *Inductivley Coupled plasma mass spectrometry handbook.* Blackwell Pub. .

Nightingale, M. (2010). *Water-CO2-Rock Interactions at the Pembina Cardium CO2 Monitoring Pilot.* Calgary: University of Calgary.

Ohno, T., Shinohara, A., Kohge, I., Chiba, M., & Hirata, T. (2004). Isotopic Analysis of Fe in Human Red Blood Cells by Multiple Collector-ICP-Mass Spectrometry. *Analytical Sciences, 20*, 617-621.

Pavlov, A. A., & Kasting, J. F. (2002). Mass-Independent Fractionation of Sulfur Isotopes in Archean Sediments: Strong Evidence for an Anoxic Archean Atmosphere. *Astrobiology, 2*, 27-41.

Percak-Dennett, E. M., Beard, B. L., Xu, H., Konishi, H., Johnson, C. M., & Roden, E. E. (2011). Iron isotope fractionation during microbial dissimilatory iron oxide reduction in simulated Archaean seawater. *Geobiology, 9*, 205-220.

Romanek, C., Xhang, C., Li, Y., Horita, J., Vali, H., Cole, D. R., & Phelps, T. J. (2003). Carbon and hydrogen isotope fractionations associated with dissimilatory iron-reducing bacteria. *Chemical Geology*, 5-16.

Rouxel, O. J., Bekker, A., & Edwards, K. (2005). Iron Isotope Constraints on the Archean and Paleoproterozoic Ocean Redox State. *Science, 307*, 1088-1091.

Rouxel, O., & Auro, M. (2010). Iron isotope variations in costal seawater determined by Multicollector ICP-MS. *Geostandards and Goeanalytical Research, 34*, 135-144.

Rudge, J. F., Reynolds, B. C., & Bourdon, B. (2009). The double spike toolbox. *Chemical Geology, 265*, 420-431.

Saito, N. (1984). Selected Data on ion exchange seperations in radioanalytical chemistry. *Pure & Analytical Chemistry, 56*, 523-539.

Schoenberg, R., & von Blanckenburg, F. (2005). An assessment of the accuracy of stable Fe isotope ratio measurements on samples with organic and inorganic matrices by high-resolution multicollector ICP-MS. *International Journal of Mass Spectrometry, 242*, 257-272.

Sharma, M., Polizzotto, M., & Anbar, A. D. (2001). Iron Isotopes in hot Springs Along the Juan de Fuca Ridge. *Earth and Planetary Science Letters, 194*, 39-51.

Siebert, C., Nägler, T. F., & Kramers, J. D. (2001). Determination of Molybdenum isotope fractionation by double-spike multicollector inductively coupled plasma mass spectrometry. *Geochemistry Goephysics Geosystems, 2*, 2000GC000124.

Stenberg, A., Malinovsky, D., Rodushkin, I., Andrén, H., Pontmér, C., Öhlander, B., & Baxter, D. C. (2003). Seperation of Fe from whole blood matrix for precise isotopic ratio measurements by MC-ICP-MS: a comparison of different approaches. *Journal for analytical atomic spectrometery, 18*, 23-28.

Taylor, P. D., Maeck, R., & De Bièvre, P. (1992). Determination of the absolute isotopic composition and atomic weight of a reference sample of natural iron. *International Journal of Mass Spectrometry and Ion Processes, 121*, 111-125.

ThermoFinnigan. (2003). Finnigan Neptune hardware manual. Bremen, Germany: Product Marketing, Thermo Electron Corporation.

Thomas, R. (2008). *Practical Guide to ICP-MS A Tutorial for Beginners: Second Edition* . Boca Raton, FL: CRC Press.

Urey, H. C. (1947). The Thermodynamic Properties of Isotopic Substances. *Journal of Chemical Society*, 562-581.

Vargas, M., Kashefi, K., Blunt-Harris, E., & Lovley, D. (1998). Microbiological evidence for Fe(III) reduction on Early Earth. *Nature, 395*, 65-67.

Walczyk, T., & von Blanckenburg, F. (2002). Natural Iron Isotope Variations in Human Blood. *Science, 295*, 2065-2066.

Walczyk, T., & von Blanckenburg, F. (2005). Deciphering the iron isotope message of the human body. *International Journal of Mass Spectrometry, 242*, 117-134.

Wessling-Resnick, M. (2000). Iron Transport. *Annual Reviews in Nutrition, 20*, 129-151.

Weyer, S., & Schwieters, J. B. (2003). High Precision Fe isotope measurements with high mass resolution MC-ICPMS. *International Journal of Mass Spectrometry, 226,* 355-368.

Wiederhold, J. G., Teutsch, N., Kraemer, S. M., Halliday, A. N., & Kretzschmar, R. (2007). Iron isotope fractionation in oxic soils by mineral weathering and podzolization. *Physical Chemistry of Soils and Aquifers: A special Issue in Honor of Garrison Sposito, 71*, 5821-5833.

Woosley, S. E., & Heger, A. (2002). The evolution and explosion of massive stars. *Reviews of Modern Physics, 26*, 1015-1071.

Wu, L., Beard, B. L., Roden, E. E., & Johnson, C. M. (2011). Stable Iron Isotope Fractionation Between Aqueous Fe(II) and Hydrouns Ferric Oxide. *Environmental Science & Technology, 45,* 1847-1852.

Yang, L. (2009). Accurate and precise determination of isotopic ratios by MC-ICP-MS: A review. *Mass Spectrometry Reviews, 28*, 990-1011.

Zymela, S. (1996). *Carbon, Oxygen and Strontium isotopic composition of diagenic calcite and siderite from the upper Cretaceous formation of Western Alberta.* Hamilton, Ontario : McMaster University .

Appendix

Permission for Figure 4

ELSEVIER LICENSE
TERMS AND CONDITIONS
Sep 05, 2013

This is a License Agreement between Breege McKiernan ("You") and Elsevier ("Elsevier") provided by Copyright Clearance Center ("CCC"). The license consists of your order details, the terms and conditions provided by Elsevier, and the payment terms and conditions.

All payments must be made in full to CCC. For payment instructions, please see information listed at the bottom of this form.

Supplier	Elsevier Limited The Boulevard,Langford Lane Kidlington,Oxford,OX5 1GB,UK
Registered Company Number	1982084
Customer name	Breege McKiernan
Customer address	4501 37th Street NW Apt. 1208 Calgary , AB T2L2J5
License number	3137970597498
License date	Apr 28, 2013
Licensed content publisher	Elsevier
Licensed content publication	International Journal of Mass Spectrometry
Licensed content title	High precision Fe isotope measurements with high mass resolution MC-ICPMS
Licensed content author	S Weyer,J.B Schwieters
Licensed content date	1 May 2003
Licensed content volume number	226
Licensed content issue number	3
Number of pages	14
Start Page	355
End Page	368
Type of Use	reuse in a thesis/dissertation
Portion	figures/tables/illustrations
Number of figures/tables/illustrations	1
Format	electronic

Are you the author of this Elsevier article?	No
Will you be translating?	No
Order reference number	
Title of your thesis/dissertation	Accurate and precise iron isotope amount ratios measured by multi-collector inductively coupled plasma mass spectrometer
Expected completion date	May 2013
Estimated size (number of pages)	
Elsevier VAT number	GB 494 6272 12
Permissions price	0.00 USD
VAT/Local Sales Tax	0.0 USD / 0.0 GBP
Total	0.00 USD

Permission for Figure 5

From: "Bouman, Claudia" <claudia.bouman@thermofisher.com>

Date: 30 April, 2013 3:02:12 AM MDT

To: Michael Wieser <mwieser@ucalgary.ca>

Subject: RE: Permission to use Thermo diagram

Hello Michael,

You can tell Breege she can use the figure for her thesis, provided TFS is mentioned to have given permission.

How are you doing?

Glad to hear the NEPTUNE is so productive.

Here everything is well. Spring is slowly coming to Bremen (winter took much too long this time!), so we are enjoying the tulips in our garden…haha.

Best regards,
Claudia

From: Michael Wieser [mailto:mwieser@ucalgary.ca]
Sent: Monday, April 29, 2013 10:18 PM
To: Bouman, Claudia

Subject: Permission to use Thermo diagram

Hello Claudia,

Breege McKiernan, my MSc student, is writing her thesis on Fe isotopes. She would like to include a figure that I think was created by Thermo in Bremen which shows the layout of the Neptune. I have copied it below. Can you please tell me who I should contact to get permission to reproduce this diagram in a thesis?

By the way, the Fe is now running very well on Neptune and we are now working on S and Cu. The fun never stops here in Calgary....

Moin, eh

Michael.

Permission for Figure 3

MINERALOGICAL SOCIETY OF AMERICA
3635 Concorde Pkwy Ste 500 • Chantilly VA 20151-1110 • USA
Tel: 1 (703) 652-9950 • Fax: 1 (703) 652-9951 • Internet: www.minsocam.org

May 1, 2013

Miss Breege Agnus McKiernan
University of Calgary
Dept Geoscience
2500 University Dr NW
Calgary AB T2N 1N4
Canada

e-mail: bmckiern@ucalgary.ca

Dear Miss. McKiernan:

I received your e-mail message of 2013-05-01 requesting permission to reproduce the following figure in your thesis "Accurate and Precise Iron Isotope Amount Ratios Measured by Multi-Collector Inductively Coupled Plasma Mass Spectrometer", University of Calgary:

Figure Number(s): 5 from Francis Albarède and Brian Beard, Analytical Methods for Non-Traditional Isotopes, *Reviews in Mineralogy and Geochemistry*, January 2004, v. 55, p. 113-152.

It is with pleasure that we grant you permission to reproduce theis figure without cost in this and all subsequent editions of this work, its ancillaries, and other derivative works, in any form or medium, whether now known or hereafter developed, in all languages, for distribution throughout the world on the condition that the authors are properly cited and that reference is given to the original publication of the Mineralogical Society of America.

Sincerely,

J. Alexander Speer
Executive Director, MSA